

**Peptide-Based Biosensors and Light-Activatable Proteins:
Tools for Studying Cell Signaling and Developing Cancer Diagnosis**

Weichen Xu

A dissertation submitted to the faculty of the University of North Carolina at Chapel Hill in partial fulfillment of the requirements for the degree of Doctor of Philosophy in the UNC Eshelman School of Pharmacy (Division of Chemical Biology and Medicinal Chemistry).

Chapel Hill
2012

Approved by:

David Lawrence PhD

Nancy Allbritton PhD

Michael Jarstfer PhD

Qisheng Zhang PhD

Klaus Hahn PhD

© 2012
Weichen Xu
ALL RIGHTS RESERVED

ABSTRACT

**WEICHEN XU: Peptide-Based Biosensors and Light-Activatable Proteins:
Tools for Studying Cell Signaling and Developing Cancer Diagnosis
(Under the direction of David Lawrence)**

Protein kinases play central roles in almost all aspects of normal and abnormal cell functions. Therefore, methods that provide sensitive, selective and controllable measurement of kinase activity should prove useful for studying cell signaling events. Moreover, easy to operate, generalizable strategies are in high demand for disease diagnosis. This dissertation described the development and application of peptide-based kinase biosensors and strategies to control enzyme activities by light. First, we developed a highly sensitive peptide-based biosensor that employs capillary electrophoresis to measure Src activity in prostate cell lysates as well as in single living cells. Our studies revealed that there is a direct correlation between cell aggressiveness and the fraction of cellular Src that is in the active state. We also determined that pTyr-527 level of Src is a poor indicator of inactive Src. In addition, we have demonstrated that two or more kinases can be simultaneously monitored using this technique. Second, aimed at unraveling the distinct roles of the Src family kinases Fyn and Lck in T cell activation, we developed a highly selective, potent, and light-deactivatable Fyn inhibitor. This inhibitor provides a way of selectively activating Fyn kinase by light. We have also discovered that attaching a profluorescent dye rendered this peptide cell permeable. Third, we described a new strategy for the construction of a profluorescent light-activatable

cAMP-dependent protein kinase (PKA) via active site-directed peptide-based affinity labeling. This modified PKA displays minimum catalytic activity and low fluorescence. Light illumination restored enzymatic activity and induced stress fibers lose in living cells. A 6.2-fold fluorescence enhancement was also observed.

The strategies developed in these studies provided powerful tools to elucidate the relationship of kinase activity with disease stages and the complex cell signaling networks. With these tools in hand, we are hoping to advance our knowledge of a basic biological phenomenon as well as providing future diagnostic tool for cancer patients.

Dedication

I dedicate this work to my parents Mr. Xiaodong Xu and Ms. Li Li, and my fiancé Dr. Zhancheng Zhang, who are always there to help, support, inspire and love me through the course of this dissertation and my life.

Acknowledgements

I give my truehearted thanks to my advisor, Dr. David Lawrence, for his scientific guidance throughout my graduate study and research. This dissertation would not have been possible without his support. His insight, determination, critical thinking and positive attitude all inspired me to dedicate myself to hard work and becoming a true scientist. I thank him for nurturing me to become a proud chemical biologist. I have received great inheritance from the Lawrence laboratory and hope to pass it on in my future life.

I am also very grateful to Dr. Nancy Allbritton. Her broad knowledge in biology and analytical chemistry, her great attention to details and her cheerful encouragement have helped me through some hard times and eventually accomplished the project that I am so proud of. I also owe my deepest gratitude to Dr. Hsien-ming Lee, not only for his invaluable help and scientific inspirations, but for his professional skills and close mentorship. Dr. Lee is not only a great mentor to me, but also a close friend. I will never forget those tough but happy days when we tried to finish the project together. I also want to thank my committee members Dr. Michael Jarstfer, Dr. Qisheng Zhang, and Dr. Klaus Hahn. They have provided me with wonderful ideas for my projects and helped me finish my Ph.D training smoothly.

I am so fortunate to have many of my colleagues and friends to support and help me. First, I want give my thanks to the current and former members of the Lawrence Lab.

I thank Dr. Qunzhao Wang for his help and suggestion in peptide chemistry. I thank Dr. Haishan Lee for providing invaluable scientific training for me during my rotation. I want to thank Dr. Melanie Priestman for sharing her comprehensive knowledge in biology and microscopy, her help in preparing this dissertation, and also her friendship. I also thank Dr. Jennifer Shell, Dr. Robert Hughes, Dr. Vyas Sharma, and Dr. Thomas Shell for their help with my dissertation and scientific discussions. I want to thank Weston Smith, Luong Nguyen, Finith Jernigan, Nate Oien, Collin O'Banion and Ana Kamilaris for their help with my research projects. I want to give my special thanks to Danielle Cook. She is one of my truest friends. She has inspired me to work hard, to be a true scientist and to enjoy American life.

I would also like to thank my collaborators and friends in the Allbritton Lab: Angie Proctor, Ryan Phillips, Abby Turner and Jazz Dickenson. I want to give my special thanks to Angie. She is the most organized, detail oriented and lovable person I have ever met. I have learned so much from her. She always selfishlessly give me so much help not only on my project and dissertation, but also in life.

Dr. Lee Graves of the Department of Pharmacology is not a member of my thesis committee, but he has nonetheless provided indispensable help for part of the work presented in this dissertation. I thank him for his guidance and help.

I also thank the funding sources that have made my studies possible. The prostate cancer project is funded by NIH grant 1R01CA140173.

Preface

Chapter 2 and chapter 3 represent unpublished research that was designed and performed by myself. Chapter 4 represents work done in collaboration with Dr. Hsien-ming Lee. The paper was published previous to writing this dissertation with the following citation:

Lee, H-M., Xu, W., and Lawrence, D.S. (2011). Construction of a Photoactivatable Profluorescent Enzyme Via Proximity Labeling. *J. Am. Chem. Soc.* 133, 2331–2333.

Permission to include the article in its entirety in a Ph.D dissertation was retained from American Chemical Society as explained at <http://pubs.acs.org.libproxy.lib.unc.edu/page/copyright/permissions.html>

All copyrighted material included in this dissertation is used with permission from the relevant copyright holders.

Table of Contents

Abstract.....	iii
Dedication.....	v
Acknowledgements	vi
Preface	viii
Table of Contents	ix
List of Tables	xi
List of Schemes.....	xii
List of Figures	xiii
List of Abbreviations.....	xvi
Chapter	
I. BACKGROUND AND SIGNIFICANCE.....	1
STRUCTURE AND REGULATION OF SRC FAMILY KINASES	1
SRC FAMILY KINASE SIGNALING	7
SRC FAMILY KINASES IN T-CELL SIGNALING.....	12
SENSING KINASE ACTIVITY.....	15
II. SRC KINASE ACTIVITY PROFILING IN PROSTATE CANCER: A CORRELATION WITH CANCER CELL INVASIVENESS.....	24
MATERIALS AND METHODS	27
RESULTS AND DISCUSSION.....	37
CONCLUSIONS	82

III.	UNRAVELING THE ROLES OF FYN AND LCK IN TCR SIGNALING BY A LIGHT-DEACTIVATABLE FYN KINASE INHIBITOR	84
	MATERIALS AND METHODS	88
	RESULTS AND DISCUSSION.....	96
	CONCLUSIONS	116
IV.	CONSTRUCTION OF A PHOTOACTIVATABLE PROFLUORESCENT ENZYME VIA PROPINQUITY LABELING	118
	MATERIALS AND METHODS	122
	RESULTS AND DISCUSSION.....	129
	CONCLUSIONS	143
	References.....	144

List of Tables

Table 1.1	Cell type specific expression of Src family kinases.	2
Table 1.2	Signaling molecules associated with Lck and FynT in T cells.	12
Table 2.1	Stability of the Src peptide sensor in prostate cell lysates.	43
Table 2.2	Peptide library for identifying selective Src substrate against EGFR.	81
Table 3.1	IC ₅₀ and selectivity of peptide inhibitors for Src, Fyn, Lck and Blk.	99
Table 3.2	IC ₅₀ and selectivity of peptide 24 , 25 and 27 for Fyn and Lck.	107

List of Schemes

Scheme 2.1 The design of cell permeable Src sensor peptide 3	68
Scheme 3.1 Synthesis of the profluorescent peptide 26	102
Scheme 3.2 The “uptake and report” design of peptide 26	103

List of Figures

Figure 1.1	Domain structure of Src family kinases.....	3
Figure 1.2	The structures of inactive and active Src family kinases.	4
Figure 1.3	The activation of Src family kinases.	5
Figure 1.4	Role of Src during cell migration.	9
Figure 1.5	Src mediate EGF- and HGF-induced epithelial-mesenchymal transition and cell migration and invasion.	10
Figure 1.6	Lck and FynT recruitment and activation upon TCR stimulation.....	13
Figure 1.7	FRET-based kinase sensor based on phosphorylation induced conformational change.	15
Figure 1.8	Different approaches to construct “caged” proteins.	23
Figure 2.1	CE-LIF separation and visualization of the Src peptide substrate 1 and its chemically synthesized phosphorylated counterpart 2	40
Figure 2.2	Src kinase-catalyzed phosphorylation of the Src substrate as a function of time.....	41
Figure 2.3	Phosphorylation kinetics of the Src substrate by lysates from nine prostate cell lines.....	42
Figure 2.4	Src kinase activities of PZ-HPV-7, RWPE1, CWR22Rv1, DU145 and PC3 prostate cell lines.....	46
Figure 2.5	Immunodepletion of Src kinase from prostate cell lysates.	48
Figure 2.6	Src activity in DU145 lysates as a function of inhibitor concentration.	49
Figure 2.7	Src protein levels in PZ-HVP-7, RWPE1, DU145, PC3 and CWR22Rv1 prostate cell lines.....	51
Figure 2.8	Fractional Src kinase activity in PZ-HVP-7, RWPE1, DU145, PC3 and CWR22Rv1 prostate cell lines.....	52
Figure 2.9	Phosphorylation status of Src in PZ-HVP-7, RWPE1, DU145, PC3 and CWR22Rv1 prostate cell lines.....	55
Figure 2.10	Total Src kinase activity in prostate cancer progression model cell lines. ...	57
Figure 2.11	Src expression levels in all prostate cell lines tested.	58

Figure 2.12	Fractional Src kinase activity in prostate cancer progression model cell lines.	59
Figure 2.13	Phosphorylation of Src in prostate cancer progression model cell lines.	60
Figure 2.14	Invasiveness of prostate cell lines assessed by Matrigel invasion assay.	62
Figure 2.15	Single cell analysis of Src kinase activity in DU145 cells by CE.	65
Figure 2.16	Uptake of peptide 3 by prostate cells.	69
Figure 2.17	CE-LIF separation and visualization of Src sensor and Akt sensor.	71
Figure 2.18	Kinase-catalyzed phosphorylation of Src and Akt sensors as a function of time as assessed by CE-LIF.	73
Figure 2.19	Phosphorylation and degradation of Src sensor and Akt sensor in DU145 and PC3 cell lysate.	76
Figure 2.20	Radiolabeled ATP kinase assay.	77
Figure 2.21	Phosphorylation of Src sensor and EGFR sensor by Src or EGFR kinase. ...	80
Figure 3.1	A light-deactivatable Src family kinase inhibitor.	87
Figure 3.2	Fluorescence microscopy imaging of peptide 26 uptake by Jurkat T cell. .	105
Figure 3.3	Immobilized peptide 25 selectively pulls-down Fyn over Lck from Jurkat cell lysate.	109
Figure 3.4	TCR induced phosphorylation of Pyk2 and LAT requires Src family kinase activity.	111
Figure 3.5	Effect of Lck selective inhibitor damnacanthal treatment on Pyk2 and LAT phosphorylation.	114
Figure 3.6	Effect of the cell permeable Fyn selective inhibitor 26 treatment on Pyk2 and LAT phosphorylation.	115
Figure 4.1	The uncage-and-report design of a caged profluorescent PKA.	121
Figure 4.2	Design of the caged profluorescent PKA.	130
Figure 4.3	Structure of the caging agent 28	131
Figure 4.4	Caging agent 28 labeling PKA reaction is driven by protein-ligand recognition.	132
Figure 4.5	Mass spectrometry characterization of caged PKA.	135

Figure 4.6	Actin staining of untreated and CPT-cAMP-treated REF52 cells.	137
Figure 4.7	Morphology change in wtPKA injected REF52 cell.	138
Figure 4.8	Stress fibers in photolyzed non-microinjected cells were retained.	139
Figure 4.9	Microinjected REF52 cells in the absence of illumination.	140
Figure 4.10	Photolysis of caged PKA induced stress fiber disappearance and fluorescence increase.....	141
Figure 4.11	TAMRA fluorescence prior to and after photolysis.	142

List of Abbreviations

ACN – Acetonitrile

ADP – Adenosine 5'-diphosphate

Ahx – L-2-aminohexanoic acid

Ala – Alanine

Aloc – Allyloxycarbonyl

AM – Acetoxymethyl ester

AML – Acute myeloid leukemia

ANP linker – 3-N α -Fmoc-amino-3-(2-nitrophenyl)propionic acid

APC – Antigen presenting cell

AR – Androgen receptor

ATP – Adenosine 5'-triphosphate

Ba – 3-Methoxy-4-nitrobenzoic acid

BGP – β -glycerophosphate

Bis-Tris – Bis(2-hydroxyethyl)amino-tris(hydroxymethyl)methane

Blk – B lymphocyte kinase

Boc – t-Butyloxycarbonyl

BPE – Bovine pituitary extract

BSA – Bovine serum albumin

C – Cysteine

C subunit – Catalytic subunit

CaMKII – Ca²⁺/calmodulin-dependent protein kinase II

cAMP – Cyclic adenosine monophosphate

CaP – Prostate cancer

CD4 – Cluster of differentiation 4

CD45 – Lymphocyte common antigen

CD8 – Cluster of differentiation 8

CE-LIF – Capillary electrophoresis-laser induced fluorescence

CFDA-SE – Carboxyfluorescein diacetate-succinimidyl ester

CPM – Counts per minute

CPP – Cell penetrating peptide

CPT-cAMP – 8-(4-Chlorophenylthio) adenosine-3',5'-cyclic monophosphorothioate

CRY2 – Cryptochrome 2

CSK – C-terminal Src kinase

Cys – Cysteine

Cys – Cysteine

D – Aspartic acid

Dap – 2,3-Diaminopropionic Acid

DCM – Dichloromethane

DHFR – Dihydrofolate reductase

DIC – N,N'-Diisopropylcarbodiimide

DIPEA – N,N-Diisopropylethylamine

DMEM – Dulbecco's modified eagle medium

DMF – N,N-Dimethylformamide

DNA – Deoxyribonucleic acid

Dock180 – Dedicator of cytokinesis

DPBS – Dulbecco's phosphate buffered saline

DTT – Dithiothreitol

E – Glutamic acid

ECB – Extracellular buffer

ECL – Enhanced chemiluminescence

ECM – Extracellular matrix

EDTA – Ethylenediaminetetraacetic acid

EGF – Epidermal growth factor

EGFR – Epidermal growth factor receptor

ELMO1 – Engulfment and cell motility protein 1

Em – Emission

EMEM – Eagle's minimal essential medium

EMT – Epithelial-mesenchymal transition

EPL – Expressed protein ligation

eq (equiv) – Equivalent

ER – Estrogen receptor

ERK – Extracellular signal-regulated kinase

ESI-MS – electrospray ionization-mass spectrometry

Ex – Excitation

F – Phenylalanine

FAK – Focal adhesion kinase

FAM – Carboxyfluorescein

FBS – Fetal bovine serum

FCS – Fetal calf serum

FGFR – Fibroblast growth factor receptor

FITC – Fluorescein isothiocyanate

Fmoc – N-9-Fluorenylmethoxycarbonyl

FRET – Fluorescence resonance energy transfer

FynT – Fyn kinase T cell specific isoform

G – Glycine

Glu – Glutamic acid

Gly – Glycine

H – Histidine

HBSS – Hank's balanced salt solution

HCTU – O-(1H-6-Chlorobenzotriazole-1-yl)-1,1,3,3-tetramethyluronium
hexafluorophosphate

HEPES – 4-(2-hydroxyethyl)-1-piperazineethanesulfonic acid

HGF – Hepatocyte growth factor

HGFR – Hepatocyte growth factor receptor

Hna – 1,4,5,6,7,7-hexachloro-5-norbornene-2,3-dicarboxylic acid

HOBT – Hydroxybenzotriazole hydrate

HPLC – High-performance liquid chromatography

HRP – Horseradish peroxidase

I – Isoleucine

IGFR – Insulin-like growth factor

IgG – Immunoglobulin G

IL-2 – Interleukin-2

IL-8 – Interleukin-8

Ile – Isoleucine

IPA – Isopropyl alcohol

IPTG – Isopropyl- β -D-thiogalactoside

ITAMs – Immunoreceptor tyrosine-based activation motifs

ivDde – 4,4-dimethyl-2,6-dioxocyclohex-1-ylidene

JNK – Jun N-terminal kinase

K – Lysine

K-SFM – Keratinocyte-serum free medium

LAT – Linker for activation of T cells

Lck – Lymphocyte-specific protein tyrosine kinase

LOV – Light-oxygen-voltage

Lys – Lysine

MALDI-TOF – Matrix assisted laser desorption/ionization- time of flight

MAPK – Mitogen-activated protein kinase

Met – Methionine

MHC – Major histocompatibility complex

miR – Micro RNA

MK2 – MAP kinase-activated protein kinase 2

MMP – Metalloproteinases

MOPS – 3-(N-Morpholino) propanesulfonic acid

MS/MS – Tandem mass spectrometry

N – Asparagine

Nd:YAG – Neodymium-doped yttrium aluminium garnet

NHS – N-Hydroxysuccinimide

NK cells – Natural killer cells

NMM – N-methylmorpholine

NR – Nuclear receptor

OBzl – O-Benzyl

Orn – Ornithine

OtBu – t-butyl ester

P – Proline

P/S – Penicillin/Streptomycin

p130Cas – Crk-associated substrate

p190RhoGAP – Rho GTPase activating protein

PAG – Phosphoprotein associated with GEMs

pbf – 2,2,4,6,7-pentamethyl-dihydrobenzofuran-5-sulfonyl

PBS – Phosphate buffered saline

PBST – Phosphate buffered saline with Tween 20

PDGF – Platelet-derived growth factor

PDGFR – Platelet-derived growth factor receptor

PDMS – Polydimethyl siloxane

PEG – Polyethylene glycol

PEP – PEST domain-enriched tyrosine phosphatase

PEST – Proline-, glutamic acid-, serine-, and threonine-rich

PET – Polyethylene terephthalate

PhyB – Phytochrome B

PI3K – Phosphoinositide 3-kinase

PKA – Protein kinase A or cAMP-dependent protein kinase

PKC – Protein kinase C

PKG – Protein kinase G or cGMP-dependent protein kinase

PKI – PKA inhibitor

PL – Photo linker

PR – Progesterone receptor

PTK – Protein tyrosine kinase

PTP – Protein tyrosine phosphatase

pTyr – Phosphorylated tyrosine

PVDF – Polyvinylidene fluoride

pY – Phosphorylated tyrosine

PyBop – Benzotriazole-1-yl-oxy-tris-pyrrolidino-phosphonium hexafluorophosphate

Pyk2 – Proline-rich tyrosine kinase 2

R – Arginine

Rac1 – Ras-related C3 botulinum toxin substrate 1

REF – Rat embryo fibroblasts

RFU – Relative fluorescence units

RT – Room temperature

RTK – Receptor tyrosine kinase

SDS – Sodium dodecyl sulfate

SDS-PAGE – Sodium dodecyl sulfate-polyacrylamide gel electrophoresis

SEM – Standard error of the mean

Ser – Serine

SFK – Src family kinase

SH – Src Homology

SHP-1 – SH2 domain-containing phosphatase 1

SLP-76 – SH2 domain-containing leukocyte protein of 76 kDa

T – Threonine

T-ALL – T-adult lymphoblastic leukemia

TAMRA – Carboxytetramethylrhodamine

TAT – Trans-activating transcriptional activator

TBS – Tris Buffered Saline

tBu – t-Butyl

TCR – T cell receptor

TFA – Trifluoroacetic acid

Thr – Threonine

TIS – Triisopropylsilane

TrpR – Tryptophan repressor

Trt – Trityl

Tyr – Tyrosine

UV – Ultraviolet

Val – Valine

VEGFR – Vascular endothelial growth factor receptor

WASP – Wiskott–Aldrich syndrome protein

wt – Wild type

ZAP-70 – Zeta-chain-associated protein kinase 70

β A – 3-aminopropanoic acid

β Ala – 3-aminopropanoic acid

CHAPTER I

BACKGROUND AND SIGNIFICANCE

Structure and Regulation of Src Family Kinases

Src kinase family members. Protein tyrosine kinases (PTKs) play central roles in cell signaling pathways by catalyzing phosphoryl transfer from ATP to the tyrosine residues on the protein substrates. Based on sequence homology, the 90 identified tyrosine kinases are divided into the receptor PTK family (58 members) and the non-receptor PTK family (32 members). Src kinase family is one of the 10 subfamilies further divided from the non-receptor PTK family, and has attracted much attention (Robinson et al., 2000). To date, there are over 10,000 papers published that involve the study of Src family kinases (SFKs). The 9 members of Src kinase family are: Src, Fyn, Lck, Hck, Blk, Lyn, Fgr, Yes, and Yrk. Members of this family are expressed in different cell types as listed in **Table 1.1** (Parsons and Parsons, 2004; Benati and Baldari, 2008).

Src kinase family member	Pattern of expression	Isoforms
Src	Ubiquitous	Neuron specific isoforms
Yes	Ubiquitous	
Yrk	Ubiquitous	
Fyn	Ubiquitous	T cell specific isoform (FynT)
Lck	T cells, NK cells, brain	
Blk	B cells	
Lyn	B cells, myeloid cells, brain	Two alternatively spliced forms

Fgr	B cells, myeloid cells	
Hck	Myeloid cells	Two different translational starts

(Parsons and Parsons, 2004; Benati and Baldari, 2008)

Table 1.1 Cell type specific expression of Src family kinases.

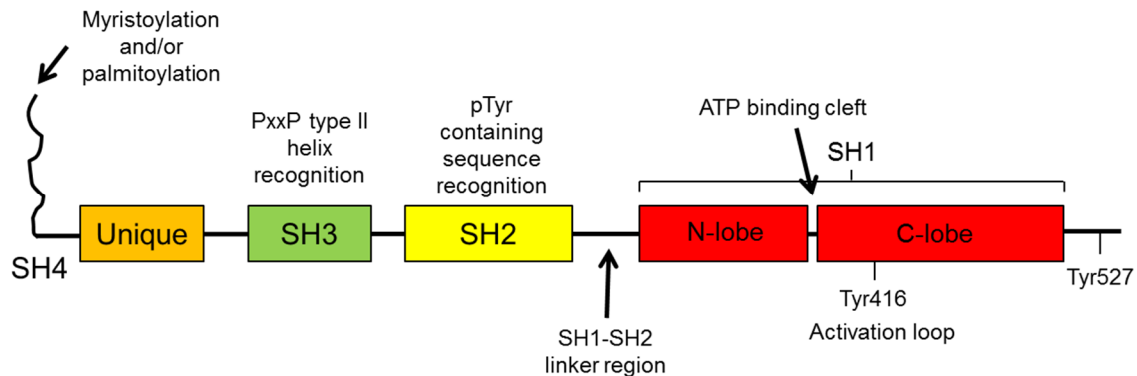
Src family kinase domain structure. SFKs share a conserved multidomain structure that contains SH1 (kinase domain), SH2 (phosphotyrosine containing sequence binding domain), SH3 (proline-rich sequence binding domain) and SH4 (membrane targeting region) domains. SFK also has a divergent “unique” domain between SH4 and SH3 domains (**Fig. 1.1**) (Boggon and Eck, 2004). The kinase domain (SH1) is composed of the N-terminal lobe and the C-terminal lobe. ATP binding and phosphoryl transfer occur at the cleft between these two lobes. The C-terminal lobe contains a peptide substrate binding site and an activation loop, where the critical regulatory tyrosine residue (Tyr-416 in Src) resides (Xu et al., 1997).

The SH2 domain has a highly conserved recognition pocket for phosphorylated tyrosine residue (pTyr), and a more divergent hydrophobic residue binding pocket that specifically recognize different pTyr containing sequences. The preferred SH2 domain binding sequence for SFKs is pTyr-Glu-Glu-Ile (Eck et al., 1993). SH2 domains serve as protein-protein recognition and interaction modules, mediating important regulatory events in cell signaling pathways.

The SH3 domain was initially characterized as a β -barrel structure that comprises the “PxxP” type II helix recognition site (Feng et al., 1994). However, recent studies have found that interaction of SH3 domain with other signaling molecules is not limited to

proline-rich sequences (Jia et al., 2005; Li, 2005; Kaneko et al., 2008), suggesting a much more diverse role of SH3 domain in cell signal transduction.

The N-terminal membrane localization region (SH4) in SFKs contains a consensus Met-Gly-Cys sequence for myristoylation and palmitoylation. The lipid modification is necessary for the localization of SFKs to the plasma membrane (Resh, 1999). The “unique” domain is different for each Src family members, but its function for most members is still unclear. However, the unique domain of Lck kinase has been shown to contain a “CxxC” motif that mediates interactions of Lck with T cell coreceptors CD4 and CD8 (Shaw et al., 1990; Turner et al., 1990), and also regulates selection of Lck specific substrates and biological functions of T cells (Carrera et al., 1995).



(Boggon and Eck, 2004; Benati and Baldari, 2008)

Figure 1.1 Domain structure of Src family kinases.

Src family kinase activity regulation. The widely accepted model of SFKs activity regulation is based on the phosphorylation and dephosphorylation of two critical residues, tyrosine 416 and 527 (p60Src, will be used in this chapter to indicate the equivalent sites in SFKs). Tyr-416 is located in the activation loop of kinase domain, and Tyr-527 is located in the C-terminal tail. Phosphorylation of Tyr-527 is catalyzed by C-terminal Src kinase (CSK). The crystal structures (**Fig. 1.2**) of the autoinhibited Src kinase showed that pTyr-527 docks into the SH2 domain phosphotyrosine recognition pocket, which facilitates the SH3 domain to form intramolecular interaction with the polyproline-type II helix of the SH1-SH2 linker region and also the N-lobe of kinase domain. As a consequence of the SH3 interaction, the two lobes of the kinase domain are pushed closer, and results in blocking of ATP binding cleft and burying of Tyr-416. Switching to the active conformation is induced either by dephosphorylation of pTyr-527 or SH2 and SH3 domain binding partners, or a combination of the two. As a result, the SFKs employ an “open” conformation, and Tyr-416 becomes available for autophosphorylation (Boggon and Eck, 2004; Benati and Baldari, 2008).

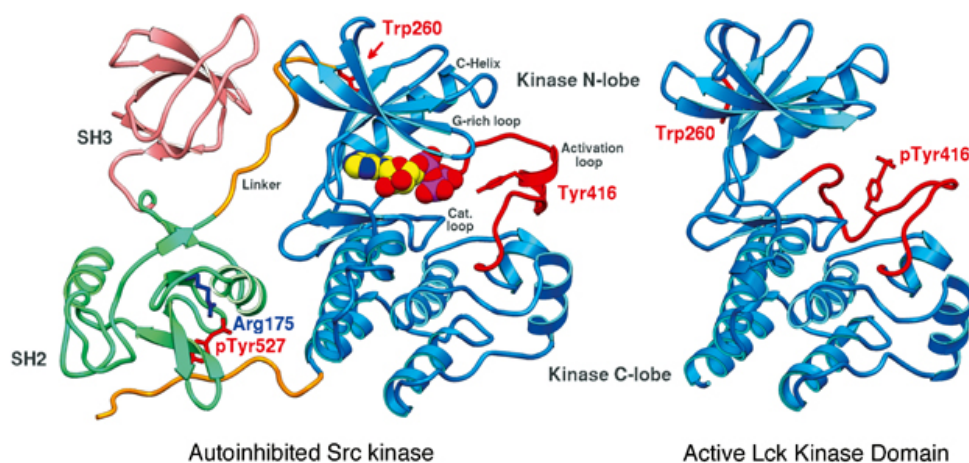


Figure 1.2 The structures of inactive and active Src family kinases.

Reprinted from Titus, J Boggon and Michael, J Eck. (2004). Structure and regulation of Src family kinases. *Oncogene* 23, 7918-7927. © 2004 Nature Publishing Group, used with permission.

The SFK activity regulation model described above is based on the crystal structures of N-terminal truncated forms of SFKs. Therefore, the position and role of myristoylation and palmitoylation in full-length SFKs is not clear. Resh and co-workers have recently found that myristoylation and membrane association positively regulate Src kinase activity, but render it more susceptible to ubiquitin-mediated degradation than their nonmyristoylated counterpart (Patwardhan and Resh, 2010). This confirmed the previous findings by Hakak *et al.* that activation of Src increase the extent of polyubiquitination (Hakak and Martin, 1999). However, their study also suggested that membrane binding plays a role in Src activation. They proposed that myristoylation mediates insertion and alignment of Src to lipid bilayers, which may facilitate an optimal conformation for Tyr-416 phosphorylation and kinase activity (**Fig. 1.3**) (Patwardhan and Resh, 2010).

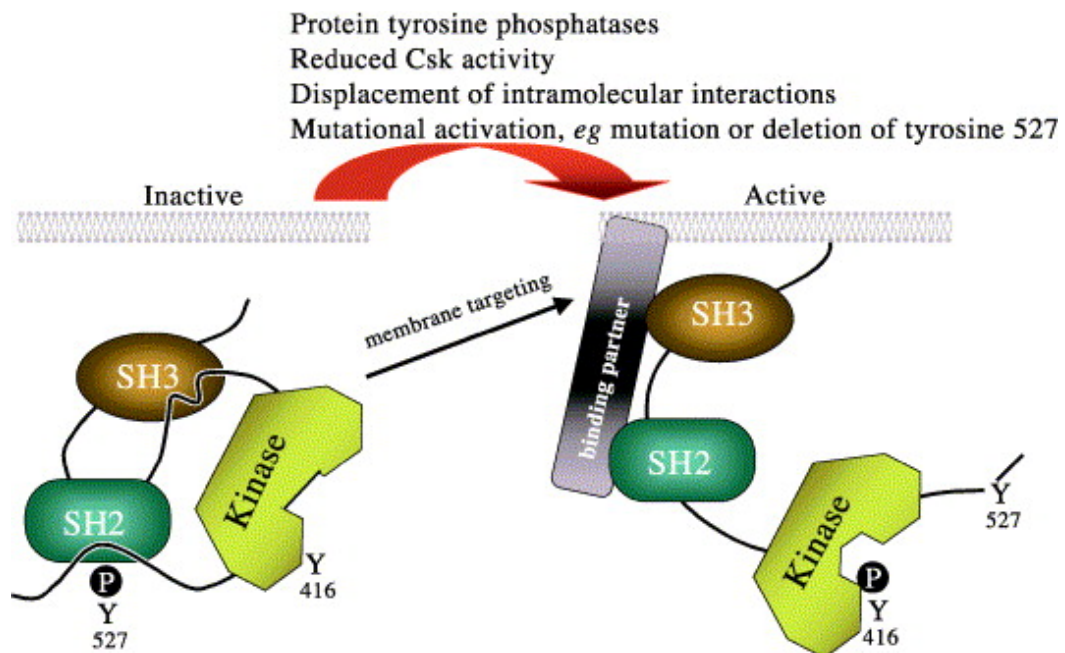


Figure 1.3 The activation of Src family kinases.

Reprinted from Margaret, C. Frame. (2002). Src in cancer: deregulation and consequences for cell behaviour. *Biochimica et Biophysica Acta* 1602, 114-30. © 2002 Elsevier Science, used with permission.

SFKs activity is often assessed by the phosphorylation levels of Tyr-416 and Tyr-527. Higher pTyr-416 level indicates more active Src, and pTyr-527 indicates inhibited Src. However, the SFKs activity regulation model described above suggests that SFKs are activated through dissociation of the SH2 and SH3 domains from the kinase domain. Therefore, interaction of the SH2 and SH3 domains with higher affinity binding partners should be able to generate an active kinase without dephosphorylating pTyr-527. Indeed, a short pTyr containing peptide that binds to Src SH2 domain is able to enhance kinase activity (Liu et al., 1993). Knight and co-workers have determined that 20% kinase activity is retained in Src kinase that consists of the pTyr-527-SH2 complex and pTyr-416. Furthermore, Src kinase activity can also be regulated by phosphorylation on serine and threonine residues. Lydon *et al.* showed that phosphorylation by serine/threonine kinase Cdc2 on Thr-34, Thr-46, and Ser-72 partially activates pTyr-527 containing Src kinase (Roskoski, 2005). Due to the complex phosphorylation and conformational regulation of SFKs, their activity should not be assessed solely by Tyr-416 and Tyr-527 phosphorylation levels.

Src Family Kinase Signaling

Src family kinase signaling in cancers. Src family kinases have been implicated in many types of cancers. In colon cancer, a mutation that results in a C-terminal tail truncated Src kinase was identified, which leads to enhanced kinase activity and cancer metastasis (Irby et al., 1999). However, despite this finding, genetic mutations of SFKs are rarely detected in cancers. The major association of SFKs with cancers is through changes in protein expression, phosphorylation, and enzymatic activity. These changes have been observed in a variety of human malignancies, including prostate cancer, breast cancer, colorectal cancer, lung cancer, pancreatic endocrine tumor and hematologic malignancies (Benati and Baldari, 2008; Kim et al., 2009).

SFKs interplay with receptor tyrosine kinases to regulate cancer cell proliferation and survival. SFKs play important roles in cancer cell signaling through bidirectional interaction with multiple receptor tyrosine kinases (RTKs) and downstream signaling proteins. These RTKs include epidermal growth factor receptor (EGFR), platelet-derived growth factor receptor (PDGFR), insulin-like growth factor 1 receptor (IGFR-1), fibroblast growth factor receptor (FGFR), vascular endothelial growth factor receptor (VEGFR), hepatocyte growth factor receptor (HGFR) and others (Bromann et al., 2004; Kim et al., 2009). Src is believed to associate with activated RTKs through its SH2 domain, thereby releasing the inhibitory intramolecular conformation, and allowing the enzyme to adopt an open conformation that leads to Tyr-416 phosphorylation and increased catalytic activity. Activated Src not only regulates downstream proteins, but also reciprocally phosphorylates and regulates RTKs, particularly EGFR, PDGFR and IGFR-1 (Benati and Baldari, 2008).

The synergistic roles played by EGFR and Src may have particularly important clinical relevance since both tyrosine kinases are frequently overexpressed in breast cancer (Abram and Courtneidge, 2000). Studies have shown that Src tightly associates with activated EGFR and is required for EGFR induced mitogenesis. Overexpression of Src can increase EGF-stimulated DNA synthesis and tumor cell proliferation (Belsches et al., 1997; Kong et al., 2003). Other studies also indicated a role of SFKs in growth factor stimulated DNA synthesis and mitogenesis, although the requirement of SFKs may depend on cell types and the cellular context in the studies (Bromann et al., 2004).

Src signaling in cancer cell migration and invasion. Cancer patients often suffer from metastasized tumors. Much attention has been devoted for developing diagnostics and therapeutics for metastatic cancer. In order for tumor cells to become metastatic, they need to acquire abilities to migrate, degrade the extracellular matrix (ECM), invade the stroma and enter the lymph or vascular system to reach a distant site (Geho et al., 2005). SFKs not only support tumor cell survival and mitogenesis during local and metastatic growth, but have a more profound role in reorganizing actin cell cytoskeleton, disrupting cell-cell and cell-matrix adhesion, altering cell morphology and ultimately promoting cell migration and invasion.

Integrins are transmembrane receptors that cluster in specific cell-matrix adhesions to organize ECM and cell cytoskeleton, and interact with several structural and signaling proteins including Src, focal adhesion kinase (FAK), paxillin, talin, tensin and others (Berrier and Yamada, 2007). Integrin-mediated adhesion induces FAK phosphorylation, which creates a binding site for Src SH2 domain (Mitra and Schlaepfer, 2006). The cytoplasmic tail of $\beta 3$ integrins can also directly interact with Src SH3

domain, promoting Src activation (Huveneers and Danen, 2009). Therefore, Src is recruited and activated at the adhesion and protrusion leading edge during cell migration. Activated Src then recruits and activates the scaffold protein p130Cas, which binds Dock180 and ELMO1 through association with the adaptor protein Crk. The Dock180-ELMO1 complex serves as a guanine-exchange factor to activate Rac1 and induce actin-driven cell protrusions (Huveneers and Danen, 2009). Src also mediates suppression of Rho through phosphorylating p190RhoGAP, which is important for relieving contractile forces during migration. At the cell's trailing edge, Src recruits ERK/MAPK and calpain, which induces proteolytic cleavage to promote adhesion disassembly and cell-matrix detachment (Fig. 1.4) (Guarino, 2009).

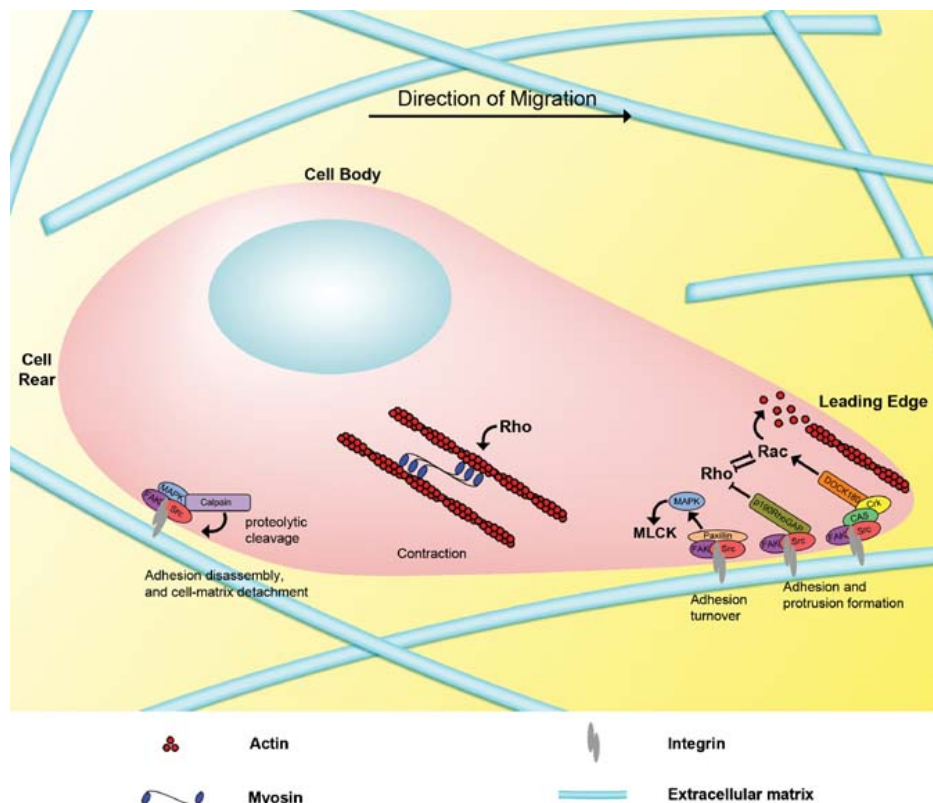


Figure 1.4 Role of Src during cell migration.

Reprinted from Marcello, Guarino. (2010). Src signaling in cancer invasion. Journal of Cellular Physiology 223, 14-26 © 2010 Wiley-Liss, Inc., used with permission.

Src also induces activation of the PI3K/Akt pathway either through direct binding of PI3K to the Src SH3 domain or phosphorylation of PI3K. PI3K plays a central role in cell migration by generating asymmetrical signaling that establishes cell polarity. Src mediated PI3K/Akt activation can also enhance tumor cell survival during growth, invasion and metastasis due to the anti-apoptotic effect of Akt (Guarino, 2009).

Epithelial cells become migratory through the epithelial-mesenchymal transition (EMT), during which the cell-cell junctions are disrupted. Src is required for EGF- and HGF-induced EMT by phosphorylating the E-cadherin- β -catenin complex, thus altering the interaction between the two proteins and thereby interfering with E-cadherin functionality (**Fig. 1.5**) (Behrens et al., 1993; Frame, 2002). Furthermore, for tumor cells to invade, they not only need to acquire the migratory phenotype, but also have to translocate through matrix barriers. Src is known to mediate “mesenchymal-type” invasion by promoting the expression of matrix degrading proteases, such as metalloproteinases (MMPs) (Kuo et al., 2006; Wang and McNiven, 2012).

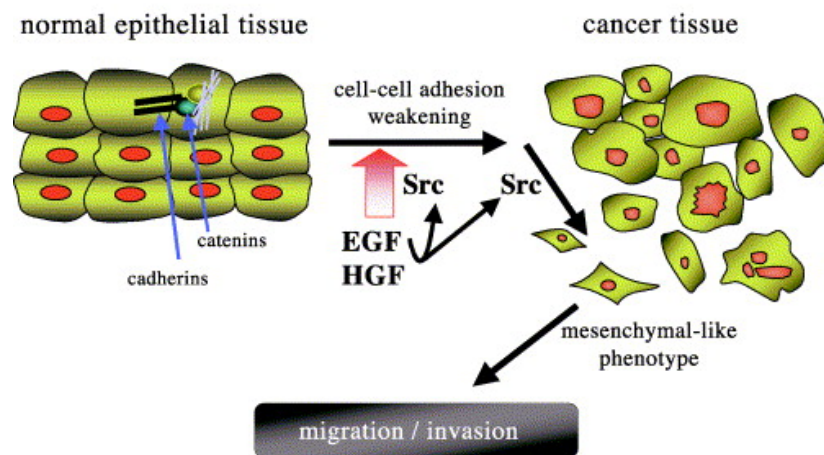


Figure 1.5 Src mediate EGF- and HGF-induced epithelial-mesenchymal transition (EMT) and cell migration and invasion.

Reprinted from Margaret, C. Frame. (2002). Src in cancer: deregulation and consequences for cell behaviour. *Biochimica et Biophysica Acta* 1602, 114-30. ©2002 Elsevier Science, used with permission.

The Interplay of Src with sex steroid receptors in cancer. Sex steroid hormones including estrogen, progesterone and androgen are key regulators in the development and progression of endocrine-related cancers. These hormones function through estrogen receptor (ER), progesterone receptor (PR) and androgen receptor (AR), respectively. These receptors are members of the nuclear receptor (NR) superfamily, and function as transcription factors to regulate gene expression (Gao et al., 2002). Src has been suggested to play a role in hormone receptor signaling and resistance. Studies have shown that blocking Src interaction with AR or ER strongly inhibits prostate cancer or breast cancer growth (Saad and Lipton, 2010). Prostate and breast cancer patients who receive hormone-deprivation/blocking therapies often develop androgen-independent prostate cancer or antiestrogen-resistant breast cancer, which results in a poor prognosis. Src kinase has been demonstrated to contribute to hormone-independent tumor growth by transactivating AR/ER mediated signaling through other mechanisms, including growth factor and cytokine receptor activation (Hiscox et al., 2006; Mellado et al., 2009). Moreover, active Src kinase can also drive the transition of prostate cancer from the androgen-dependent to -independent type (Unni et al., 2004).

Src family kinases in hematologic malignancies. Src family members are also key players in hematologic malignancies. Increased Hck and Lyn activities are evident in Bcr-Abl positive cells (Danhauser-Riedl et al., 1996). Overexpression of Lck has been found in acute myeloid leukemia (AML) and T-adult lymphoblastic leukemia (T-ALL) (Benati and Baldari, 2008).

Src Family Kinases in T-Cell Signaling

Lck and FynT (the T cell specific isoform of Fyn) are the predominant SFKs found in T cells. They are believed to have overlapping and distinct functions during T cell receptor (TCR) proximal signaling. Lck associates with CD4 and CD8 receptors through cysteine residues in the “unique” domain (Turner et al., 1990; Kim et al., 2003), whereas the “unique” domain of FynT interacts with the TCR-CD3 complex (zur Hausen et al., 1997). The SH2 and SH3 domains of Lck and FynT also exhibit different binding specificities. Different molecules have been shown to interact with Lck or FynT, as demonstrated by coimmunoprecipitation experiments (**Table. 1.2**) (Zamoyska et al., 2003).


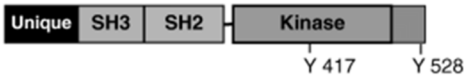
Molecules shown to associate with:	
Lck 	Cell surface: CD4 & CD8, CD45, CD22, IL-2R Intracellular: ZAP-70, PI-3K, c-cbl, SAM68, MAPK, RasGAP, raf 1, LckBP1, Lad/TSA _d
Fyn 	Cell surface: TCR, CD2, IL-2R, Fas Intracellular: ZAP-70, PI-3K, c-cbl, SAM68, Pyk2, SAP/SLAM, Shc, Gab-2

Table 1.2 Signaling molecules associated with Lck and FynT in T cells.

Adapted from Zamoyska, R., Basson, A., Filby, A., Legname, G., Lovatt, M., and Seddon, B. (2003). The influence of the src-family kinases, Lck and Fyn, on T cell differentiation, survival and activation. *Immunological Reviews* 191, 107–118. © 2003 Blackwell Munksgaard, used with permission.

Activities of Lck and FynT are not only regulated by domain binding, but also by phosphorylation and dephosphorylation. Phosphatase CD45 is responsible for the dephosphorylation of both pTyr-416 and pTyr-527. pTyr-416 can also be

dephosphorylated by other phosphatases including PEP, PTP-PEST and SHP-1 (Salmond et al., 2009). Lck also contains a serine phosphorylation site that is not present in FynT. Serine/threonine kinase MAPK/ERK phosphorylation of this site leads to changes in Lck SH2 binding affinity to phospho-proteins (Stefanová et al., 2003).

The different roles of Lck and FynT can also be attributed to their different cellular localizations. Lck is often found at plasma membrane, whereas FynT is intracellular and colocalizes with the centrosome and microtubules (Ley et al., 1994). It is still unclear how each kinase is specifically recruited and activated upon T cell stimulation. One possible mechanism proposed by Julius and co-workers is that Lck is activated outside of lipid rafts, and then recruited into rafts (Filipp et al., 2003). This translocation is required for Fyn colocalization and activation (Filipp et al., 2008) (**Fig. 1.6**).

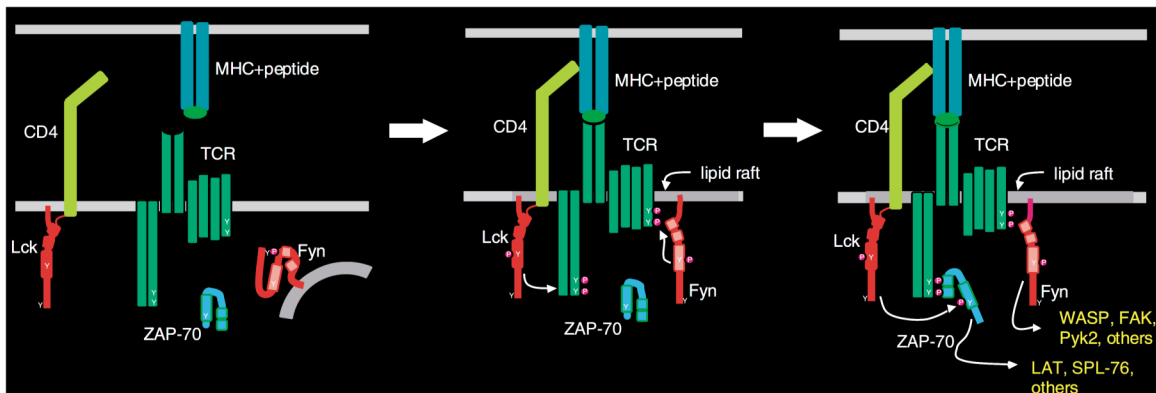


Figure 1.6 Lck and FynT recruitment and activation upon TCR stimulation.

Reprinted from Palacios, E.H., and Weiss, A. (2004). Function of the Src-family kinases, Lck and Fyn, in T-cell development and activation. *Oncogene* 23, 7990–8000. © 2004 Nature Publishing Group, used with permission.

Upon T cell stimulation, activated Lck phosphorylate CD3 and ζ -chain ITAMs, leads to recruitment and activation of ZAP-70, which then phosphorylates an adapter protein LAT. LAT is central to the recruitment of multiple signaling molecules that leads to T cell activation. Activated FynT is believed to also contribute to activating some of these pathways, and can partially compensate for loss of Lck (Samelson, 2002). However, FynT is also sufficient to initiate some signaling pathways, as demonstrated in studies using Lck deficient cell lines. For example, FynT alone can activate MAPK/ERK or PI3K upon TCR stimulation (Lovatt et al., 2006; Salmond et al., 2009).

In addition to positive regulation of TCR signaling, Lck and FynT also play a feedback inhibition role in T cell signaling pathways. Stimulation of TCR and coreceptors in a Fyn deficient T cell caused more IL-2 production and faster cell proliferation. This hyperactivity of Fyn-deficient T cells was not observed by TCR activation (anti-CD3 stimulation) alone, which suggests the involvement of Lck in the hyperactive phenotype (Filby et al., 2007). Moreover, FynT phosphorylation of PAG, which is a transmembrane adaptor protein, is required for recruiting CSK to the vicinity of SFKs, indicating a negative feedback loop (Yasuda et al., 2002; Davidson et al., 2007).

Sensing Kinase Activity

As the complex regulation mechanisms of kinases and their important roles in cell signaling and diseases are revealed, the ability to measure kinase activity in living cells and understand precise regulation in a spatiotemporal manner has become critical. Therefore, biosensors and “caged” enzymes aiming to visualize or/and control kinase activity, dynamics and localization have been developed.

FRET-based sensors. Fluorescence resonance energy transfer (FRET) is the transfer of energy from the donor to the acceptor fluorophore, which strongly depends on donor and acceptor distance and orientation. One major class of FRET-based kinase biosensors is based on the phospho-amino acid binding induced orientation change between the donor and acceptor. When the target kinase is activated, the substrate sequence of the biosensor become phosphorylated, and then binds to the adjacent phospho-amino acid binding domain. As illustrated in **Fig. 1.7**, this binding result in an orientation change of the fluorescent proteins, thus inducing a FRET change (VanEngelenburg and Palmer, 2008).

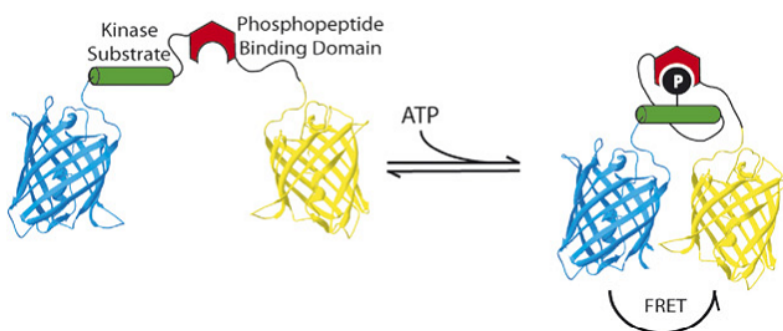


Figure 1.7 FRET-based kinase sensor based upon phosphorylation induced conformational change.

Reprinted from VanEngelenburg, S.B., and Palmer, A.E. (2008). Fluorescent biosensors of protein function. *Current Opinion in Chemical Biology* 12, 60–65. © 2008 Elsevier Science, used with permission.

This type of FRET-based kinase sensors has been developed for a variety of kinases, and new biological phenomena have been discovered. Tsien and co-workers are among the first to develop FRET-based kinase sensors, which include sensors for Abl, Src, EGFR, PKB, PKC and PKA. Studies using these sensors have lead to some interesting findings. For example, PDGF-induced Abl activity is strongest in membrane ruffles (Ting et al., 2001); local mechanical stimulation induces directional and long range Src activation (Wang et al., 2005); phosphorylation of the PKC sensor coincides with calcium oscillations (Violin et al., 2003), and PKB signaling is more rapid in the cytosol than in the nucleus (Kunkel et al., 2005). Umezawa and co-workers also used a FRET based PKB/Akt sensor to discover that activated PKB localizes to subcellular compartments, and different stimuli triggers different localization (Sasaki et al., 2003). Studies using FRET sensors to monitor the activity of other kinases, including ERK (extracellular signal-regulated kinases) (Sato et al., 2007), JNK (Jun N-terminal kinase) (Pereira et al., 2011) and MAPK (mitogen-activated protein kinase) (Timm et al., 2011) have also been published.

The FRET pair can also be introduced onto a kinase itself, if the kinase employs a conformational change upon activation. This approach has been used to monitor several kinases in living cells, including PKB/Akt (Calleja et al., 2003, 2007), Ca^{2+} /calmodulin-dependent protein kinase II (CaMKII) (Takao et al., 2005; Erickson et al., 2011), ERK2 (Fujioka et al., 2006) and MAP kinase-activated protein kinase 2 (MK2) (Neininger et al., 2001).

The FRET-based kinase sensors usually give 10-35% signal change. There has been a significant effort to improve the response, notably by adjusting fluorophore

distance and orientation, or changing FRET partners (Zhang et al., 2005; Allen and Zhang, 2006). Although these sensors are advantageous in the aspect that they are genetically encoded and don't require cellular delivery, the small FRET signal change and other possible issues including donor-to-acceptor stoichiometry, bleed-through and cross excitation, and donor/accepter orientation all lead to difficulties in designing and analyzing FRET-based kinase sensing (Kremers et al.).

Fluorescent peptide-based sensors. Peptide-based sensors are advantageous in that they can be easily synthesized, are relatively small, and can be modified to contain functional groups to achieve high affinity and specificity. The traditional way of assessing kinase activity using peptide substrates is radioactive ATP-based assays, where phosphorylation is quantified by the amount of radiolabeled gamma phosphate transferred to the substrate. However, these types of assays are discontinuous and require special handling of radioactive materials.

In the past decade, fluorescent peptide-based kinase sensing systems have been developed and proved useful in biological systems. One such system is capillary electrophoresis with laser induced fluorescence (CE-LIF)-based kinase activity measurement. The synthetic peptide substrate for the target kinase is labeled with a fluorophore. The nonphosphorylated substrate and the kinase phosphorylated product can be separated and quantitatively detected by CE-LIF, therefore allowing a measurement of target kinase activity in cell lysate as well as in living cells. Several peptide-based sensors have been developed using this technique, including sensors for PKA, PKB, PKC, CamKII, cdc2K, Src and EGFR (Meredith et al., 2000; Rauf et al., 2010; Li et al., 2011 and the studies described in **Chapter 2**). CE offers several significant advantages: high

resolution, high sensitivity, minimum sample consumption, high sample capacity, short detection time and automated high-throughput analysis (Pang et al., 2004; Wang and Audet, 2009). These features not only allow single cell level analysis and multiplexed kinase measurement, but also provide drug screening and disease diagnosis applications. The drawback, however, is that the assays are discontinuous. Moreover, live cell application requires peptide delivery and the sensors lack spatial resolution (Wang and Audet, 2009).

A popular continuous peptide-based kinase sensing is based on phosphorylation induced fluorescence change. Because peptide sensing strategy doesn't rely on FRET, the fluorescence response is generally over 100%, which can significantly improve sensitivity (Lawrence and Wang, 2007). The phosphorylation induced fluorescence change can be achieved by several mechanisms. One type of kinase sensor initially developed by Lawrence and co-workers and then further developed by Imperiali and co-workers is based on chelation enhanced fluorescence (CHEF). The substrate peptides contain a chelation sensitive fluorophore, which exhibit enhanced fluorescence upon phosphate group mediated metal binding. CHEF-sensors for a variety of kinases have been developed, including PKC, Src, Abl, IRK, PKB, MK2, Pim2, PKA and p38 α (Chen et al., 2002; Shults and Imperiali, 2003; Luković et al., 2008; González-Vera et al., 2009; Stains et al., 2011; also reviewed in González-Vera, 2012).

Environmentally sensitive fluorophores is another strategy for developing kinase sensors. Most of these fluorophores exhibit weak fluorescence in aqueous solutions, but bright fluorescence in non-polar solvent or hydrophobic environment. One strategy is to place an environmentally sensitive fluorophore on the peptide substrate close to the

phosphorylation site. Kinase-mediated phosphorylation modifies the local polarity and thus induces a fluorescence change (Yeh et al., 2002b). Another strategy utilizes the phospho-peptide recognition protein domains. Binding of a protein domain upon peptide phosphorylation will embed the fluorophore in a hydrophobic pocket, thus enhancing fluorescence (Wang and Lawrence, 2005). Environmentally sensitive fluorophores-mediated kinase sensing has also been successfully applied in living cells. Hahn and co-workers have developed a Src kinase sensor, in which a solvent-sensitive merocyanine dye was conjugated to a monobody that contain SH3 domain binding motif. When the Src kinase becomes activated, the SH3 domain is released from the “closed” conformation and recognized by the monobody. This binding induces a fluorescence enhancement of the dye, which is possibly due to the decrease in water-exposed surface area. Using this sensor, they found that Src kinase with an “open” conformation localizes to dorsal ruffles during cell protrusion (Gulyani et al., 2011).

Another kinase induced fluorescence increase is through disruption of fluorescence quenching. Fluorophores can be quenched via static and collisional mechanisms by several amino acids, including Trp, Met, Tyr and His (Chen et al., 2010). This phenomenon has been used to develop kinase sensors, since phosphorylation could disrupt the interaction and cause fluorescence increase. Pyrene labeled sensors have been developed by Lawrence *et al.*, in which up to 4.7-fold fluorescence increase was observed upon kinase-induced phosphorylation (Wang et al., 2006b; Wakata et al., 2008). Fluorophores with longer excitation and emission wavelength, such as cascade yellow, oregon green and cascade blue, have also been used for this type of kinase sensor and applied to cell-based systems (Wang et al., 2006c). The ability to use fluorophores with

different wavelengths also allowed the development of a multicolor sensing system for two or more kinases (Wang et al., 2010b). Lee and colleagues have developed another quenching strategy based on micelle formation. Phosphorylation introduces negative charges and thus disrupts the micelle, which leads to a 4-6 fold fluorescence increase (Sun et al., 2005). In addition, fluorescence fold change has been significantly enhanced (>60-fold) using a “deep quench” strategy also developed by Lawrence and co-workers. A quencher molecule non-covalently interacts with the substrate peptide. Kinase phosphorylation induces the phospho-peptide binding to a protein domain, thereby disrupting the quencher interaction (Sharma et al., 2007).

Peptide-based kinase sensors have been developed rapidly over the past few years. However, only a few have been applied to biological systems. Current peptide-based kinase biosensors need to be improved in their sensitive, specificity, protease resistance and photophysical properties, as well as cell delivery.

Photoactivatable (“caged”) proteins. The complex spatial and temporal regulation of cell signaling networks provides a challenge in elucidating the role of intracellular protein activity and its affect on cellular behavior. Therefore, in the past decade, much attention has been given to developing photoactivatable (“caged”) proteins, whose activities can be spatially and temporally controlled using light in a living cell system.

Several techniques have been developed to construct “caged” protein derivatives. The most utilized approach to cage proteins is by modifying key active site residues, most commonly lysine or cysteine, using photo-cleavable moieties (**Fig. 1.8A**). Proteins caged using this strategy include G-actin (Marriott, 1994), myosin (Marriott and

Heidecker, 1996), β -galactosidase (Golan et al., 1996) and PKG (Priestman et al., 2011). The difficulties commonly associated with this strategy are: (a) lack of precise control of modification for proteins that contain multiple reactive residues, and (b) not all proteins contain reactive residues that regulate enzymatic activity. Molecular biology, however, has provided alternative strategies that allow specific modification. One way is using site-directed mutagenesis to introduce reactive residues (e.g., cysteine) at key active sites (Chang et al., 1995; Ghosh et al., 2004), or to generate single reactive residue mutant (Chang et al., 1998). Another strategy pioneered by Schultz and co-workers (Wang et al., 2006a) is unnatural amino acid mutagenesis, which allows direct protein expression with the desired caging groups at specific sites of the target protein. A variety of proteins have been caged using unnatural amino acid mutagenesis (reviewed in Lee et al., 2009; Riggsbee and Deiters, 2010). Single key residue modification has also been described using an enzyme-directed caging protocol (Zou et al., 2002).

Proteins can also be caged through expressed protein ligation (EPL). This approach allows synthetic small peptides that contain multiple modifications (*e.g.*, photo-cleavage site, fluorophores and quenchers) to ligate to proteins via native amide bond (Hahn and Muir, 2004; Pellois et al., 2004; Hahn et al., 2007). Another strategy of caging enzymes is using caged small molecule effectors (Kawakami et al., 2008; Karginov et al., 2010; Riggsbee and Deiters, 2010; Priestman et al., 2011), or inhibitors that can be destroyed by light (Li et al., 2008a) (**Fig. 1.8B**). Several caged small molecule effectors have been developed to control protein expression, including caged doxycycline, ecdysone, estradiol, tamoxifen, and isopropyl- β -D-thiogalactoside (IPTG) (Riggsbee and Deiters, 2010). Nagamune *et al.* developed a caged PI3K SH2 domain binding peptide, in

which the critical tyrosyl phosphate moiety is protected by a photolabile group. Microinjecting this peptide into living cells and followed by UV irradiation induced light-dependent PI3K activation (Kawakami et al., 2008). Dieters and co-workers used a caged rapamycin to induce protein dimerization by light in living cells (Karginov et al., 2010). In addition, Lawrence *et al.* have reported a coumarin-caged cAMP that was used in conjunction with nitrobenzyl-caged PKG to achieve wavelength-distinct photoactivation of PKA and PKG in living cells (Priestman et al., 2011). Deiters *et al.* have recently developed an inhibitor-like caging strategy, in which protein function is sterically blocked by bulky PEG polymers attached to lysine residues through a photo-labile linker. Upon UV irradiation, the PEG photocage will be removed to release the native protein (Georgianna et al., 2010).

The use of light-responsive LOV (light-oxygen-voltage) domain from plant phototropin to cage protein activity has become popular in recent years. LOV contains an α helix that docks with the rest of the domain in the dark but undocks upon blue light (450–500 nm) irradiation. This large conformational change enables allosteric regulation of proteins fused to the LOV domain. Activities of proteins including Rac1 (Wu et al., 2009), DHFR (Lee et al., 2008a) and TrpR (Strickland et al., 2008) have been controlled using this strategy. This approach is attractive not only because it allows genetic expression of the caged proteins, but also the fusion protein activity can be reversibly controlled in the presence and absence of light. In addition to LOV, other light-responsive proteins such as PhyB (Leung et al., 2008; Levskaya et al., 2009), and CRY2 (Kennedy et al., 2010) are also being used for the spatiotemporal control of cell signaling proteins (**Fig. 1.8C**).

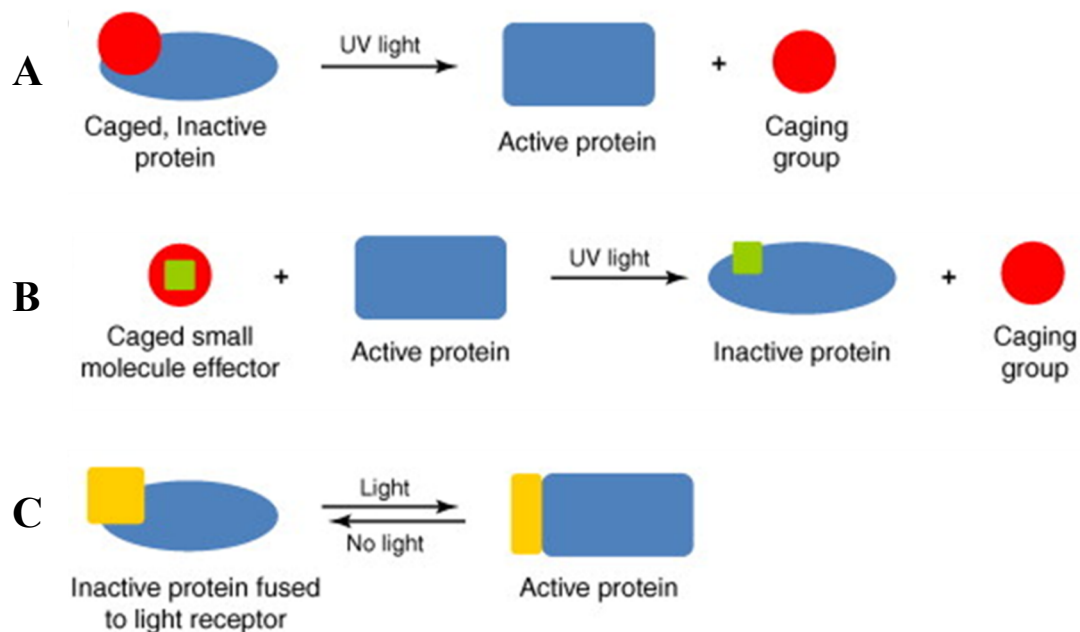


Figure 1.8 Different approaches to construct “caged” proteins.

(A) Key residues modified by photo-cleavable groups. (B) Control of protein function by light using caged small molecule effectors. (C) Reversible regulation of protein activity by light-responsive domains.

Adapted from Chad W. Riggsbee, Alexander Deiters. (2010). Recent advances in the photochemical control of protein function. *Trends in Biotechnology*. 28, 468-475. © 2010 Elsevier, used with permission.

CHAPTER II

SRC KINASE ACTIVITY PROFILING IN PROSTATE CANCER: A CORRELATION WITH CANCER CELL INVASIVENESS

Conventional strategies for identifying the biochemical basis of tumorigenesis and metastasis rely upon the search for aberrant up- (or down-) regulated genes and proteins. Although this approach has led to life-saving discoveries (Gora-Tybor and Robak, 2008), many areas of cancer diagnosis, treatment, and prognosis remain intractable. For example, a majority of men diagnosed with prostate cancer (CaP; e.g. >200,000 American men/year), a typically slow growing disease, will eventually die from other disorders. For these patients, treatment is both unnecessary and expensive, with the cost of a typical radical prostatectomy running approximately \$5000 - \$7500 (based on data from 2007) (Bolenz et al., 2010). On the other hand, a significant fraction of CaP patients will find themselves dealing with the deadly metastatic form of the disease: approximately 27,000 American men die from CaP each year (Wolf et al., 2010). The absence of clear-cut biochemical markers precludes the design of a satisfactory treatment protocol at the time of diagnosis. In short, a burning and unresolved issue in the field of CaP is how to distinguish between the benign and deadly forms of the disease at the time of diagnosis.

Metastasis is dependent, in part, on the ability of cells to separate from the parent tumor and migrate toward growth factor gradients emanating from nearby blood vessels. Migration is a highly spatial phenomenon mediated by the directed formation of

invadopodia, protease-active protrusions displayed by metastatic cancer cell lines and by patient-derived tumor cells (Buccione et al., 2009). Invadopodia promote the breakdown of the extracellular matrix in a machete-like fashion, a behavior required for the subsequent invasion of surrounding tissue. The protein tyrosine kinase Src is both sufficient and necessary for invadopodia formation and function (Bowden et al., 2006; Buccione et al., 2009; Kelley et al., 2010). This is due, at least in part, to the Src kinase-mediated phosphorylation of cortactin, an action that triggers the cofilin-promoted assembly of F-actin in invadopodia (Oser and Condeelis, 2009; Mader et al., 2011). In addition, Src is known to play a critical role in promoting protrusions at the leading edge, an essential element of migratory behavior that is likewise a cofilin-dependent process. Recently, it has been proposed that the cofilin pathway in metastatic cells is globally inhibited, yet contains spatially-localized pockets of dynamic activity (Soon, 2007). In short, the intracellular topography of this key signaling pathway may form the biochemical basis of metastatic potential. In addition to invasion, Src has also been implicated in the transition to and maintenance of androgen-independent growth, another hallmark of aggressive CaP (Fizazi, 2007; Tatarov et al., 2009).

Given the critical role that Src plays as a trigger for invadopodia formation and function as well as in directing cell movement, we wondered if a relationship exists between Src kinase activity and the known invasive behavior of various prostate cell lines. Furthermore, we decided to place a constraint on the fashion by which we addressed this conjecture: can we devise and employ a method to assess Src activity that might eventually prove applicable to patient samples? In particular, prostate biopsies furnish only a limited supply of cells. Furthermore, primary cells are challenging to grow in

culture and difficult to transfect, thereby placing significant demands on any method that seeks to assess the kinetic properties of protein kinases. Although there are a number of available methods to sample protein kinase activity, including a variety of genetically-encoded and peptide-based probes that detect kinase activity by a fluorescence change, these are unlikely to be useful in evaluating kinase activity in primary cells (Rothman et al., 2005; Lawrence and Wang, 2007; Sharma et al., 2008; Li et al., 2008b; Uri et al., 2010; Newman et al., 2011). With these challenges in mind, we have developed a capillary electrophoresis (CE)-based strategy for sampling Src kinase activity. CE is an extraordinarily sensitive method (Kovarik and Allbritton, 2011), which is essential when sample quantity is limited (e.g. patient biopsies). Furthermore, CE instruments are commercially available that are operated in clinical labs (Jabeen et al., 2006). In this project, we developed a selective and sensitive approach for quantifying the enzymatic activity of the Src kinase in large cell populations as well as in single cells. Furthermore, we evaluated the relationship between Src activity and cellular invasiveness across a series of normal and cancerous prostate cell lines and identified a positive correlation between fractional enzymatic activity and invasiveness.

Materials and Methods

Peptide synthesis. Analytical grade reagents N,N-dimethylformamide (DMF), dichloromethane (DCM), N,N-diisopropylethylamine (DIPEA), acetonitrile (ACN), trifluoroacetic acid (TFA) and other common reagents were purchased from Fisher or Sigma-Aldrich. Fmoc amino acids, O-(1H-6-chlorobenzotriazole-1-yl)-1,1,3,3-tetramethyluronium hexafluorophosphate (HCTU), N-hydroxybenzotriazole (HOBT) and NovaSyn TGR resins were obtained from NovaBiochem. Fmoc-Orn(Aloc)-OH was obtained from Bachem. 5-carboxyfluorescein (5-FAM) was purchased from Anaspec. The non-phosphorylated peptide-resin Fmoc-Orn(Aloc)-Glu(OtBu)-Glu(OtBu)-Glu(OtBu)-Ile-Tyr(tBu)-Gly-Glu(OtBu)-Phe-Orn(Aloc)-amide-Resin and the phosphorylated peptide-resin Fmoc-Orn(Aloc)-Glu(OtBu)-Glu(OtBu)-Glu(OtBu)-Ile-Tyr(PO(OBzl)OH)-Gly-Glu(OtBu)-Phe-Orn(Aloc)-amide-Resin were synthesized using a standard Fmoc peptide synthesis protocol on the Prelude automatic peptide synthesizer (Protein Technologies). Briefly, amino acid (5 equiv), HCTU (5 equiv) and DIPEA (10 equiv) were mixed with TGR resin in DMF and reacted with nitrogen bubbling mixing for 10 min at room temperature. Fmoc deprotection was achieved by using 20% piperidine in DMF for 20 min. The allyloxycarbonyl (Aloc) protecting group on the ornithine (Orn) residues was selectively removed with 3 equivalent of tetrakis (triphenylphosphine) palladium $[Pd(PPh_3)_4]$ in chloroform/acetic acid/N-methylmorpholine (37:2:1). The Orn residues were then acetylated using acetic anhydride/DIPEA (4:1) and the N-terminal Fmoc protecting group was subsequently removed. The free N-terminus was then exposed to 5-FAM (5 equiv), HOBT (10 equiv) and N,N'-diisopropylcarbodiimide (DIC, 15 equiv) in DMF overnight, followed by

incubating with 30% piperidine for 15 min. The peptides were cleaved with TFA/H₂O/TIS (triisopropylsilane) (95:2.5:2.5) and purified via HPLC (Waters), and their structures confirmed by ESI-Mass Spectrometry (Agilent Technologies). C₈₁H₉₇N₁₃O₂₇ (peptide **1**) calculated Mass: 1684.7, found (ESI+) 1684.0 and C₈₁H₉₈N₁₃O₃₀P (peptide **2**) calculated Mass 1764.7, found 1764.0.

Cell permeable Src sensor peptide **3** was prepared by mixing free N-terminal amine containing peptide with 1.5 equivalent of carboxyfluorescein diacetate, succinimidyl ester (CFDA-SE, AnaSpec) in anhydrous DMF, and react in the presence of 10 equiv of anhydrous DIPEA for 2 h. Reaction mixture was then purified by HPLC and confirmed by ESI-MS. C₈₅H₁₀₃N₁₃O₂₉ (peptide **3**) calculated Mass: 1770.8, found 1768.2.

Peptides **9-14** were synthesized in a similar fashion described above. Briefly, the peptide backbones were prepared using a peptide synthesizer, and followed by 5-FAM coupling on the free N-terminal amine. All the peptides were HPLC purified and confirmed by ESI-MS. C₆₃H₆₇N₉O₂₁ (peptide **9**) calculated Mass: 1286.2, found 1285.6; C₆₅H₆₉N₉O₂₃ (peptide **10**) calculated Mass: 1344.3, found 1343.8; C₆₄H₆₉N₉O₂₁ (peptide **11**) calculated Mass: 1300.3, found 1300.0; C₆₆H₇₁N₉O₂₃ (peptide **12**) calculated Mass: 1358.3, found 1357.8; C₆₃H₆₇N₉O₂₁ (peptide **13**) calculated Mass: 1286.2, found 1286.0; C₆₃H₆₉N₉O₁₉ (peptide **14**) calculated Mass: 1256.3, found 1256.0.

Cell culture and cell lysate preparation. All cell lines were acquired from ATCC and grown in a humidified incubator at 37 °C with 5% CO₂. PZ-HPV-7, RWPE1, WPE1-NA22, WPE1-NB14, WPE1-NB11 and WPE1-NB26 cell lines were cultured in Keratinocyte Serum Free Medium (K-SFM) supplied with 0.05 mg/mL bovine pituitary extract (BPE) and 5 ng/mL epidermal growth factor (EGF) (all provided as a kit from

Invitrogen), and 1% penicillin/streptomycin (P/S; Invitrogen). 22Rv1 cells were cultured in RPMI 1640 medium (Invitrogen) supplemented with 10% heat-inactivated fetal bovine serum (HI-FBS, Invitrogen) and 1% P/S. DU145 cells were cultured in Eagle's Minimum Essential Medium (EMEM, ATCC) supplemented with 10% HI-FBS and 1% P/S. PC3 cells were cultured in F-12K medium (ATCC) supplemented with 10% HI-FBS and 1% P/S. Cell lysates were prepared as followings: confluent cells were first trypsinized and collected into 15 mL tubes and then washed 3 times with 10 mL ice cold Dulbecco's phosphate-buffered saline buffer (DPBS, no calcium, no magnesium, Invitrogen). The cells were lysed by M-PER mammalian protein extraction reagent mixed with 5/100 (v/v) Halt protease and phosphatase inhibitor cocktail EDTA-free (Thermo Fisher Scientific), and rotated for 10 min at 4 °C. Cell debris was removed by centrifuging samples at 14,000 x g for 10 min at 4 °C. The total protein concentrations were determined by comparing to known concentrations of bovine serum albumin (BSA) using the Dc Protein assay (Bio-Rad).

Capillary electrophoresis. Capillary electrophoresis was performed on a ProteomeLab PA800 system equipped with a laser-induced fluorescence (LIF) detector (Beckman Coulter). The LIF was excited using the 488 nm argon laser. A fused-silica capillary (30/20 cm total/effective length, 50/360 µm inner/outer diameter) was used for separation (Polymicro Technologies). Prior to installation, capillaries were pretreated with 0.1 M NaOH for 12 h, distilled water for 1 h, 0.1 M HCl for 6 h and distilled water again for 12 h. For samples containing Src or/and Akt substrates, the concentrated samples were diluted in 100 mM Borate/100 mM SDS buffer at pH 7.7 (final volume no less than 20 µL) and hydrodynamically injected and separated at 25 °C at a constant

voltage of 12 kV. The running buffer was 100 mM Borate/100 mM SDS buffer at pH 7.7. For samples containing EGFR substrates, the concentrated samples were diluted in 100 mM Borate buffer at pH 7.5 and hydrodynamically injected and separated at 25 °C at a constant voltage of 12 kV. The running buffer was 140 mM Borate/70 mM SDS buffer at pH 7.7. Before each run, the capillary was rinsed with 0.1 M NaOH, distilled water, and then the running buffer for 2 min under 20 psi pressure. Data was collected and analyzed using 32 Karat Software (Version 8.0, Beckman Coulter).

Protein kinase phosphorylation assay. Kinase assay reagents including 4-morpholinepropanesulfonic acid (MOPS), ethylenedinitrilotetraacetic acid (EDTA), magnesium chloride (MgCl_2) and adenosine 5'-triphosphate disodium salt hydrate (ATP) were purchased from Sigma Aldrich. The pure Src kinase phosphorylation assays were performed with a total volume of 40 μL from the following stock solutions: 30.9 μL of H_2O , 0.5 μL of 1.14 mM substrate stock solution, 4 μL of 10X Src kinase reaction buffer (80 mM MOPS, 2 mM EDTA, 40 mM MgCl_2 , pH 7.0), 0.6 μL of 100 ng/ μL active Src kinase (Millipore 14-326), 4 μL of 10 mM ATP. Final concentration of the assay solution was 8 mM MOPS, 0.2 mM EDTA, 4 mM MgCl_2 , 1.5 ng/ μL Src kinase, 14.25 μM substrate, and 1 mM ATP. Assays were initiated by adding ATP. At each time point, 2 μL of the reaction mixture was removed and diluted with 8 μL 0.1 M HCl to stop the reaction.

The Src and Akt kinase phosphorylation assays were performed in a similar fashion, but the final concentration of the assay solution was 8 mM MOPS, 0.2 mM EDTA, 4 mM MgCl_2 , 0.25 ng/ μL Src kinase or/and Akt1 kinase (S473D, Millipore 14-453), 15 μM Src substrate or/and Akt substrate, and 1 mM ATP. The EGFR and Src

kinase phosphorylation assays were performed using a total assay volume of 15 μ L, and the final concentration of the assay solution was 8 mM MOPS, 0.2 mM EDTA, 4 mM MgCl_2 , 10 mM MnCl_2 , 0.1 $\mu\text{g}/\mu\text{L}$ BSA, 0.05 mM DTT, 1.7 ng/ μL Src kinase or 6 ng/ μL EGFR kinase (Millipore 14-531), 40 μM Src substrate or EGFR substrate, and 1 mM ATP.

Cell lysate phosphorylation assays were also performed similarly as described above under the following conditions: 2.5 $\mu\text{g}/\mu\text{L}$ cell lysate, 6.75 mM Tris (pH 7.5), 1 mM ATP, 4 mM MgCl_2 , 57 μM substrate in the absence or presence of different concentrations of tyrosine kinase inhibitors Gleevec (imatinib mesylate) or AZD0530 (Selleck Chemicals). Assays were initiated by adding substrate(s).

Western blot experiments. Primary antibodies Src (36D10): #2109, Yes: #2734, Phospho-Src Family (Tyr416): #2101, Phospho-Src (Tyr527): #2105, and α -tubulin (DM1A): #3873 were purchased from Cell Signaling Technology; anti-Fyn: 610163 and anti-Lck: 551047 were purchased from BD Pharmingen Biosciences; anti-Lyn (H-6): sc-7274 was obtained from Santa Cruz Biotechnology. Secondary antibodies (Amersham ECL anti-rabbit or anti-mouse IgG, horseradish peroxidase linked species specific whole antibody from donkey) were obtained from GE Healthcare. SDS-PAGE gel electrophoresis was performed using NuPage 4-12% Bis-Tris precast gel (Invitrogen), running at 200 V for 50 – 60 min. Gels were transferred to PVDF membranes using iBlot dry blotting system (Invitrogen) for 7 min. Blocking, antibody incubation, and washes were performed on SNAPid protein detection system (Millipore). Specifically, the membranes were first blocked using 0.5% non-fat milk in 1X PBS buffer supplemented with 0.1% Tween-20 (PBST) for 1 min. After removing the blocking buffer, the

membranes were incubated with primary antibodies for various times (non-phospho antibodies were diluted 1.7:1000 in blocking buffer and incubated for 15 min (X2); phospho-antibodies were diluted 1.7:1000 in PBST and incubated for 3 h. The membranes were washed with PBST 3 times following manufacture's instruction. Then secondary antibodies (1:1000 dilution in blocking buffer for non-phospho protein detection; 1:1000 dilution in PBST for phospho-protein detection) were applied for 15 min. The membranes were subsequently washed with PBST (X3), 0.5% NaCl (X3) and PBS (X3). The blots were detected by Amersham ECL Plus (GE Healthcare) and the chemiluminescence images were obtained by the FluoChemFC2 system (Alpha Innotech). The densitometry analysis of the bands was performed using the AlphaView software.

Immunodepletion of Src kinase from cell lysates. A Pierce Classic IP kit was employed for these experiments. The immune complex was formed by mixing (via rotation) 500 µg of cell lysate with 5 µg of Src antibody Src (36D10): 2109 or 5 µg bovine serum albumin (BSA) as control overnight at 4 °C. The immune complex was then captured by mixing (via rotation) the cell lysate-antibody mixtures with Pierce protein A/G agarose; the BSA control was mixed with Pierce control agarose resin for 1 h at 4 °C. Both treatments (with antibodies and with bovine serum albumin) were separately repeated (3 h exposure time to antibodies/bovine serum albumin and 1 h agarose-capture). Finally, the pre-cleared lysate was collected and concentrated using the Vivaspin 500 centrifugal concentrator, 10 kD (GE Healthcare) for western blot analysis and kinase assays.

Single cell capillary electrophoresis. Custom made cell chambers were prepared by utilizing polydimethyl siloxane (PDMS, Sylgard 184) to glue a silicon O-

ring to a glass coverslip (Fisher). The day before use, DU145 cells in suspension were diluted in 500 μ L of complete media, plated on the chamber, and incubated in a 5% CO₂ humidified incubator at 37 °C. Single cell capillary electrophoresis was performed using a custom-made CE-LIF system, as described previously (Kottegoda et al., 2008; Proctor et al., 2012). Briefly, capillaries (30 μ m inner diameter, 360 μ m outer diameter, total length 38 cm with an effective length 21.5 cm) were conditioned with 0.1 M NaOH for 12 h, distilled water for 1 h, 0.1 M HCl for 6 h and distilled water again for 12 h. To initiate electrophoresis, the inlet reservoir was held at ground and a voltage of -10 kV was applied to the outlet. The electrophoretic buffer was 300 mM Borate buffer at pH 7.5. Each new chamber of cells was first washed with a constant flow of extracellular buffer (ECB; 135 mM NaCl, 5 mM KCl, 1 mM MgCl₂, 1 mM CaCl₂, and 10 mM HEPES, pH 7.4, 25 °C) for 4 min. Microinjection was performed using an Eppendorf Transjector 5246 and InjectMan system. 114 μ M peptide **1** and 90X phosphatase inhibitor cocktail mixture (diluted from 100X phosphatase inhibitor cocktail 2, Sigma-Aldrich) was microinjected into a single cell (200 hPa, 1 s). For cells not treated with Src inhibitor, the ECB flow was kept on until 20 s after the microinjection. For inhibitor-treated cells, the ECB flow was halted and replaced with 1 mL of inhibitor-containing ECB for 5 min. The ECB flow was turned on (40 s total) after microinjection to remove any residual peptides from the extracellular environment. The microinjected cell was incubated for 2 min prior to lysis by a focused Nd:YAG laser (Sims et al., 1998). The lysate from the single cell was immediately loaded into the capillary via electrokinetic injection and electrophoresed. Data was collected with custom software (LabVIEW 9.0.1, National Instruments) and analyzed by Origin (version 7.5, OriginLab Corporation).

Fluorescence microscopy. Cells were plated on glass bottom dish the day before experiment and let adhere in a 37 °C, 5% CO₂ humidified incubator. The cells were washed with ECB buffer once before treated with cell permeable Src sensor **3** for 30 min at 37 °C. Peptide **3** stock solution (in anhydrous DMSO, stored at -80 °C) was diluted in ECB buffer to reach a final concentration of 5 µM. After removing peptide containing buffer, the cells were washed with ECB buffer again. Transmitted light images and fluorescein fluorescence images were taken using an inverted Olympus IX81 microscope with transmitted light and FITC filter cube.

Matrigel invasion assay. Invasion assay was performed using BD BioCoat™ Tumor Invasion System. One key component of the tumor invasion system is the BD FluoroBlok™ insert, which contains polyethylene terephthalate (PET) membrane that blocks 490-700 nm light transmission. Therefore, fluorescence from cells in the top chamber is shielded from bottom-reading fluorescence plate readers and microscopes, whereas cells that invaded through the membrane to the bottom chamber can be easily detected without cell scraping and manual cell counting (BD Biosciences, 2010). The other key component is the BD Matrigel™ Matrix coating, which is a biologically active extracellular matrix preparation extracted from the Engelbreth-Holm-Swarm mouse sarcoma (BD Biosciences, 2008).

The 24-multiwell tumor invasion system was warmed up to room temperature, and rehydrated with 500 µL serum free media (according to the cell line to be used) in a 37 °C, 5% CO₂ incubator for 2 h. The rehydrating media was then carefully removed without disturbing the Matrigel and the membranes. Prostate cells were grown in their complete media (as described in the **Cell culture and cell lysate preparation** section) to

~80% confluency in T75 flasks. The cells were washed with 10 mL DPBS, and lifted with 3 mL 0.53 mM EDTA, pH 8.0. Serum free medium (7 mL) was added to the detached cells, and centrifuge at 200 x g for 5 min to remove supernatant. The cells were then resuspended in serum free media containing 0.1% BSA. 500 μ L cell solution containing 5×10^4 cells (counted using Scepter 2.0 handheld automated cell counter, Millipore) were added to the upper chamber of each well, and 750 μ L complete medium (without antibiotics) was added to the lower chamber. The plate was then incubated at a 37 °C, 5% CO₂ incubator for 24 h. The cells were labeled with calcein acetoxymethylester (calcein AM, BD Biosciences), a non-fluorescent, cell-permeable dye that becomes fluorescent after being hydrolyzed in live cells. The PET membrane can block >99% of calcein fluorescence (Ex = 494 nm, Em = 517 nm) (BD Biosciences, 2006). 100 μ g calcein AM powder was first dissolved in 40 μ L DMSO, then diluted in 20 mL Hank's balanced salt solution (HBSS) to reach the final concentration of 5 μ g/mL. The calcein AM solution was added to a new BD Falcon™ 24 well plate at 500 μ L/well. The upper chamber from the invasion system was taken out after incubation. The media was carefully removed and the chamber was transferred to the calcein AM containing plate. The cells in the upper chamber were labeled as well with 300 μ L calcein AM solution. Labeling was allowed at 37 °C, 5% CO₂ incubator for 1 h. The fluorescence reading from bottom and top was separately taken using a SpectraMax Gemini™ EM fluorescence plate reader at 494 nm excitation and 517 nm emission.

Akt kinase assay using radiolabeled ATP. Radiolabeled ATP kinase assays were performed with assistance from Dr. Lee Graves. 0.5 ng/ μ L active Akt1 kinase (S473D, Millipore 14-453) were spiked into assay solutions with a total volume of 20 μ L.

Assay solutions contain: (1) Cell lysis buffer (CLB, 150 mM NaCl, 9.1 mM Na₂HPO₄, 1.7 mM NaH₂PO₄, 1.0% nonidet P-40, 0.5% deoxycholic acid, pH 7.4) (2) kinase buffer (8 mM MOPS, 0.2 mM EDTA, 4 mM MgCl₂), (3) RWPE1 cell lysate prepared in CLB, (4) RWPE1 cell lysate from (3) with addition of 46 mM β-glycerophosphate (BGP), and (5) RWPE1 cell lysate from (3) heat inactivated at 100 °C for 10 min. In addition, 10 mM MgCl₂, 13.4 μM Akt substrate (peptide **6**) or H₂O for background controls were present in all assays. A mixture of 1 mM ATP and [γ-³²P]ATP was used to initiate kinase reaction. The reaction mixtures were incubated for 30 min at 37 °C. Then the solution containing the substrate peptide was spotted onto phosphocellulose paper squares to capture the peptides. The papers were then washed in phosphoric acid extensively to remove unreacted [γ-³²P]ATP. Liquid scintillation fluid (ScintiSafe Econo 2, Fish Scientific) was added to the dried papers, and the radioactivity was measured by a Multipurpose Scintillation Counter LS6500 (Beckman Coulter).

Results and Discussion

The Src protein kinase is the founding member of the Src kinase subfamily of nonreceptor protein tyrosine kinases. The catalytic activity of these enzymes is regulated, in part, via phosphorylation (Roskoski, 2005). Specifically, full activation of Src is dependent upon phosphorylation at Tyr-416. By contrast, Tyr-527 phosphorylation inhibits catalytic activity, by promoting an intramolecular interaction with the enzyme's SH2 (and SH3) domains. Indeed, the level of phosphorylated Tyr-527, as revealed by Western blot analysis, is often taken as a measure of inactive enzyme. However, this interpretation is fraught with danger. Although the low *in vitro* catalytic activity of pTyr-527 Src is indisputable, the corresponding activity of the same enzyme in a biological environment is less certain. Upon interaction of the SH2 or SH3 domains of the Src enzyme with other proteins, the inhibitory pTyr-527 residue is released, which generates fully active pTyr-527 Src (Moarefi et al., 1997; Thomas et al., 1998; Zheng et al., 2000). Indeed, this process is recapitulated by short pTyr-containing peptides that, upon binding to Src's SH2 domain, disrupt the intramolecular inhibitory pTyr-527 interaction and thereby activate kinase activity (Liu et al., 1993; Alonso et al., 1995; Boerner et al., 1996). Consequently, pTyr-527 status is not necessarily indicative of an inhibited enzyme *per se*, but rather of an enzyme that is potentially primed and ready to be "switched on" by interaction with an appropriate accessory protein. In short, high pTyr-527 Src levels could represent inhibited enzyme, activated enzyme, or some variant in-between. This uncertainty highlights the need to sample Src kinase directly via its ability to phosphorylate a target substrate.

A variety of peptide-based substrates have been described to assay kinase activity. Generic ELISA- (Rijksen et al., 1996) and γ - ^{32}P -ATP-based (Braunwaler et al., 1996) methods are two of the most common, and very sensitive, strategies used for assessing activity with pure enzyme under *in vitro* conditions. In addition, fluorophore-labeled peptides (Wang and Lawrence, 2005; Wang et al., 2006b, 2006c, 2010b; Lawrence and Wang, 2007), as well as GFP-based proteins, have been described that exhibit a fluorescent response to phosphorylation, thereby allowing Src kinase activity to be continuously sampled in live cells via fluorescent microscopy (Ting et al., 2001; Wang et al., 2005). A biosensor that generates a fluorescent readout through binding to the “open” conformation of Src kinase has also been described (Gulyani et al., 2011). Although the latter technologies furnish a window into the biochemical basis of cell behavior, it is less readily translated into a routine and economical methodology for the rapid screening of the limited number of cells available in patient samples.

CE is an ultrasensitive method by which small amounts of analytes are separated and quantified, via the application of an electric field and subsequent detection of the analytes (Borland et al., 2008). The Src kinase catalyzes the transfer of the γ -phosphoryl group from ATP to the tyrosine residue of the substrate, which results in a change of the electrophoretic mobility. The latter enables separation of the starting nonphosphorylated peptide substrate from the final phosphorylated product (Li et al., 2001, 2004; Sims and Allbritton, 2003).

Design and synthesis of the Src kinase sensor. Based on the optimal Src substrate sequence identified from an oriented peptide library (Songyang et al., 1995), we developed the Src kinase substrate: 5-FAM-Orn(Ac)-Glu-Glu-Glu-Ile-Tyr-Gly-Glu-Phe-

Orn(Ac)-amide (peptide **1**), where Tyr represents the site of phosphorylation. Ornithine (Orn) residues were placed on each terminus of the peptide sequence, in the event that the peptide proved to display poor selectivity for Src versus other protein kinases. We have previously shown that side chain modification of active site-directed peptides with unnatural substituents can dramatically enhance the selectivity for the target protein kinase (*vide infra*) (Lee and Lawrence, 1999, 2000; Shen et al., 2001; Yeh et al., 2002a; Lee et al., 2004, 2008b; Li and Lawrence, 2005). Both the non-phosphorylated and the phosphorylated forms [5-FAM-Orn(Ac)-Glu-Glu-Glu-Ile-pTyr-Gly-Glu-Phe-Orn(Ac)-amide (peptide **2**)] of the peptide were prepared via solid-phase peptide synthesis. 5-FAM (5-carboxyfluorescein) was chosen as the fluorophore for substrate and product detection by laser-induced fluorescence (LIF).

The separation of the non-phosphorylated substrate and the phosphorylated product by CE-LIF is shown in **Fig. 2.1**. A 1:1 mixture of the peptides was loaded into the capillary. Under the separation conditions described in the **Capillary electrophoresis** section, the substrate peptide **1** emerges at 240 s, whereas the phosphorylated product peptide **2** appears at 290 s. Growth of the latter was monitored, as a function of time, by incubating peptide **1** with active Src kinase. The 290 s peak was confirmed to be the phosphorylated product by spiking with synthetic phospho-peptide (peptide **2**). The kinetics of phosphorylation were obtained by evaluating collected time point samples via CE-LIF and quantifying the extent of phosphorylation via integration of the individual peaks. Src substrate phosphorylation is essentially complete within 3 min under the assay conditions used in these experiments that employed pure Src enzyme (**Fig. 2.2**). By contrast, subsequent experiments in cell lysates (*vide infra*) proceed at a more leisurely

pace. In the latter case, initial rate kinetics (<10% peptide phosphorylation) were acquired within 10 min of cell lysate incubation. (**Fig. 2.3**)

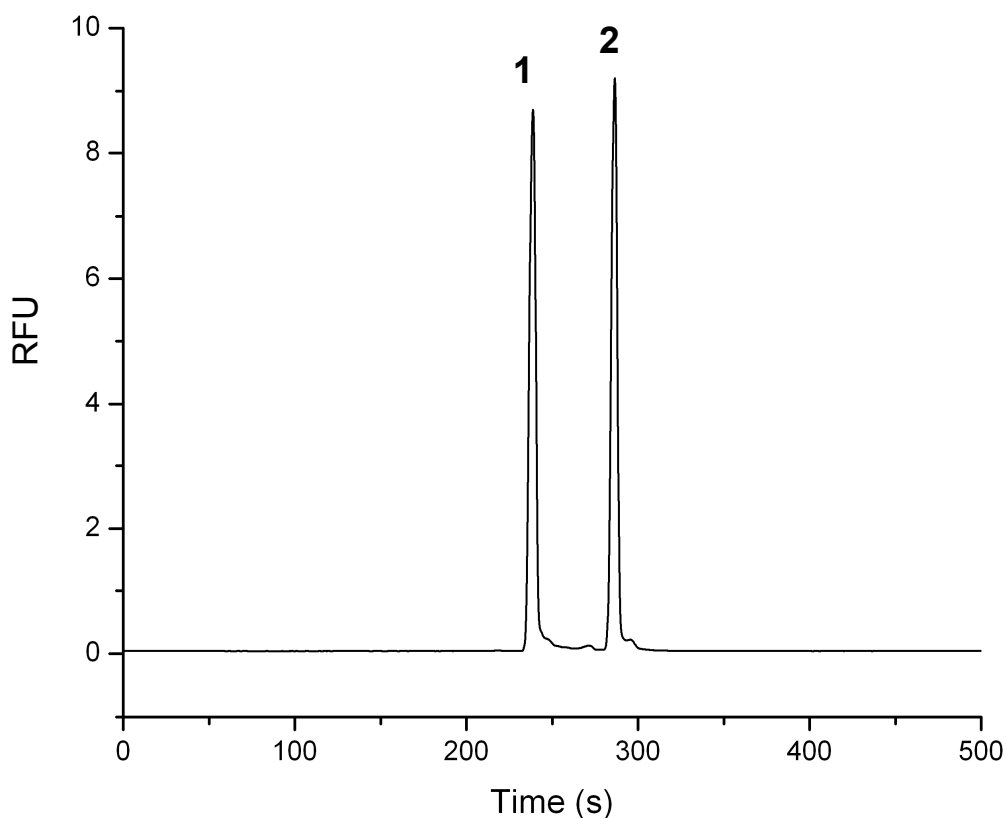


Figure 2.1 CE-LIF separation and visualization of the Src peptide substrate **1 and its chemically synthesized phosphorylated counterpart **2**.**

A 1:1 mixture of Src kinase substrate peptide **1** and its chemically synthesized phosphorylated counterpart peptide **2** was diluted in the CE running buffer (100 mM Borate/100 mM SDS buffer at pH 7.7) and hydrodynamically loaded into the capillary and separated at a constant voltage of 12 kV. The substrate peptide **1** emerges at 240 s, and the phosphorylated product peptide **2** appears at 290 s. (RFU = relative fluorescence units).

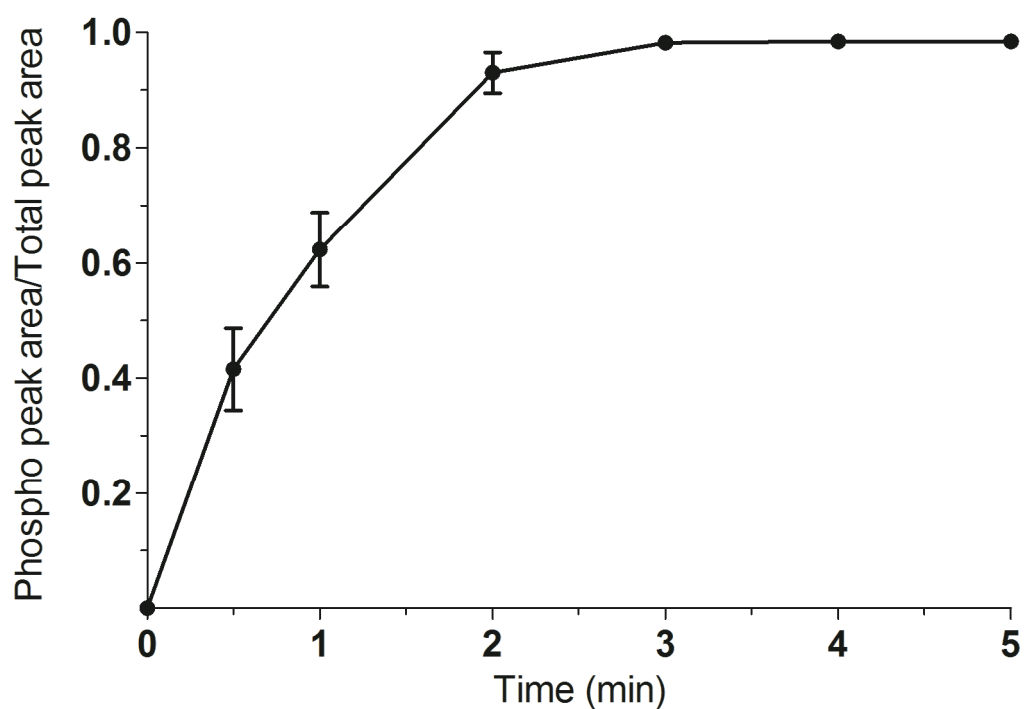


Figure 2.2 Src kinase-catalyzed phosphorylation of the Src substrate as a function of time..

Phosphorylation rate of Src substrate peptide 1 catalyzed by pure active Src kinase was assessed using the collected time point samples via CE-LIF. The extent of phosphorylation was quantified via integration of the individual peaks. All experiments were performed in triplicate. Error bars are showing SEM.

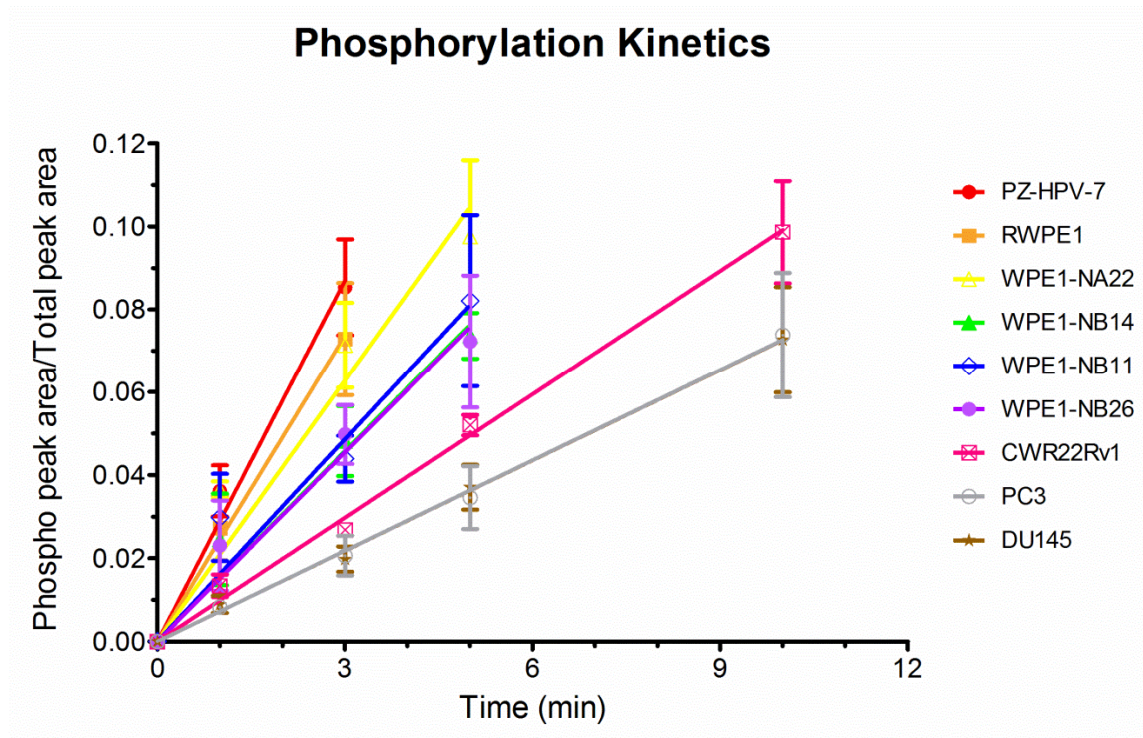


Figure 2.3 Phosphorylation kinetics of the Src substrate by prostate cell lysates.

Phosphorylation rates were derived by plotting the fraction of peptide phosphorylated [phosphopeptide peak area/(phosphopeptide + unphosphorylated peptide area)] versus time. Assays were limited to less than 10% total peptide phosphorylation in order to insure that initial rate kinetics were obtained.

Stability of the Src kinase peptide substrate in prostate cell lysates. Peptides commonly suffer protease-catalyzed degradation in cells as well as in cell lysates (Proctor et al., 2012). Consequently, prior to examining Src kinase-catalyzed phosphorylation of peptide **1** with lysates, we monitored the stability of the peptide as a function of time. Cells were lysed using Pierce's M-PER mammalian cell lysis buffer and, in the absence of ATP and Mg^{2+} (i.e. no observable kinase activity), the lysate was added to Src substrate peptide **1**. The stability of the peptide in the presence of lysate from the nine prostate cell lines is shown in **Table 2.1**. Only approximately 10% of the peptide is degraded after 1 h. Since the phosphorylation rate is measured within 10 min of incubation, the peptide is sufficiently stable for our needs.

Cell Line	% Remaining parent peptide
PZ-HPV-7	92.4 ± 0.2
RWPE1	91.0 ± 0.6
WPE1-NA22	92.4 ± 0.8
WPE1-NB14	91.4 ± 1.2
WPE1-NB11	89.8 ± 1.5
WPE1-NB26	91.0 ± 1.5
22Rv1	91.2 ± 1.8
DU145	92.9 ± 0.5
PC3	89.2 ± 2.2

Table 2.1 Stability of the Src peptide sensor in prostate cell lysates.

Cells were lysed with M-PER protein extraction reagent without protease or phosphatase inhibitors. Approximately 90% of the parent peptide is still present, as assessed by CE, after 1 h incubation in the various cell lysates. Experiments were performed in triplicate.

Assessment of Src activity in prostate cell line lysates. Tatarov *et al.* recently found a diminished survival rate in androgen-independent CaP patients with high levels of pTyr-416 Src (Tatarov et al., 2009). However, although pTyr-416 is necessary for Src kinase activity, it is not sufficient. As noted above, it is unclear what affect the presence or absence of a phosphorylated Tyr-527 residue has on Src activity given the possible existence of nearby protein binding partners. Src activity, as opposed to phosphorylation status, is a key point since recent preclinical and clinical studies have revealed that Src inhibitors, in particular dasatinib and saracatinib, hold significant promise for the treatment of CaP (Edwards, 2010). Both of these inhibitors target the ATP binding pocket of Src and therefore this form of therapy only makes sense for patients who actually display enhanced Src kinase activity. Consequently, we examined whether any correlation exists between total Src kinase activity and cell invasiveness using a series of prostate cell lines.

Our initial studies focused on the non-invasive immortalized normal prostate epithelial cell lines PZ-HPV-7 and RWPE1 and the highly invasive CaP cell lines DU145 and PC3. We also investigated Src activity in the non-metastatic CWR22Rv1 cell line, which exhibits androgen-independent growth, a characteristic behavior of advanced stage CaP (Hsieh and Wu, 2009) correlated with the Src kinase (Tatarov et al., 2009).

Our studies assessed the initial rate kinetics (i.e. <10% of product formation) of peptide phosphorylation (**Fig. 2.3**). We found that Src kinase activity (as a function of total protein content) is high in the non-invasive cell lines (PZ-HVP-7 and RWPE1) and low in the invasive cell lines (DU145 and PC3) as well as in the cell line displaying androgen-independent growth (22Rv1) (**Fig. 2.4**). This general trend is at variance with

the general notion that high Src activity correlates with prostate cell line aggressiveness (i.e. invasive behavior and androgen-independent growth). Previous reports have noted that high levels of pTyr-416 are present in the most aggressive CaPs and it has been assumed, throughout the literature, that pTyr-416 and Src activity directly correlate with one another. One possible conclusion derived from our data is that the generally accepted notion that pTyr-416 levels serve as a barometer of Src activity is faulty. However, we investigated whether there might be alternative explanations for the unexpected relationship between Src activity and cell line invasiveness illustrated in **Fig. 2.4**. One possibility is that the Src substrate peptide **1** is phosphorylated by other protein tyrosine kinases thereby rendering the apparent inverse relationship between Src activity and cell invasiveness misleading.

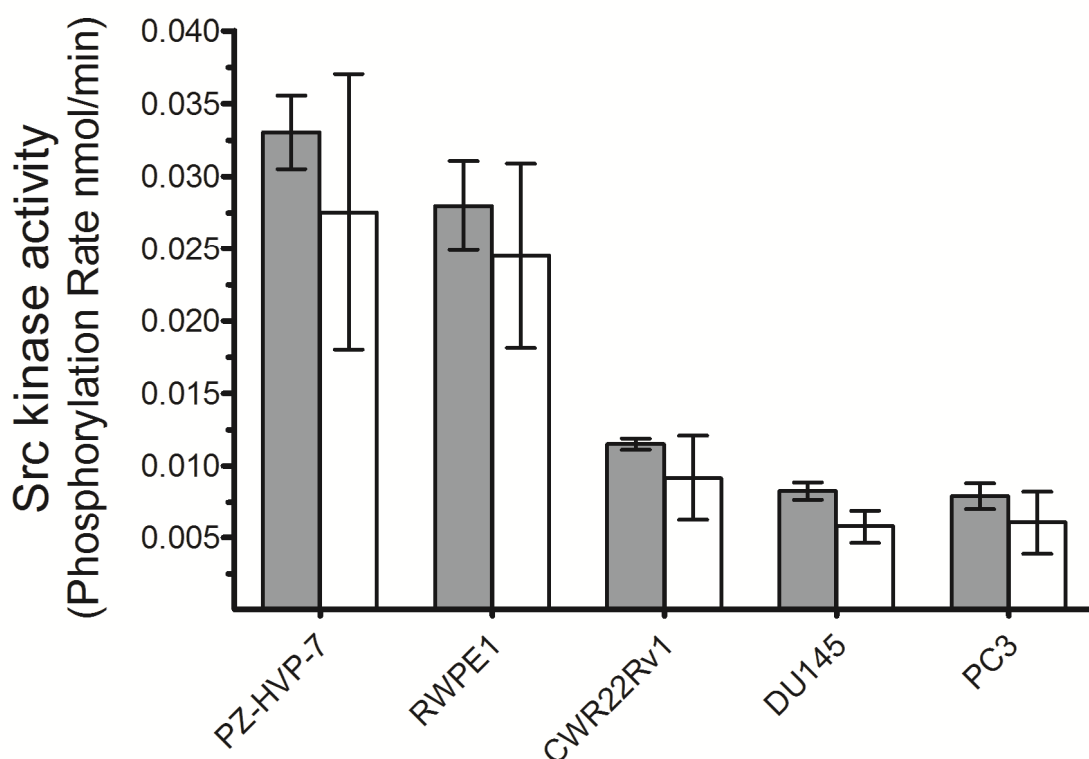


Figure 2.4 Src kinase activities of PZ-HPV-7, RWPE1, CWR22Rv1, DU145 and PC3 prostate cell lines.

Total Src kinase activities measured by CE-LIF in non-invasive (PZ-HPV-7, RWPE1), invasive (DU145, PC3), and androgen-independent (CWR22Rv1) prostate cell line lysates. Grey bars are phosphorylation rates of peptide 1 by whole cell lysates (normalized by total protein content). White bars are phosphorylation rates by cell lysates due to Src kinase alone after subtracting non-Src background phosphorylation of peptide 1. All experiments were performed in triplicate. Error bars are showing SEM. The 1-tailed t-test comparison values of Src kinase activity in noninvasive (PZ-HPV-7, RWPE1) versus invasive/androgen-independent (DU145, PC3, CWR22Rv1) cell lines is 0.0015.

Assessment of the selectivity of peptide 1 for Src in prostate cell lines. We examined the Src-selectivity of peptide **1** using CaP cell lysates depleted of Src (**Fig. 2.5**). Although Src-free cell lysates are able to phosphorylate peptide **1**, they do so to a much lesser extent (<20%) than with whole cell lysates containing Src. This is illustrated in **Fig. 2.4**, where the white bars represent Src kinase activity in which background (i.e. non-Src) kinase activity has been subtracted out. The contaminating tyrosine kinases that may be responsible for the low level of Src substrate phosphorylation in the absence of Src could be one or more of the eight other members of the Src family kinases (SFK). Indeed, several SFK family members, such as Fyn, Brk, Lyn Lck and Yes are known to present in prostate cell lines (Chang et al., 2007). Nonetheless, given the relatively modest level of peptide **1** phosphorylation by Src-free lysates, we decided that peptide **1** is, for our present needs, sufficiently Src selective.

We also assessed the ability of the peptide **1**/CE-LIF method to detect Src activity by using a combination of two known Src inhibitors. Imatinib (marketed as Gleevec), which is used to treat chronic myelogenous leukemia and other cancers, is an Abl-selective inhibitor with demonstrated weak anti-Src activity. Imatinib blocks kinase activity by serving as a competitive inhibitor of ATP. Like imatinib, saracatinib (AZD0530) is a competitive inhibitor of ATP, but displays a high selectivity and robust potency for Src. For example, the IC₅₀ values of imatinib and saracatinib with isolated Src enzyme are 24.4 μ M (Dar et al., 2008) and 2.7 nM (Green et al., 2009), respectively. Using DU145 cell lysates, we found that the potent Src inhibitor saracatinib blocks peptide **1** phosphorylation with a submicromolar IC₅₀, whereas the correspondingly poor Src inhibitor imatinib displays an IC₅₀ that is in excess of 100 μ M (**Fig. 2.6**). These

results are consistent with the notion, exemplified by the Src depletion experiments that the peptide 1/CE-LIF method serves as an efficient and selective Src activity detection modality.

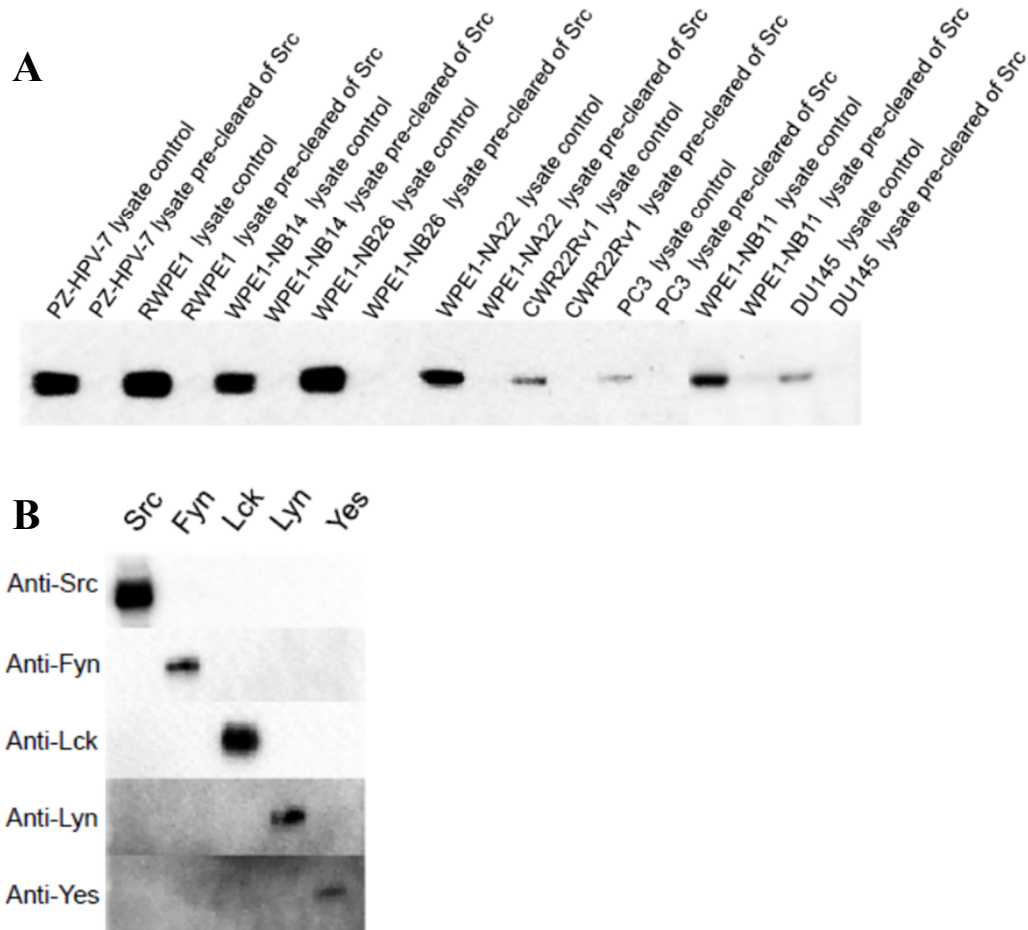


Figure 2.5 Immunodepletion of Src kinase from prostate cell lysates.

(A) Western blots of Src kinase in lysates with or without pre-clearance of Src. (B) The Src antibody used in immunodepletion displays no cross reactivity against other Src family kinases investigated. 2.4 μ g of purified Src family tyrosine kinase member was loaded into each lane and exposed to the Src antibody employed in the immunodepletion experiment as well as other antibodies specifically against the Src kinase family members.

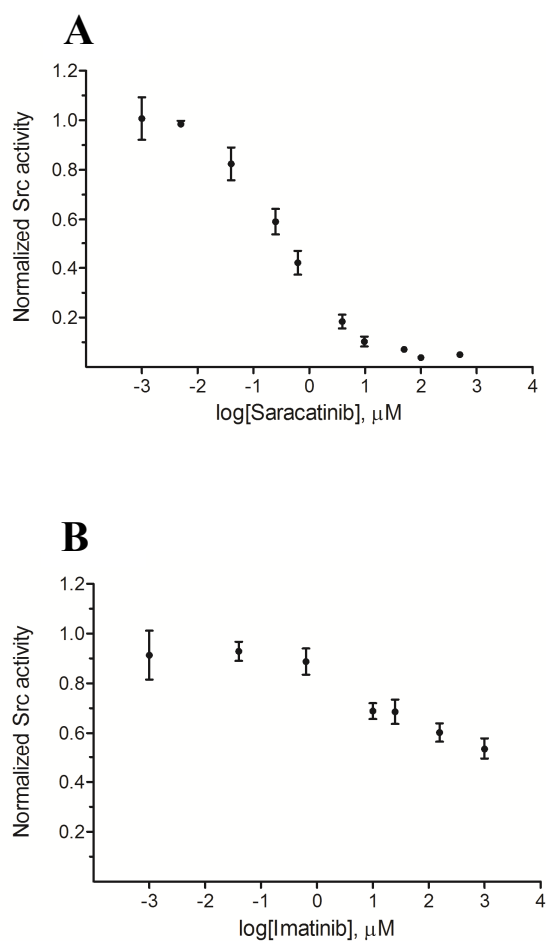


Figure 2.6 Src activity in DU145 lysates as a function of inhibitor concentration.

Normalized Src activity (where 1.0 is defined as activity in the absence of inhibitor) in DU145 lysates as a function of log [inhibitor] (μM). (A) Where inhibitor = saracatinib (AZD0530) and (B) where inhibitor = imatinib (Gleevec). All experiments were performed in triplicate. Error bars are showing SEM.

Src expression levels in prostate cell lines. Src activity is higher in non-aggressive cell lines and lower in aggressive cell lines (**Fig. 2.4**), which appears to be inconsistent with the general notion that Src plays a key role in carcinogenesis, metastasis, and the transition to the androgen-independent state. However, it occurred to us that total Src content may vary from one cell line to the next, which could dramatically alter the apparent and surprising conclusion that Src activity and CaP aggressiveness display an inverse relationship.

Src content was quantified by western blot analysis (**Fig. 2.7A**) and normalized relative to α -tubulin (**Fig. 2.7B**). We found that the invasive cell lines, as well as the androgen-independent cell line, display less Src than the corresponding non-invasive, androgen-dependent cell lines. With the data from **Fig. 2.7** in hand, we subsequently plotted “fractional Src activity” (i.e. total Src activity/total Src content) versus cell line “aggressiveness” (**Fig. 2.8**). The latter reveals a significant difference between fractional Src activity in normal versus aggressive (i.e. invasive or androgen-independent) cell lines ($p = 0.0015$).

Why is the total Src content greater in the PZ-HVP-7 and RWPE1 cell lines? One possible mechanism is the known sensitivity of activated Src, relative to its non-activated counterpart, to ubiquitin-mediated degradation (Hakak and Martin, 1999; Harris et al., 1999). Consequently, cell lines that are under intense activated Src pressure might, ironically, display lower Src content than less aggressive cells. In addition, two recent studies suggest a second mechanism by which Src levels are regulated. Majid *et al.* reported that the micro RNA (miR) miR-205 downregulates the expression of Src at both the mRNA and protein levels, thereby inhibiting Src-mediated signaling pathways (Majid

et al., 2011). Interestingly, Bhatnagar *et al.* have shown that the more invasive the prostate cell line the higher the miR-205 level (Bhatnagar et al., 2010).

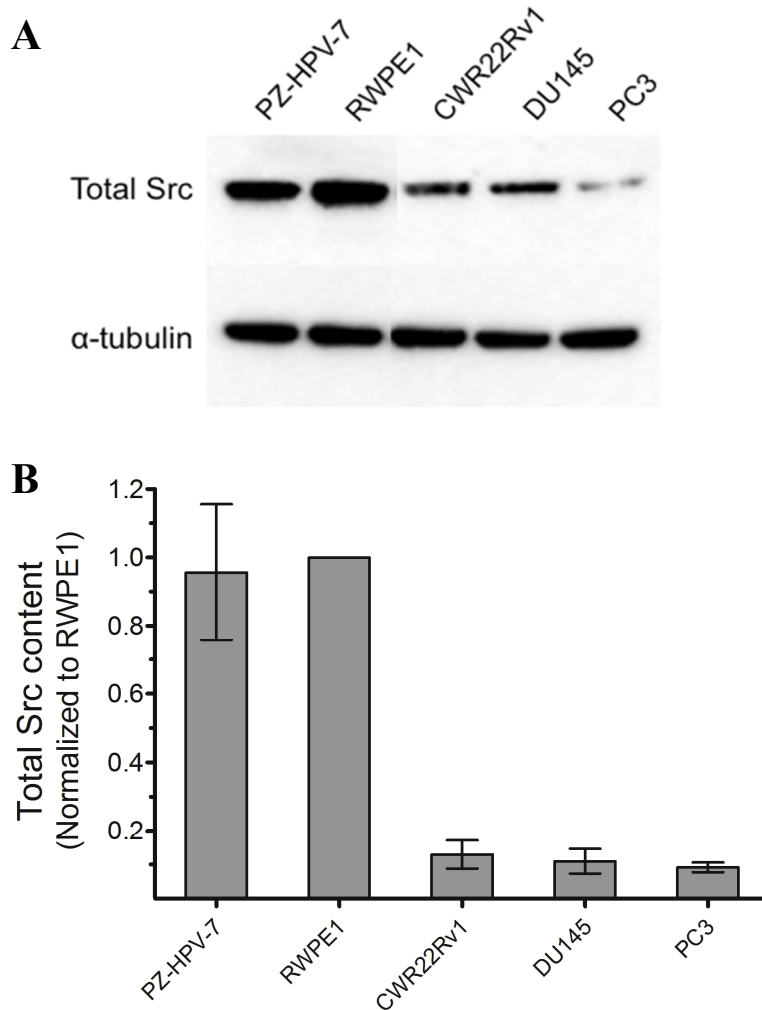


Figure 2.7 Src protein levels in PZ-HVP-7, RWPE1, DU145, PC3 and CWR22Rv1 prostate cell lines.

(A) Prostate cell lysates were probed for total Src, where α -tubulin was used as the loading control. (B) Intensities of each band from the Western blots were measured and normalized to the corresponding α -tubulin control, and then compared to cell line RWPE1 (RWPE1 as 1). All experiments were performed in triplicate. Error bars are showing SEM.

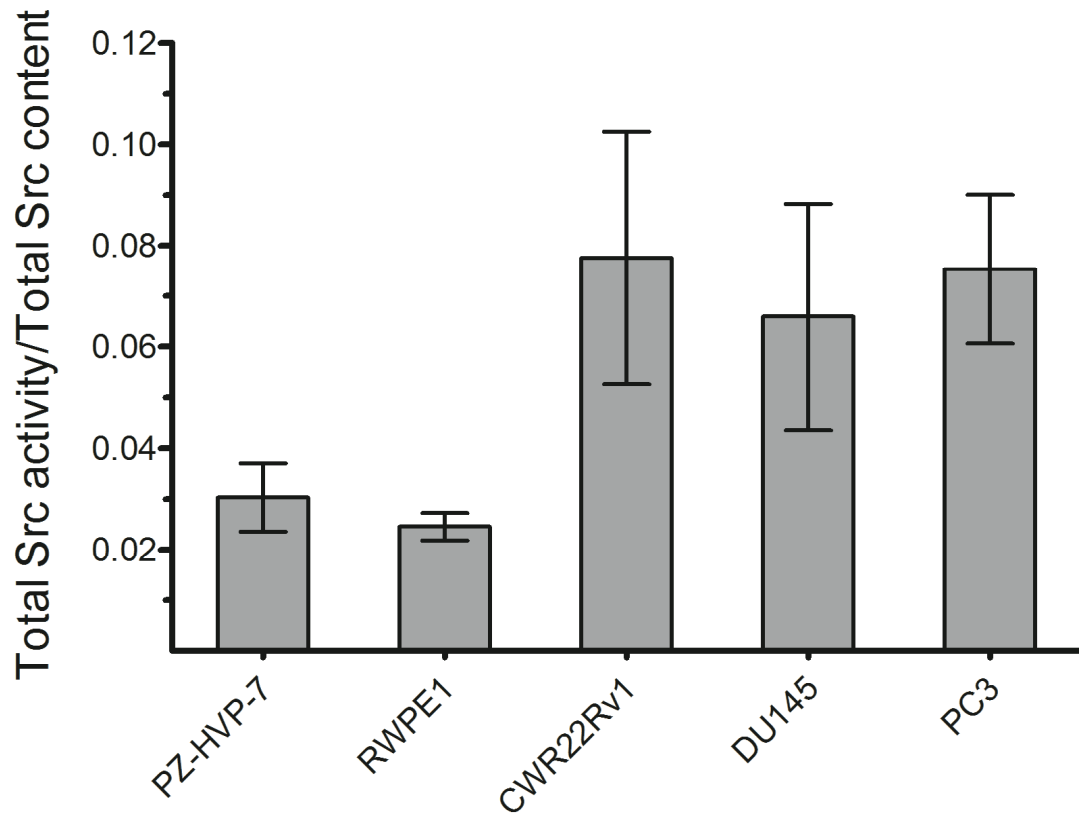


Figure 2.8 Fractional Src kinase activity in PZ-HVP-7, RWPE1, DU145, PC3 and CWR22Rv1 prostate cell lines.

Fractional Src kinase activity as assessed by measured Src activity (**Fig. 2.4**) divided total Src protein content (**Fig. 2.7**). All experiments were performed in triplicate. Error bars are showing SEM. The 1-tailed t-test comparison p-value of Src kinase activity in noninvasive (PZ-HPV-7, RWPE1) versus invasive/androgen-independent (DU145, PC3, CWR22Rv1) cell lines is 0.0015.

Src phosphorylation status in prostate cell lines. Evans and colleagues recently reported that the Src inhibitor AZD0530 is most effective against prostate cell lines that have the highest ratio of active-to-total Src (Chang et al., 2008). In the latter study, “active Src” was taken to be pTyr-416 Src. These investigators also reported that cells with the lowest (pTyr-416 Src/total Src) ratios express the most Src. We also measured the levels of pTyr-416 via Western blot analysis and plotted pTyr-416 Src/total Src (fractional pTyr-416) versus cell line aggressiveness. As is evident from **Fig. 2.9B**, a relationship analogous to that depicted in **Fig. 2.8** is apparent. These results allow us to conclude that pTyr-416 is a good indicator of catalytically active enzyme in prostate cell lines. Furthermore, the general observation that total Src content is lower in phenotypically aggressive prostate cell lines is consistent with the proteasomal and miR mechanisms described above.

We also examined what relationship, if any, exists between the level of pTyr-527 Src and cell line aggressiveness. A plot of the ratio of pTyr-527 Src/total Src (fractional pTyr-527) (**Fig. 2.9C**) versus cell lines reveals a pattern similar to that in **Figs. 2.8** and **2.9B**, namely aggressive cell lines display high “fractional Src activity” (**Fig. 2.8**), high fractional pTyr-416 content (**Fig. 2.9B**), and high fractional pTyr-527 content (**Fig. 2.9C**). Phosphorylation at Tyr-527 is considered to be inhibitory due to the formation of an intramolecular interaction that blocks Src kinase activity (Roskoski, 2005). However, as we’ve noted (*vide infra*), the pTyr-527 Src enzyme can be activated in the presence of phosphorylated peptides and proteins that disrupt the inhibitory interaction. In short, although pTyr-527 Src is inactive in purified form, the opposite appears to be true in cell

lysates. Consequently, we conclude that pTyr-527 Src levels are not a useful barometer of inactive Src and, rather, may actually be a more appropriate prognosticator of Src activity. A recent model of metastatic behavior known as “local excitation/global inhibition” poses the conjecture that aggressive tumor cells, relative to their non-aggressive counterparts, are able to generate highly localized bursts of signaling activity in response to growth factor gradients (Soon, 2007). However, our results suggest that a more apt description of aggressiveness may be the ability to globally recruit signaling enzymes to local pathways that drive the cancerous phenotype. This could have the consequence of depleting key enzymatic species from other pathways, a behavior that is consistent with the local excitation/global inhibition hypothesis. Under this scenario, the fraction of total potential signaling activity, as opposed to total activity alone, is a more meaningful measure of aggressiveness.

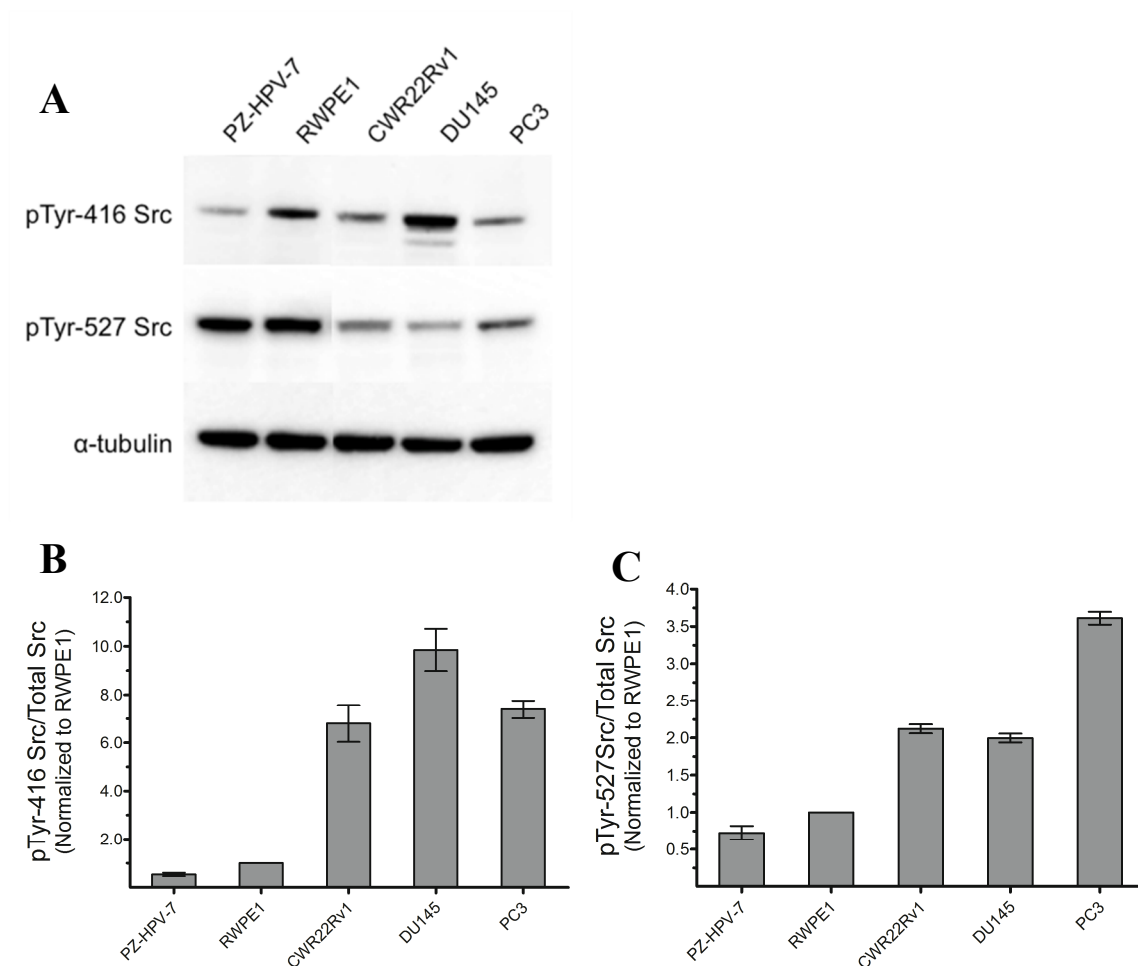


Figure 2.9 Phosphorylation status of Src in PZ-HVP-7, RWPE1, DU145, PC3 and CWR22Rv1 prostate cell lines.

(A) Prostate cell lysates were probed for Src pY416 and pY527 levels, where α -tubulin was used as the loading control. (B) pY416 levels were derived from the band intensities in the Western blots, normalized to the corresponding α -tubulin control, and then compared to cell line RWPE1 (RWPE1 as 1). (C) pY527 levels were derived from the band intensities in the western blots, normalized to the corresponding α -tubulin control, and then compared to cell line RWPE1 (RWPE1 as 1). All experiments were performed in triplicate. Error bars are showing SEM.

Src activity, expression and phosphorylation in prostate cancer progression model cell lines. In addition to the standard prostate cell lines evaluated in **Figs. 2.4 – 2.9**, we evaluated a series of N-methyl-N-nitrosourea cell lines derived from RWPE1. An advantage of these cell lines is that their relative invasiveness has been reported and displays the following order of increasing invasiveness: RWPE1, WPE1-NA22, WPE1-NB14, WPE1-NB11 and WPE1-NB26 (Webber et al., 2001). In this series of cell lines, we observed correlations analogous to those described above for Src kinase activity and aggressiveness (with the exception of WPE1-NB26). First, as we noted in **Fig. 2.4**, total Src activity decreases as a function of increasing cell line aggressiveness (**Fig. 2.10**; grey bars). Second, once background tyrosine activity is subtracted out, it is evident that the majority of observed peptide phosphorylation is due to Src (**Fig. 2.10**; white bars). Third, total Src content decreases as a function of cell line aggressiveness (**Fig. 2.11**). Fourth, fractional Src kinase activity (Src kinase activity/total Src content) increases as a function of increasing cell line aggressiveness (**Fig. 2.12**). Finally, and somewhat surprisingly, the correlation between pTyr-416 fractional levels (pTyr-416/total Src content) and cell line aggressiveness is weak, suggesting that it may be dangerous to solely rely on pTyr-416 content as a barometer of Src activity (**Fig. 2.13A**). However, we do observe a correlation, similar to that in **Fig. 2.9C**, with respect to fractional pTyr-527 content and cell line invasiveness (**Fig. 2.13B**). Curiously, one notable exception to the correlations observed for the WPE1 family is the NB26 line. The latter has received a significant amount of attention in the literature due to its highly aggressive behavior. Using total Src content and fractional Src activity as measures of aggressiveness, we would assign a non-invasive phenotype to WPE1-NB26 (i.e. similar to that of the parent cell line RWPE1). However,

since this is clearly incorrect, the invasiveness associated with this N-methyl-N-nitrosourea cell line might due to mechanisms that are independent of Src signaling.

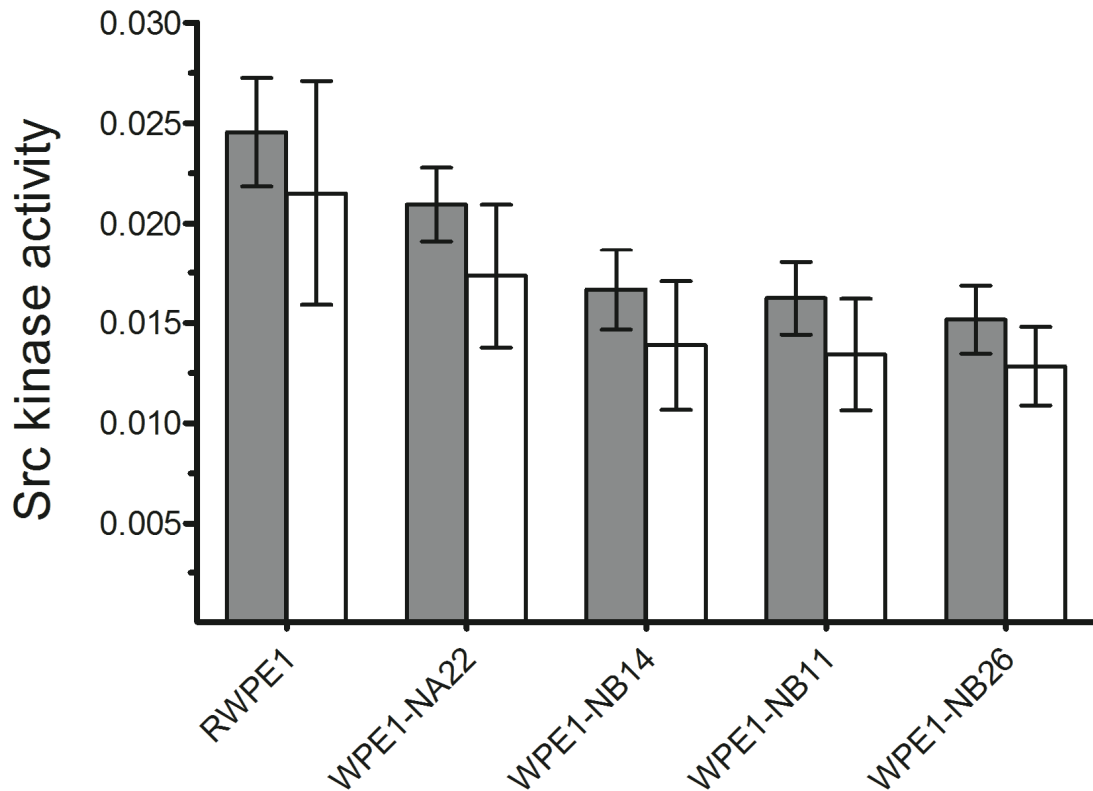


Figure 2.10 Total Src kinase activity in prostate cancer progression model cell lines.

Src-catalyzed phosphorylation rates in the RWPE1-derived cell lines WPE1-NA22, WPE1-NB14, WPE1-NB11, and WPE1-NB26 (increasing invasive ability as plotted along the x-axis). Grey bars are phosphorylation rates of Src sensor peptide **1** by whole cell lysates (normalized by total protein content). White bars are phosphorylation rates by cell lysates due to Src kinase alone after subtracting non-Src background phosphorylation of peptide **1**.

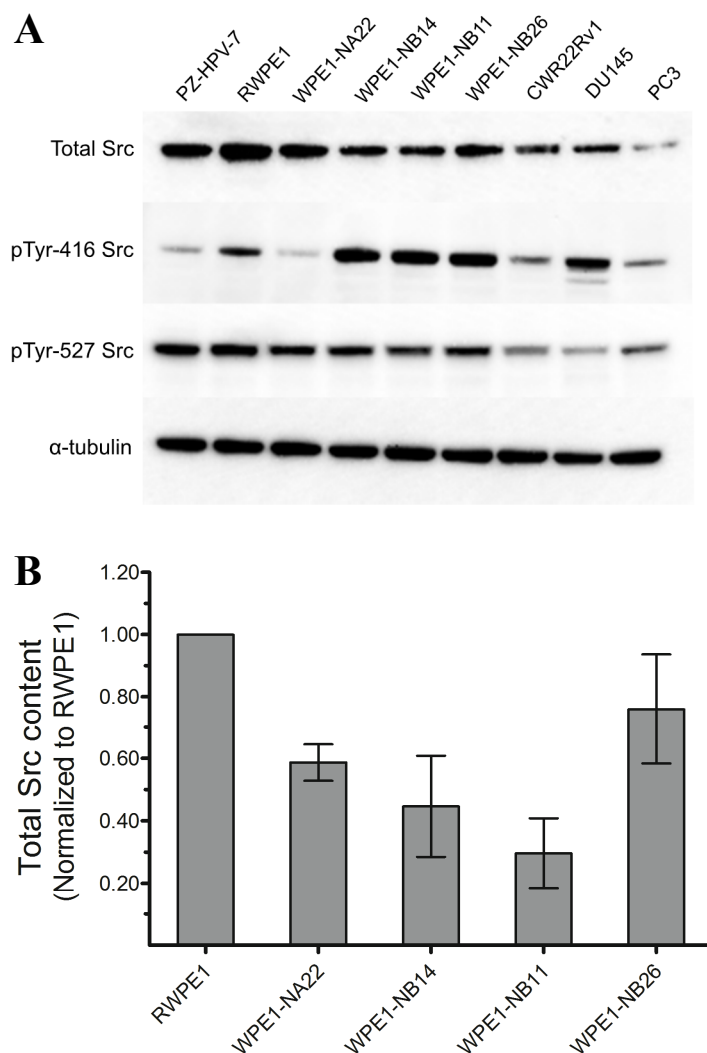


Figure 2.11 Src expression levels in all prostate cell lines tested.

(A) Prostate cell lysates were probed for total Src, pY416 Src and pY527 Src in all prostate cell lines tested, including the RWPE1-derived cell lines WPE1-NA22, WPE1-NB14, WPE1-NB11, and WPE1-NB26 (increasing invasive ability as plotted along the x-axis). α -tubulin was used as the loading control. (B) Intensities of total Src from the western blots for RWPE1-derived cell lines were measured and normalized to the corresponding α -tubulin control, and then compared to cell line RWPE1 (RWPE1 as 1). All experiments were performed in triplicate. Error bars are showing SEM.

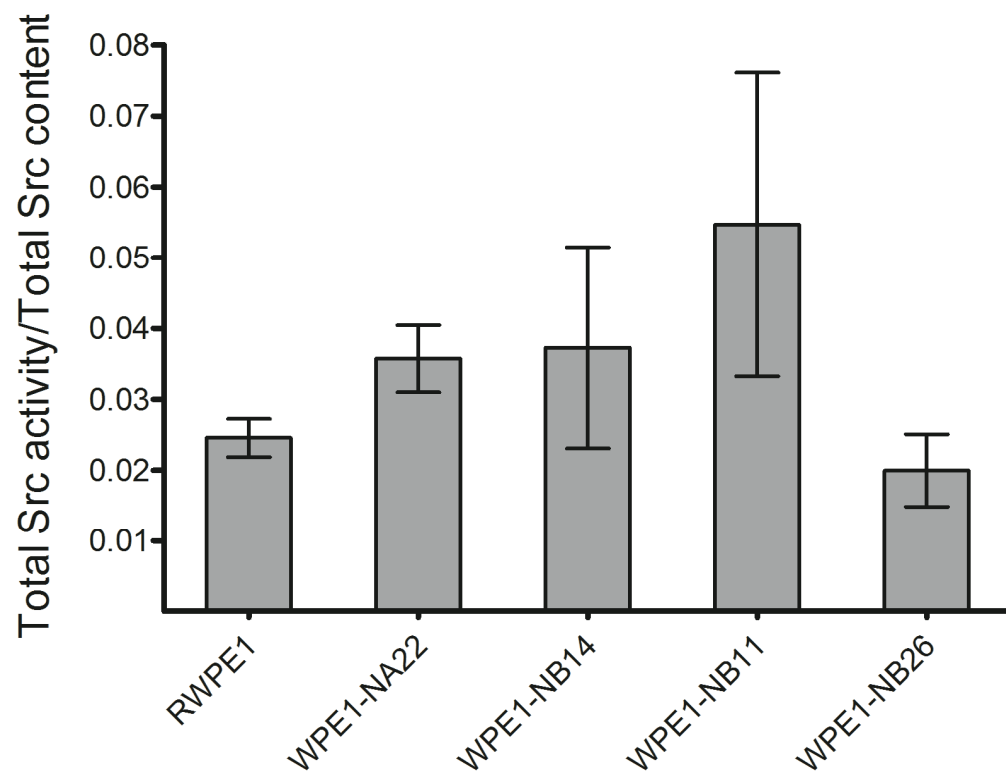


Figure 2.12 Fractional Src activity in prostate cancer progression model cell lines.

Fractional Src kinase activity was assessed by measured total Src activity (**Fig. 2.10**) divided total Src protein content (**Fig. 2.11B**).

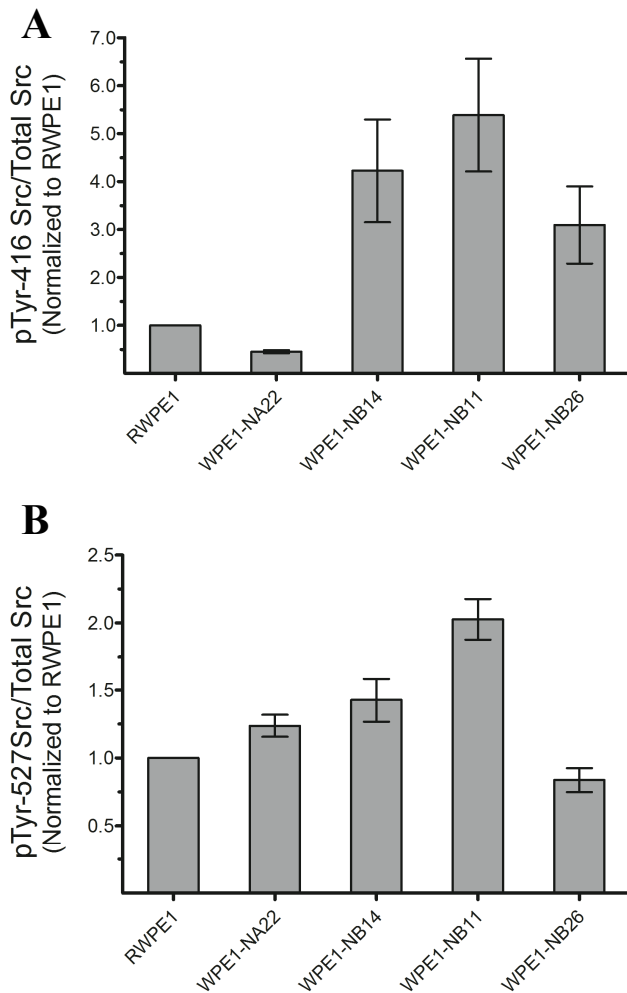


Figure 2.13 Phosphorylation of Src in prostate cancer progression model cell lines.

(A) pY416 levels of RWPE1-derived cell lines WPE1-NA22, WPE1-NB14, WPE1-NB11, and WPE1-NB26 (increasing invasive ability as plotted along the x-axis) were derived from the band intensities in the western blots (**Fig. 2.11A**), normalized to the corresponding α -tubulin control, and then compared to cell line RWPE1 (RWPE1 as 1).

(B) pY527 levels were derived from the band intensities in the western blots (**Fig. 2.11A**), normalized to the corresponding α -tubulin control, and then compared to cell line RWPE1 (RWPE1 as 1). All experiments were performed in triplicate. Error bars are showing SEM.

Assessment of cell line invasiveness. We wanted to quantitatively compare the invasiveness of all nine cell lines and determine if we can correlate invasiveness with fractional Src activity or Src phosphorylation levels. As control, we used RWPE1, WPE1-NA22, WPE1-NB14 WPE1-NB11, WPE1-NB26 and DU145 cell lines where invasiveness was already quantified (Webber et al., 2001). To determine invasiveness we used the BD tumor invasion system that contains a fluorescent light blocking membrane and Matrigel, which mimics the basement membrane. The cells were labeled with cell permeable dye and the number of cells invaded through the Matrigel quantified by fluorescence (experimental details are described in **Matrigel invasion assay** section). The percentage of total cells invaded was used as a quantitative measurement of cell line invasiveness. As shown in **Fig. 2.14**, the invasiveness measured in our experiment has variance to what was published in the literature, especially for WPE1-NA22 and WPE1-NB26 cell lines. We suspect that this is because the chemo-attractant used in our experiment is the standard cell culture medium, whereas in the previous studies, NIH/3T3 cell conditioned medium was used, which contains a variety of growth factors that might not be present in the standard culture medium (Shaw, 2005), and therefore has a different effect on cell invasion. What is interesting to note is that the invasiveness measured in our experiment seems to correlate with the pTyr-416 level of Src in RWPE1 derived cell lines (**Fig 2.13A**). However, whether there is a direct relationship between pY416-Src and invasiveness requires further determination.

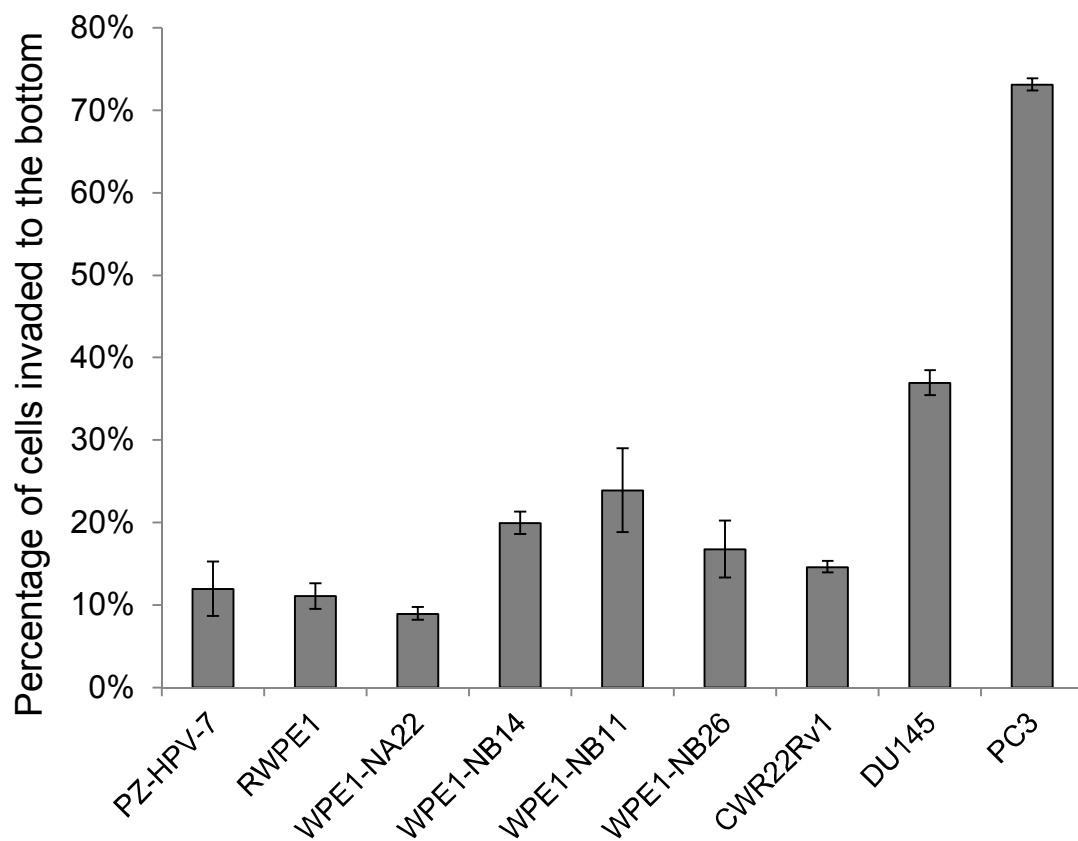


Figure 2.14 Invasiveness of prostate cell lines assessed by Matrigel invasion assay.

Cell invasion assay was performed using BD Biocoat tumor invasion system. The cells were counted by fluorescence reading after calcein AM labeling. Invasiveness is presented by the percentage of total cells that have invaded through Matrigel to the bottom chamber. All experiments were performed in triplicate. Error bars are showing SEM.

Assessment of Src activity in single prostate cells. An array of protein kinase assays has been described, including radioactive, colorimetric, and fluorescent methods (Braunwaler et al., 1996; Rijksen et al., 1996; Ting et al., 2001; Wang et al., 2005, 2006b, 2006c, 2010b; Rothman et al., 2005; Wang and Lawrence, 2005; Lawrence and Wang, 2007; Sharma et al., 2008; Li et al., 2008b; Uri et al., 2010; Newman et al., 2011). The majority of them are only appropriate for use with pure enzyme. However, a few fluorescent peptide- and GFP-based strategies have found applications in cell lysates and single cells (Wang et al., 2005; Gulyani et al., 2011). Unfortunately, the fluorescent changes displayed in single cells are typically modest, thereby requiring sophisticated and detailed one-cell-at-a-time microscopic inspection, including adjustments for photobleaching, assignment of the region of analysis, and adjustments for cell-to-cell differences in imaging parameters. By contrast, CE is not dependent upon a substrate-to-product fluorescence change, nor does this extraordinarily sensitive method require labor-intensive single cell analysis. As a consequence, CE can potentially be employed in an automated fashion, a significant advantage in a clinical setting where the operator's level of expertise is not necessarily state-of-the-art. With these potential benefits in mind, we investigated whether the CE assay described in this study could be applied to single cells.

The Src substrate peptide **1** was microinjected into DU145 cells, incubated for 2 min, each cell individually lysed with a focused Nd:YAG laser (Sims et al., 1998), the lysate immediately loaded onto the capillary via electrokinetic injection, and electrophoresed. In all DU145 samples containing peptide **1**, the corresponding phosphopeptide (peptide **2**) was observed ($14 \pm 2\%$). By contrast, no phosphorylation of peptide **1** was observed in DU145 cells pre-incubated with the potent Src inhibitor

AZD0530 (1 μ M). An analogous set of studies were performed in the presence of imatinib (1 μ M), a poor Src inhibitor. The level of phosphorylation ($15 \pm 3\%$) is essentially identical to that found in DU145 cells that had not been treated with inhibitor (**Fig. 2.15**). These studies confirm that evaluating Src activity at the single cell level is feasible and consistent with the experiments performed with lysates from large cell populations.

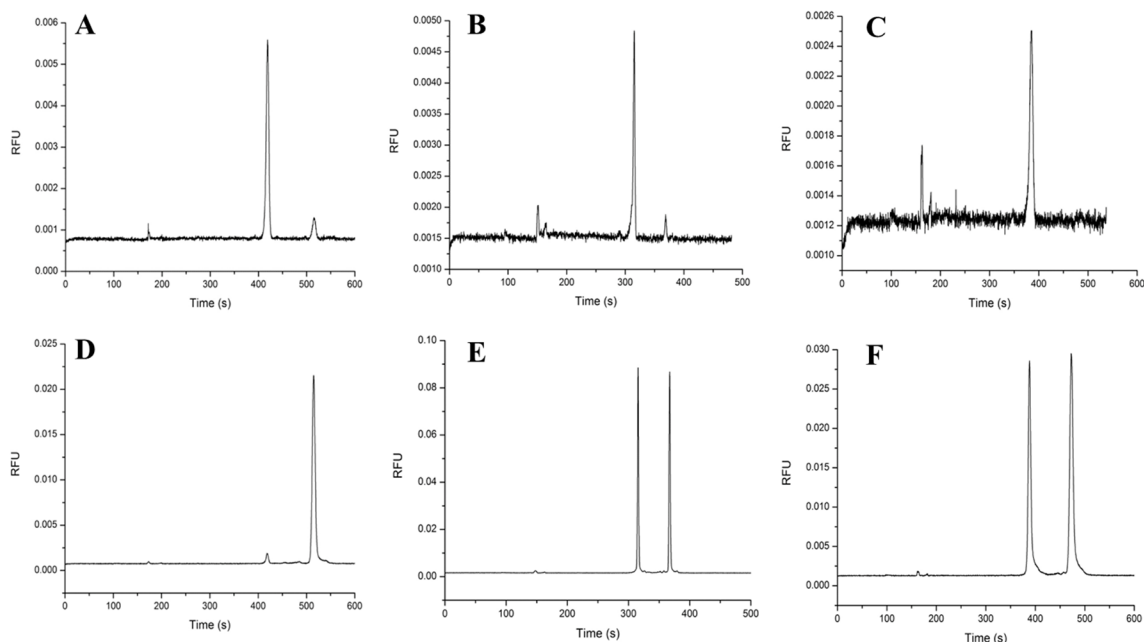


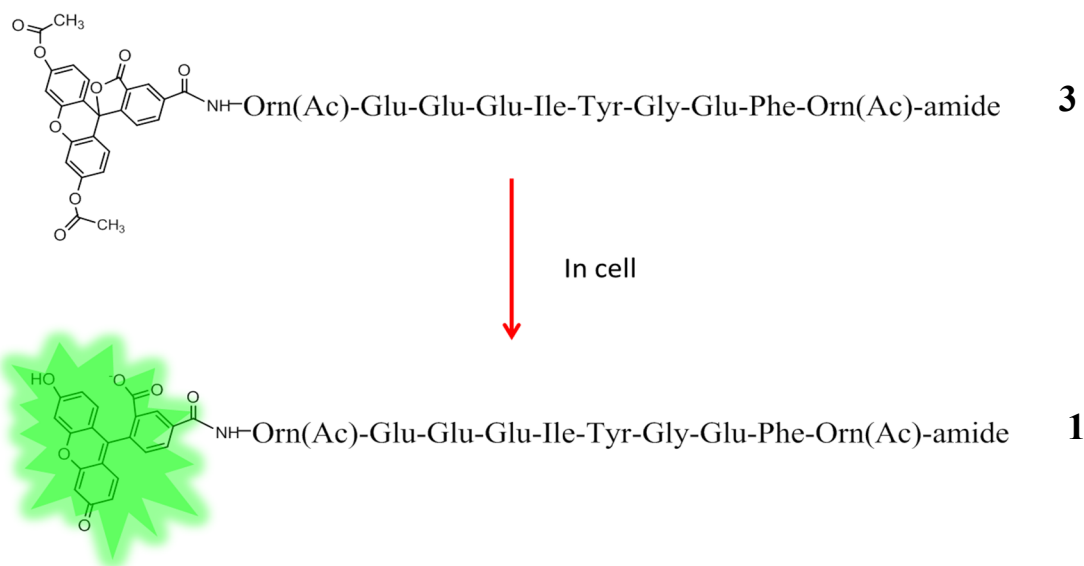
Figure 2.15 Single cell analysis of Src kinase activity in DU145 cells by CE.

(A) Cells exposed to standard media, (B) standard media and imatinib (1 μ M), and (C) standard media and AZD0530 (1 μ M). All cells were subsequently microinjected with peptide **1**, incubated for 2 min, lysed, injected into the capillary and electrophoresed. Electropherograms of (A), (B), and (C) are representative of results where $n = 5$ for each experiment. The small peak at 160 s is a component present in the media. Src substrate peptide **1** is the large peak observed approximately 100 s prior to that of the corresponding phosphopeptide. Control for (A): (D) lysate from cells exposed to standard media, microinjected with peptide **1** and incubated for 2min, then spiked with phospho standard peptide **2**; control for (B): (E) lysate from cells exposed to standard media spiked with peptide **1** and peptide **2**; control for (C): (F) lysate from cells exposed to standard media spiked with peptide **1** and peptide **2**. Controls were run either immediately prior to or following the corresponding experiments in (A), (B), and (C).

Developing cell permeable Src sensor. Although microinjection has proven successful in analyzing Src kinase activity in single cells, this technique is labor intensive and requires skilled practitioners. For routine diagnosis, a simple procedure that can be performed in a fast and automatic fashion is necessary. Therefore, we wanted to render the peptide kinase sensor cell permeable. Cellular delivery of peptides has always been a challenge for application of bioactive peptides for therapeutics and diagnosis. Many protein/peptide delivery reagents have been developed and are commercially available, such as Influx™ pinocytic cell-loading reagent (Invitrogen), Chariot™ protein delivery reagent (Active Motif) and BioPORTER® QuikEase™ protein delivery kit (Sigma Aldrich). However, the efficiency of these reagents is highly dependent on cell types and cargo properties. Moreover, materials from the delivery reagents are also introduced into cells, which might cause unwanted cellular responses. Peptide delivery has also been achieved by attaching long alkyl chains (Xie et al., 2003; Carrigan and Imperiali, 2005; Nelson et al., 2007). The disadvantages of this strategy are that additional amino acids need to be introduced into the peptide sequence for alkyl chain attachment, and the lipophilic alkyl chain is likely to raise problems in synthesis, purification and solubility.

We have discovered a novel way of synthesizing cell permeabilizing peptides, as described in **Chapter 3**. This strategy, in which the N-terminal carboxyfluorescein (FAM) on Src sensor peptide **1** is replaced with carboxyfluorescein diacetate (CFDA), is particularly suitable for this project, since no additional moieties are introduced into the original peptide chain or to the cells. Cellular hydrolysis of CFDA will result in the original FAM labeled Src sensor (**Scheme 2.1**).

The CFDA labeled Src sensor peptide **3** was prepared by reacting the free N-terminal amine containing peptide with CFDA-SE and purified by HPLC (details are described in **Peptide synthesis** section). Four prostate cell lines, DU145, PC3, RWPE1 and WPE1-NB26, were tested for the cell permeability of peptide **3**. As shown in **Fig. 2.16**, after incubating with peptide **3** for 30 min, all cell lines exhibited green fluorescence signal, indicating uptake and hydrolysis of peptide **3**. However, different fluorescence intensities were observed, which is probably due to varied uptake efficiencies by different cell types. To demonstrate that cellular uptake is facilitated by the CFDA moiety, the parent peptide **1** (labeled with FAM) was also incubated with the cells. As expected, none of the live cells showed fluorescence signals. These results, together with results from **Chapter 3**, indicate that labeling peptides with CFDA group could provide a new way of delivering peptides into cells, and at the same time, provide fluorescent molecules that can be used for fluorescent assays and microscopy studies. We do note that, however, in both studies punctate patterns were observed in cells. Additional studies are needed to identify and hopefully eliminate the punctate pattern. Moreover, optimization and more systematic studies are necessary to test the feasibility of this strategy for different peptide sequences and other cell types.



Scheme 2.1 The design of cell permeable Src sensor peptide 3.

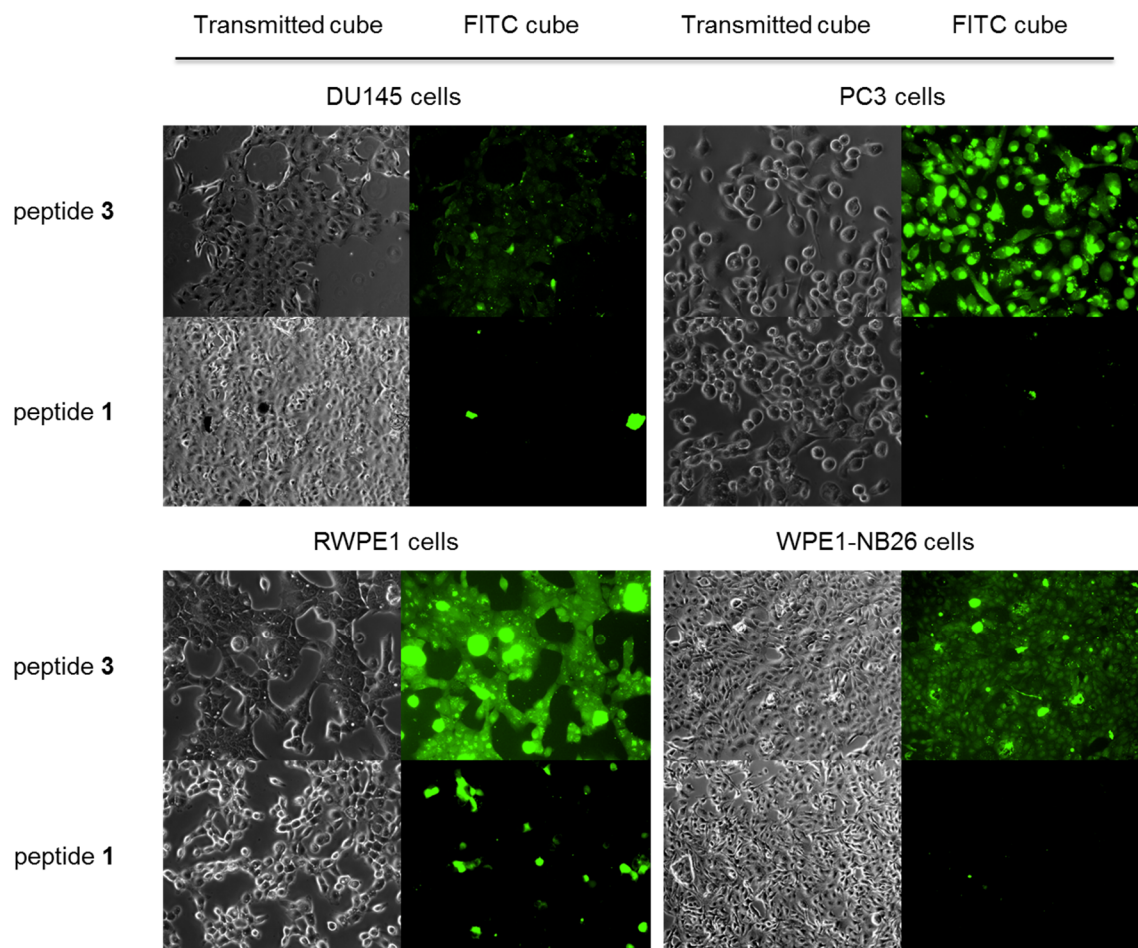


Figure 2.16 Uptake of peptide 3 by prostate cells.

Prostate cell lines DU145, PC3, RWPE1 and WPE1-NB26 were incubated with 5 μ M peptide 1 or peptide 3 in ECB buffer for 30 min. Transmitted light images and fluorescein fluorescence images were taken using an inverted Olympus IX81 microscope with transmitted light and FITC filter cube.

Simultaneous measurement of Src and Akt kinase activities. Carcinogenesis, metastasis, and the transition to the androgen independent phenotype are all complex phenomena that are mediated by the interplay of a host of signaling pathways that are themselves driven by an array of protein kinases. Therefore, the ability to measure the catalytic activity of multiple protein kinases should be useful in this regard. In addition, the profiling of multiple protein kinases could prove helpful in cancer diagnosis as well as in the design of therapeutic strategies (Wang et al., 2010b). Indeed, several kinases, including Akt, S6K and Ack have been strongly implicated as potential markers for CaP. Given the extraordinary sensitivity and resolving power of CE, it should be feasible to simultaneously monitor an array of protein kinases.

Akt is a serine/threonine kinase family that includes three closely related members, Akt1, Akt2 and Akt3 (also known as PKB α , PKB β and PKB γ , respectively). Dysregulation of Akt expression and activation has been linked to many human diseases, including prostate cancer (Ayala et al., 2004; Li et al., 2005). Akt is activated via phosphorylation on two residues: serine 473 (S473) is located in a hydrophobic motif and is phosphorylated by the rictor-mTOR complex (Sarbasov et al., 2005); threonine 308 (T308) is located in the activation loop and is phosphorylated by phosphoinositide-dependent kinase 1 (PDK1) (Alessi et al., 1997). Although S473 phosphorylation has been widely used to indicate Akt activity, studies by Vincent *et al.* have shown that pT308, but not pS473, correlates with Akt kinase activity in human non-small cell lung cancer (Vincent et al., 2011). Moreover, varied relationships exist between Akt activation status (phosphorylation level) and downstream substrate phosphorylation levels (Luo et

al., 2005). Therefore, an Akt activity sensor would prove useful in accurately assessing Akt activity and the relationship with prostate cancer progression.

Proctor *et al.* have synthesized an Akt kinase sensor (peptide **4**), 6FAM-GRPRAATFAEG-amide (manuscript in preparation). As shown in **Fig. 2.17**, due to the difference in charge to mass ratio with the Src kinase sensor, both the Akt sensor (peptide **4**) and the synthetic phosphorylated counterpart (peptide **5**) migrate differently on CE electropherogram than the Src sensor peptide **1** and peptide **2** under the same separation conditions (separation buffer: 100 mM Borate, 100 mM SDS at pH 7.4, separated at 25 °C using a constant voltage of 12 kV). Peptide **4** emerges at 380 s, peptide **5** emerges at 180 s, whereas peptide **1** appears at 220 s and peptide **2** appears at 260 s. The non-overlapping peak migration time allows us to investigate phosphorylation of peptide **1** and peptide **4** simultaneously.

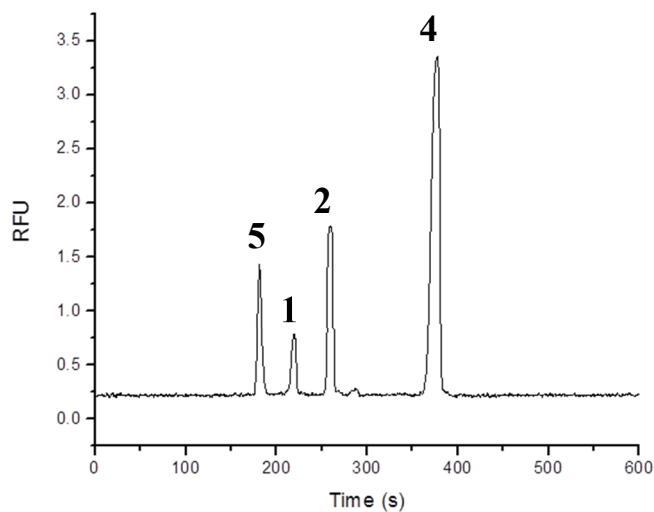


Figure 2.17 CE-LIF separation and visualization of Src sensor and Akt sensor.

The Src kinase sensor (peptide **1**, 220 s), phosphorylated counterpart (peptide **2**, 260 s), Akt kinase sensor (peptide **4**, 380 s) and phosphorylated counterpart (peptide **5**, 180 s) were separated under the same CE conditions. (RFU = relative fluorescence units)

Pure Akt1 (PKB α) kinase and Src kinase were employed to determine selectivity of peptide **1** and peptide **4** for these two enzymes. As shown in **Fig. 2.18**, Akt1 selectively phosphorylated its substrate peptide **4**, and Src selectively phosphorylated peptide **1**. No cross-reactivity was observed. This is expected since Akt is a serine/threonine kinase whereas Src is a tyrosine kinase. It is interesting to note that when both Src and Akt kinases were present, the phosphorylation rate of Akt substrate was significantly faster than when only Akt kinase was present, indicating an elevation in Akt activity (**Fig. 2.18C and D**). We suspect that the Akt kinase (a recombinant human Akt1 with S473D mutation expressed in Sf21 insect cells, purified and activated by PDK1, purchased from Millipore) is not in a fully active form, which contains unphosphorylated tyrosine residues, and when incubated with active Src in an ATP containing assay buffer, the tyrosine residues on Akt1 became phosphorylated by Src and results in elevated activity. Indeed, Src is known to phosphorylate tyrosine residues Tyr-315 and Tyr-326 on Akt both in vitro and in vivo and increase Akt activity (Chen et al., 2001a). Therefore, our results supported the model that Akt activity is not only regulated by serine/threonine phosphorylation, but by tyrosine phosphorylation as well.

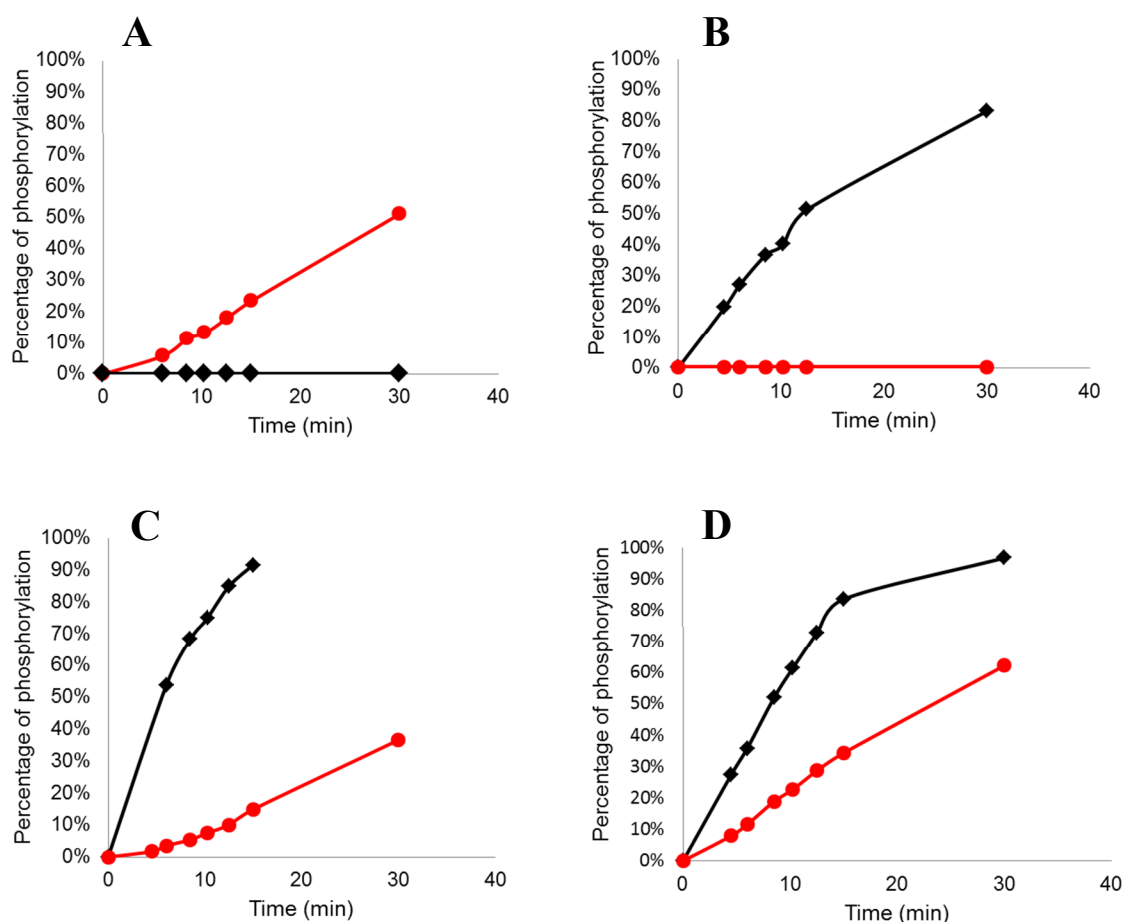


Figure 2.18 Kinase-catalyzed phosphorylation of Src and Akt sensors as a function of time as assessed by CE-LIF.

Red dots: Akt sensor peptide 4 phosphorylation; Black squares: Src sensor peptide 1 phosphorylation. (A) Both peptide 1 and peptide 4 were incubated with Akt kinase, and only peptide 4 was phosphorylated. (B) Both peptide 1 and peptide 4 were incubated with Src kinase, and only Src substrate peptide 1 was phosphorylated. (C) Peptide 1 was incubated with Src kinase, peptide 4 was incubated with Akt kinase. Both sensors were phosphorylated by their kinase. (D) Both peptide 1 and peptide 4 were phosphorylated when incubated with Src kinase and Akt kinase together.

Measure of Akt activity in prostate cell lysates. Akt activation (high S473 phosphorylation level) has been shown to play an important role in the progression of prostate cancer to the androgen-independent state using prostate tumor cell lines (Ghosh et al., 2003). However, due to the complex relationship between Akt serine/threonine/tyrosine phosphorylation levels and enzymatic activity, we wanted to use the Akt sensor to directly measure Akt activity in prostate cells.

Our initial study focused on aggressive prostate cancer cell lines DU145 and PC3. Constitutively active Akt is suggested in both cell lines, and the DU145 cell line is believed to contain higher amount of active Akt than PC3 cell line (Chen et al., 2001b). The cell lysates were prepared using M-PER protein extraction reagent and 5X Halt protease and phosphatase inhibitor cocktail. After incubating peptides **1** and **4** with either DU145 or PC3 cell lysates for 10 min, several peaks that correspond to peptidase degradation of peptide **4** appeared on the CE electropherogram and no (or very little) phosphorylation of peptide **4** was observed (**Fig. 2.19**). The fast degradation of peptide **4** has been previously observed by Proctor *et al.* in HeLa cell lysates without protease inhibitors. However, even in the presence of high concentrations of protease inhibitors, degradation of peptide **4** can not be prevented in DU145 or PC3 cell lysates. To overcome the degradation issue, Proctor *et al.* have identified the peptidase cleavage sites on peptide **4** and designed a more stable Akt substrate by replacing cleavage site amino acids with cleavage resistant or unnatural amino acids. The new stable Akt kinase sensor (peptide **6**), 6FAM-GRP-MeArg-AFTFAEG retained its substrate property. Therefore, we tested the stability and phosphorylation of peptide **6** in prostate cell lysate. However, although degradation peaks were successfully eliminated, no phosphorylation was

observed. We suspect that Akt became quickly degraded or dephosphorylated when lysing the cells. Therefore, we tried several strategies: higher concentration (20X) of protease and phosphatase inhibitor cocktail, a different cell lysis buffer [1X RIPA buffer (Millipore) with 50 mM sodium fluoride, 40 mM β -glycerophosphate, 1 mM benzamidine and 0.5 mM phenylmethanesulfonyl fluoride, adapted from the studies by Bozinovski *et al.* (Bozinovski et al., 2002)], stimulation of PC3 cells with EGF or IGF-1, and different cell lines (293T, Jurkat) known to have activated Akt. Unfortunately, none of these methods generated cell lysate that can phosphorylate Akt substrate **6**.

With assistance from Dr. Lee Graves, we performed an Akt kinase assay using radio-labeled ATP. The results are shown in **Fig. 2.20**. The same concentration of active Akt1 kinase was spiked into (1) cell lysis buffer, (2) kinase buffer (80 mM MOPS, 2 mM EDTA, 40 mM MgCl_2 , pH 7.0), (3) cell lysate [RWPE1 cells lysed in cell lysis buffer in (1)], (4) cell lysate with high concentration of serine-threonine phosphatase inhibitor β -glycerophosphate (BGP) or (5) cell lysate from (3) that has been heat inactivated for 10 min. Interestingly, after incubating Akt substrate (**peptide 6**) with the active kinase spiked assay solutions, we observed different kinase activities. The highest Akt kinase activity was observed in the kinase buffer, whereas the cell lysis buffer inhibited Akt activity to nearly 50%. From these results, we suspect that some components in the cell lysis buffer inhibit Akt activity. There is almost no Akt activity in cell lysate, and even heat inactivation of the cell lysate did not prevent a reduction in Akt activity. Initially we suspect that Akt was dephosphorylated in cell lysate, therefore we used a high concentration of serine-threonine phosphatase inhibitor BGP to prevent the spiked active Akt from dephosphorylation. However, BGP seems to have a negative effect on Akt

activity. Furthermore, the inability to recover Akt activity from heat inactivated cell lysate suggests that there may be small molecules or short peptides in the cell lysate that inhibit Akt activity.

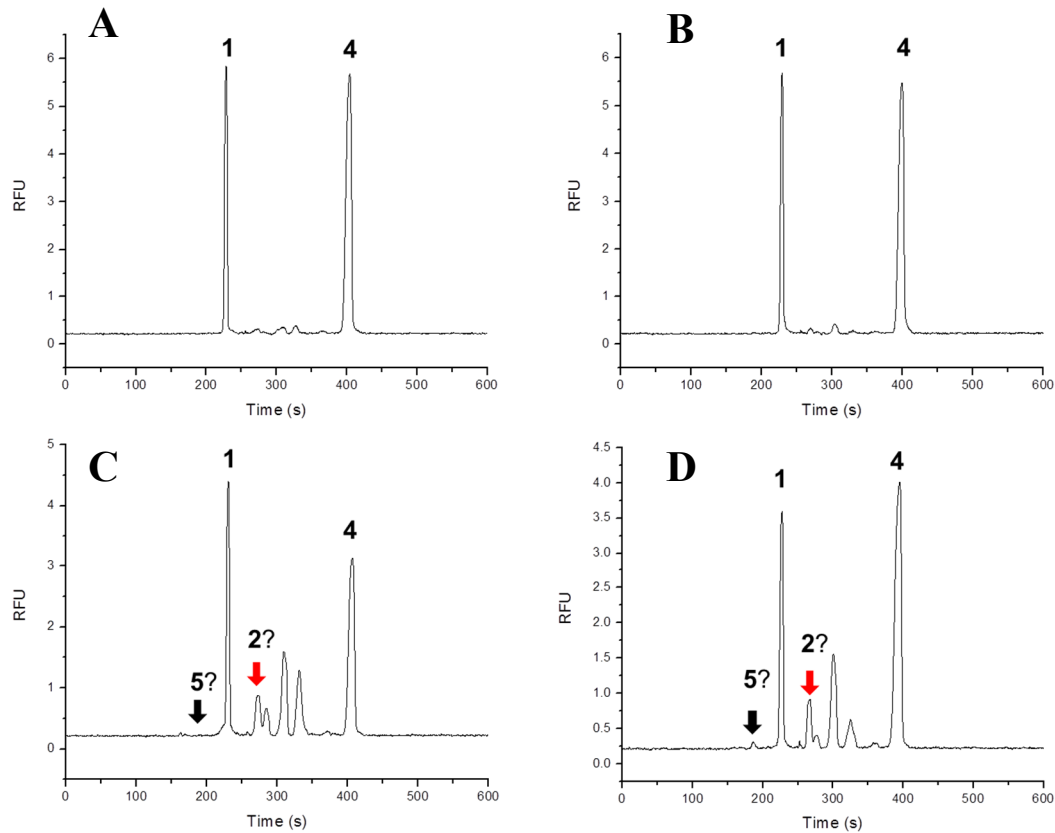


Figure 2.19 Phosphorylation and degradation of Src and Akt sensors in cell lysates.

(A) Peptide **4** and peptide **1** incubated in DU145 cell lysate for 1 min. (B) Peptide **4** and peptide **1** incubated in PC3 cell lysate for 1 min. (C) Peptide **4** and peptide **1** incubated in DU145 cell lysate for 10 min. (D) Peptide **4** and peptide **1** incubated in PC3 cell lysate for 10 min. Red arrow is where phosphorylated Src substrate (peptide **2**) should appear. However, the peak is possibly overlaid with a degradation peak from peptide **4**. Black arrow is where phosphorylated Akt sensor **5** should appear. The tiny peak in (D) is possibly peptide **5** or a degradation peak.

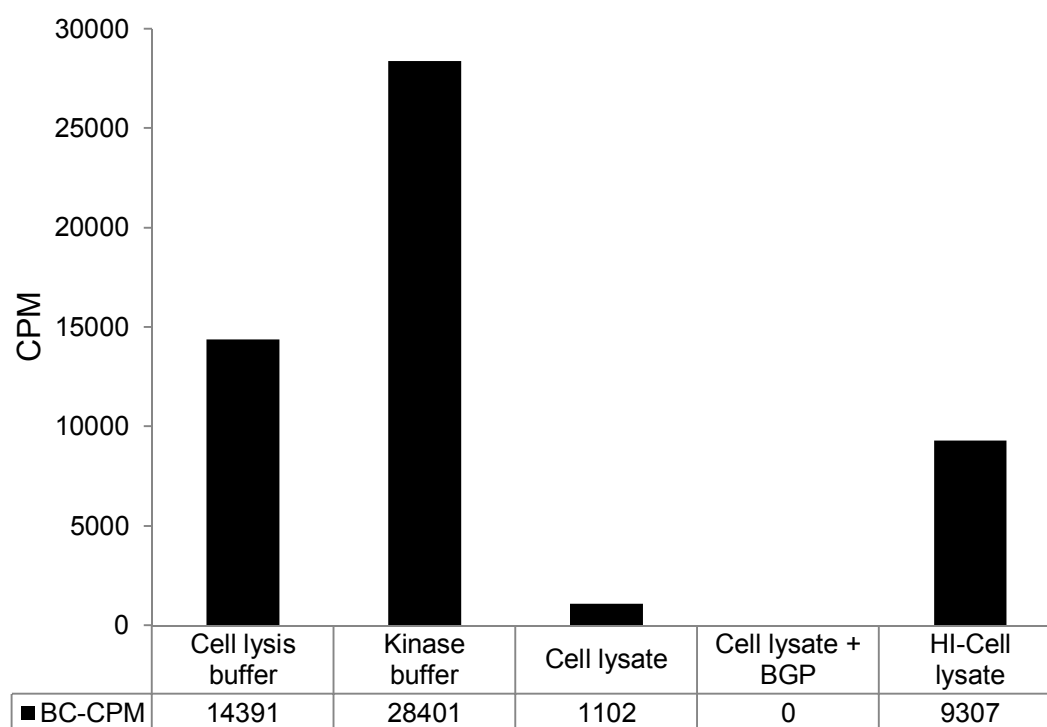


Figure 2.20 Radiolabeled ATP kinase assay.

Akt activity was measured using radiolabeled ATP assay as described in the **Akt kinase assay using radiolabeled ATP** section.

CPM = counts per minute

BC-CPM = background corrected counts per minute

Simultaneous measurement of Src and EGFR kinase activities. In addition to prostate cancer, Src kinase has also been implicated in tumor progression in other types of cancer. Src plays an important role in receptor tyrosine kinase (RTK) mediated signaling response by physically interacting with activated RTKs, serving both as a substrate and an activator to positively regulate RTK signaling (Guarino, 2009). One of the most widely studied RTKs is epidermal growth factor receptor (EGFR). Overexpression of EGFR has been indicated in ~60% cases of breast and other types of cancers, and correlates with poor patient outcomes. Studies have shown that overexpression of both EGFR and Src leads to enhanced cell migratory and invasive behavior (Dimri et al., 2007). Several small molecule inhibitors (e.g., gefitinib and erlotinib) that block EGFR enzymatic activity are currently under clinical trials. However, none of the inhibitors gave a complete response rate (Sheng and Liu, 2011). Indeed, cancer cell survival has been linked with the kinase-independent roles of EGFR (Weihua et al., 2008). Therefore, the ability to measure EGFR kinase activity, and determine the correlation between kinase activities and cancer progression will provide important information for both diagnosis and therapeutics.

Phillips *et al.* have designed and synthesized an EGFR activity sensor (peptide 7), 6FAM-EELEDDYEDDNleEE for CE analysis. They have demonstrated that peptide 7 is stable in cell lysate as well as in living cells, and can be efficiently phosphorylated in A431 cells, which contain a high level of EGFR activity. Because of the synergistic roles EGFR and Src play in cancer progression, we reasoned that it would be useful to simultaneously monitor Src and EGFR kinase activity in cancer cells. Because EGFR and Src are both tyrosine kinases and share some substrate similarities, we wanted to first

determine if the two kinase substrates (peptide **1** and **7**) are selective for their targets. As shown in **Fig. 2.21**, both kinases are able to phosphorylate their substrate efficiently. However, when incubated with active EGFR kinase, Src substrate **1** is also quickly phosphorylated. Fortunately, no EGFR activity was detected by EGFR substrate **7** in prostate cell lines PZ-HPV-7, DU145 and PC3. However, we expect that the poor selectivity of peptide **1** between Src and EGFR will make it difficult to assess individual kinase activity in cancer cells with upregulated EGFR. Therefore, we decided to make a small library of Src kinase sensors and screen for a more selective Src substrate sequence.

The library was designed based on the relative amino acid selectivity of Src and Lck kinase substrate and EGFR kinase substrate in a study published by Cantley and co-workers. They showed that Src prefers hydrophobic amino acid Ile (I) or Val (V) at the Y-1 position, whereas EGFR prefers negatively charged Glu (E) or Asp (D) at this position. Both kinases prefer E or D at the Y-2 position, but Src can also accommodate Gly (G). At the Y+2 position, E is the preferred amino acid for both substrates, however, the Src kinase family member Lck can accommodate Val (V) (Songyang et al., 1995). Based on these findings, we rationally designed and synthesized peptides **9-14** (**Table 2.2**). Phosphorylation of these peptides by EGFR or by Src kinase was examined and compared with peptide **1**. We found that all the peptides (**1** and **9-14**) were phosphorylated at a similar rate by Src kinase. In contrast, peptides **9-14** exhibited a slower phosphorylation rate than peptide **1** when incubated with EGFR kinase. The lead compound from this library is peptide **14**, which exhibits the highest selectivity for Src over EGFR. We have also examined the stability of peptide **14** in HeLa and A431 cell lysates prepared without any protease inhibitors, and no degradation peaks were observed.

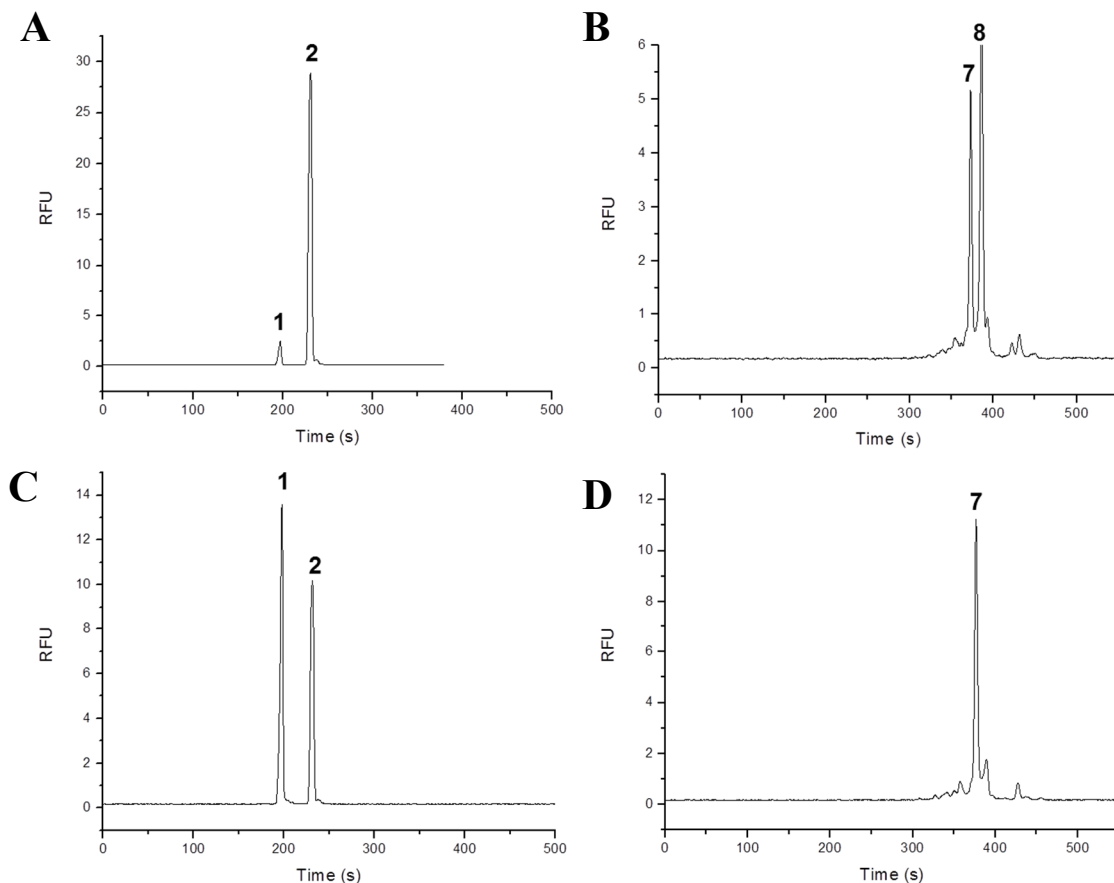


Figure 2.21 Phosphorylation of Src sensor and EGFR sensor by Src or EGFR kinase.

(A) Src sensor peptide 1 incubated with Src kinase for 1 h resulted in 93% phosphorylation. (B) EGFR sensor peptide 7 incubated with EGFR kinase for 1 h resulted in 59% phosphorylation. (C) Peptide 1 incubated with EGFR kinase for 1 h resulted in 44% phosphorylation. (D) Peptide 7 incubated with Src kinase for 1 h resulted in 8% phosphorylation. Peptide 1 (Src sensor) is the peak near 200 s; peptide 2 (phosphorylated Src sensor) is the peak near 240 s; peptide 7 is the peak near 375 s; the phosphorylated product (peptide 8) is the peak near 390 s.

A

v-Src EEEEIGEFD	E (1.7) D (1.5)	E (3.2) D (2.2)	E (2.2) D (2.0) G (1.6)	I (4.2) V (3.1) L (1.6)	Y	G (2.6) E (2.5) D (1.6)	E (2.5)	F (4.0) I (1.8) L (1.7) V (1.7)	D (2.2) E (2.1)
Lck XEXIYGVLF	X	E (1.5)	X	I (3.4) V (3.0) L (2.3) F (1.6)	Y	G (2.2) A (1.6)	V (1.6)	L (2.3) V (2.2) F (2.2) I (2.0)	F (1.7) L (1.7) V (1.6) I (1.5)
EGF receptor EEEEYFELV	E (1.6) D (1.5) R (1.5) A* (1.5)	E (2.9) D (1.8)	E (2.6) D (1.5)	E (2.5) D (2.1) I (1.6)	Y	F (2.1) V (1.9) I (1.7) E (1.5)	E (1.9) F (1.6) D (1.5)	L (1.7) I (1.7) F (1.6) V (1.5)	V (1.6)

B

	Peptide sequence	Phosphorylation rate by EGFR kinase (pmol/min)
1	5FAM-Orn(Ac)-E-E-E-I- <u>Y</u> -G-E-F-Orn(Ac)-amide	3.61
9	5FAM-E-E-G-V- <u>Y</u> -G-E-F-amide	1.36
10	5FAM-E-D-D-I- <u>Y</u> -G-E-F-amide	3.3
11	5FAM-E-E-G-I- <u>Y</u> -G-E-F-amide	2.04
12	5FAM-E-E-E-V- <u>Y</u> -G-E-F-amide	2.88
13	5FAM-E-D-G-I- <u>Y</u> -G-E-F-amide	2.16
14	5FAM-E-E-G-V- <u>Y</u> -G-V-F-amide	0.54

Table 2.2 Peptide library for identifying selective Src substrate against EGFR.

(A) Amino acid selectivity for Src, Lck and EGFR substrates.

Reprinted from Songyang, Z., Carraway, K.L., Eck, M.J., Harrison, S.C., Feldman, R.A., Mohammadi, M., Schlessinger, J., Hubbard, S.R., Smith, D.P., Eng, C., et al. (1995). Catalytic specificity of protein-tyrosine kinases is critical for selective signalling. *Nature* 373, 536–539. © 1995 Nature Publishing Group, used with permission.

(B) A small library of peptides was designed and synthesized for screening for selective Src substrates against EGFR. The phosphorylation rate of each peptide by EGFR kinase was determined as described in the **Protein kinase phosphorylation assay** section.

Conclusions

We have developed a sensitive and selective Src kinase activity sensing system. Using a series of prostate model cell lines, we have discovered that total Src activity decreases as a function of increasing prostate cell line aggressiveness. However, this unexpected (and ultimately misleading) observation is the consequence of a corresponding decrease in total Src content in the more aggressive cell lines. When the latter is taken into account (i.e. “fractional Src activity”), a positive correlation is observed between cellular aggressiveness and the fraction of cellular Src that is in the active state. In addition, we have found that pTyr-416 Src/total Src is a useful barometer of fractional Src activity for certain cell lines, although the correlation is suspect in the WPE1 cell line series. Furthermore, we found that the ratio of pTyr-527/total Src is a poor indicator of inactive Src but a good predictor of active Src.

Cancer progression is the result of aberrant regulation of signaling networks driven by a variety of protein kinases. Our observation that increased “fractional Src kinase activity” correlates with aggressiveness may represent the ability of clinically aggressive cell lines to globally recruit signaling enzymes to local pathways that drive the cancerous phenotype. This conjecture will require additional data for verification, most notably using primary cells from clinical samples. In addition, the ability to profile multiple protein kinases that are implicated in cancer development could prove helpful in cancer diagnosis and therapeutics (Wang et al., 2010b). Given the high sample capacity of CE, it should be feasible to multiplex screens of kinase activity. We have demonstrated that Src and Akt sensors can be specifically phosphorylated by purified kinases and simultaneously monitored by CE-LIF. However, even though Akt kinase does not stay

active in a cell lysate, Proctor *et al.* have observed Akt-mediated sensor peptide phosphorylation in live LNCaP cells using single cell CE analysis. Therefore, it should prove feasible to simultaneously monitor Src and Akt kinase activity in live cells. Furthermore, we have improved the Src substrate for selective phosphorylation against EGFR. It would also be interesting to assess Src and EGFR activities in cancer cells, possibly in conjunction with Akt activity measurement as well.

CHAPTER III

UNRAVELING THE ROLES OF FYN AND LCK IN TCR SIGNALING BY A LIGHT-DEACTIVATABLE FYN KINASE INHIBITOR

T-lymphocytes play key roles in the human immune system. T cells are activated by the interaction of the cell surface, multi-subunit T cell receptor (TCR) with an antigenic peptide on major histocompatibility complex (MHC) present on an antigen presenting cell (APC) (Nel, 2002; Sundberg et al., 2007). Following antigen recognition, T cell signaling pathways are activated, leading to changes in gene regulation and cell behavior. Proper induction of signaling pathways is crucial for the response to pathogens. Numerous diseases have been linked to aberrant activation of T cells (Wilkinson et al., 2005; Datta and Milner, 2011; Wiegers et al., 2011).

In the Src kinase family, FynT (the T cell isoform of Fyn) and Lck are the two members mainly expressed in T cells, and play a pivotal role in the initial signaling cascade upon TCR activation. FynT and Lck are believed to have distinct yet overlapping functionalities upon T cell stimulation (Zamoyska et al., 2003; Palacios and Weiss, 2004; Salmond et al., 2009). The differences in their specific roles can be attributed to the different localization of these two kinases in T cells. Lck is often found at the plasma membrane, whereas FynT usually localizes to the centrosome, and associate with microtubule cytoskeleton (Ley et al., 1994). Moreover, studies showed that FynT and Lck have different substrate specificities. Activated Lck phosphorylates ITAMs (immunoreceptor tyrosine-based activation motifs), leading to recruitment and activation

of ZAP-70 (zeta-chain-associated protein kinase 70), which subsequently induces the phosphorylation of T cell specific adapters, such as LAT (linker for activation of T cells) and SLP-76 (SH2 domain-containing leukocyte protein of 76 kDa). Some studies showed that activated FynT kinase can specifically phosphorylate cytoskeletal regulators, such as WASP (Wiskott–Aldrich syndrome protein), FAK (focal adhesion kinase), and Pyk2 (proline-rich tyrosine kinase 2) (Palacios and Weiss, 2004). However, controversial studies exist that indicate both Fyn and Lck can be responsible for phosphorylating some of the proteins mentioned above, such as ZAP-70, Pyk2 and LAT (Lovatt et al., 2006; Martín-Cófreces et al., 2006; Collins et al., 2010a, 2010b). Most studies aimed at unraveling the roles of Fyn and Lck were conducted by generating and using protein overexpressing, kinase deficient, or mutated cell lines. However, as Zamoyska *et al.* and Denny *et al.* have pointed out, stimulating responses in kinase-deficient or over-expressed T cells seem to “mask rather than illuminate unique signaling niches” (Denny et al., 2000; Zamoyska et al., 2003). Therefore, the assumed specific or redundant functions by Fyn and Lck might have been mistaken simply as a consequence of experimental methods.

Alternatively, using fast-acting, selective inhibitors to manipulate kinase activity in cells that contain normal protein levels should prove more useful in revealing the actual roles of the target kinase. Lck selective, cell permeable inhibitors have been developed in recent years, including synthetic small molecules (Meyn and Smithgall, 2008; Won and Lee, 2008) and natural products (Faltynek et al., 1995). Imatinib (Gleevec), which is a potent Bcr-Abl inhibitor, has recently been found to be a selective inhibitor for Lck ($IC_{50} = 2.6 \mu M$), but not Fyn or Src (Lee et al., 2010b). Damnacanthal,

an anthraquinone derivative from plant extract, is a potent and selective Lck inhibitor [Lck ($IC_{50} = 17$ nM), ~20-fold selective for Lck versus Fyn] discovered by Michne and colleagues (Faltynek et al., 1995). However, the discovery and development of Fyn selective inhibitors has a much slower progress. To the best of our knowledge, the only reported selective inhibitor for Fyn versus Lck is a bivalent peptide developed by Lawrence and co-workers, that exhibits a 900-fold selectivity for Fyn ($IC_{50} = 53 \pm 4$ nM) versus Lck ($IC_{50} = 43 \pm 4$ μ M) (Hah et al., 2006). However, applying bioactive peptides in cell signaling studies face the challenge of cellular delivery, and the ability of this peptide to penetrate a cell membrane has not been investigated.

Furthermore, cellular response is often highly regulated in time and space. During TCR signaling, enzyme activation is turned on and off within several minutes. Kinases such as Pyk2 are known to have distinct phases of activation (Collins et al., 2010a). In such cases, the conventional inhibitors are limited by the fact that the biochemical contribution of their target kinases cannot be studied in a spatiotemporal fashion. Li *et al.* have developed a strategy to cage Src kinase by a potent light-deactivatable peptide inhibitor. This peptide contains three components: the N-terminus component targets Src kinase domain, the C-terminus component contains a pTyr-Glu-Glu-Ile-Glu sequence that binds to Src SH2 domain, and a photo-cleavable group containing linker connects the two components. The bivalent inhibitor has high inhibitory potency toward Src kinase, therefore Src activity is “caged” when binding to the intact peptide. Upon light-induced cleavage at the linker region, the inhibition was destroyed and thus restored up to 90% of Src kinase activity (**Fig. 3.1**) (Li et al., 2008a).

In this project, we explored the selectivity of photo-deactivatable peptide inhibitors between Fyn and Lck, and discovered a potent and highly selective Fyn inhibitor. Furthermore, we developed a new strategy to deliver the Fyn inhibitor peptide into Jurkat T cells. With this inhibitor, we should be able to selectively control Fyn kinase activity by light inside living T cells. We believe that this inhibitor will provide a powerful tool to study the complex roles played by Fyn and Lck in TCR signaling.

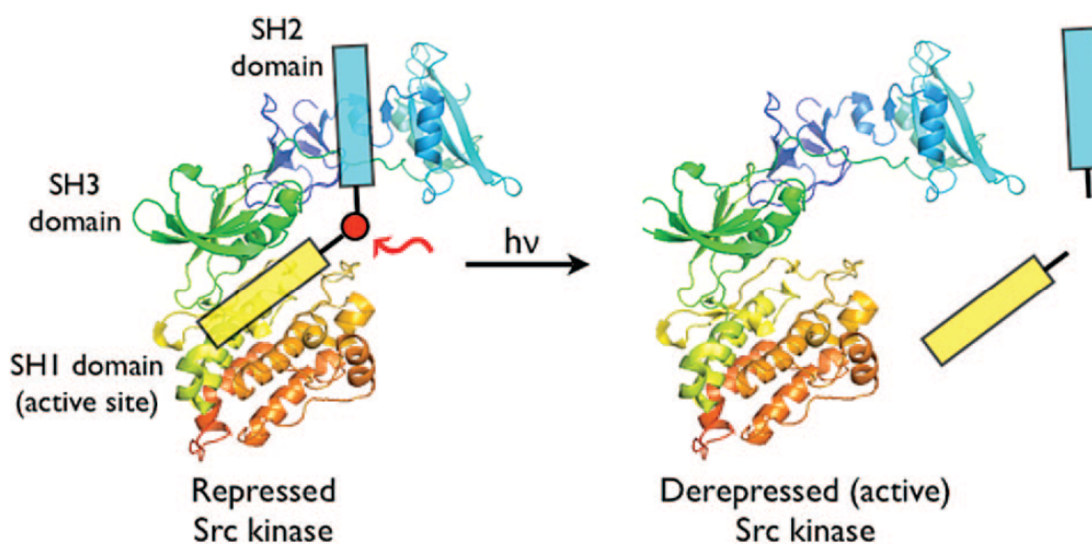


Figure 3.1 A light-deactivatable Src family kinase inhibitor.

Reprinted from Li, H., Hah, J.-M., and Lawrence, D.S. (2008). Light-mediated liberation of enzymatic activity: “small molecule” caged protein equivalents. *Journal of the American Chemical Society* 130, 10474–10475. © 2008 American Chemical Society

Materials and Methods

Peptide synthesis. 3-methoxy-4-nitrobenzoic acid (Ba) and 1,4,5,6,7,7-hexachloro-5-norbornene-2,3-dicarboxylic acid (Hna) were purchased from Sigma Aldrich. NovaSyn TGR resin, O-(1H-6-chlorobenzotriazole-1-yl)-1,1,3,3-tetramethyluronium hexafluorophosphate (HCTU), benzotriazole-1-yl-oxy-tris-pyrrolidino-phosphonium hexafluorophosphate (PyBop), N-hydroxybenzotriazole (HOBT), Fmoc-e-Ahx-OH, Fmoc-Tyr(PO(OBzl)OH)-OH, Fmoc- β -Ala-OH and other common Fmoc protected amino acids were purchased from NovaBiochem. Fmoc-Dap(Aloc)-OH and 3-N α -Fmoc-amino-3-(2-nitrophenyl)propionic acid (ANP linker) were obtained from Advanced ChemTech. (5,6)-carboxyfluorescein diacetate, succinimidyl ester (CFDA-SE) was obtained from AnaSpec. Tetrakis (triphenylphosphine) palladium (Pd(PPh₃)₄) was purchased from Strem Chemicals. Other common chemicals such as N,N-dimethylformamide (DMF), dichloromethane (DCM), N,N-diisopropylethylamine (DIPEA), triisopropylsilane (TIS), N-methylmorpholine (NMM) and trifluoroacetic acid (TFA) were obtained from Sigma Aldrich or Fisher Scientific.

Ba-E(OtBu)-E(OtBu)-E(OtBu)-I-F-G-E(OtBu)-F-Dap(Aloc)-C(trt)-ANP- β -pY(OBzl)-E(OtBu)-E(OtBu)-I-E(OtBu)-Ahx-K(Boc)-CONH₂ was synthesized on the NovaSyn TGR resin (0.2 mmol/g, 1 g resin, 0.2 mmol scale) using a standard peptide coupling protocol on a Protein Technology International Prelude peptide synthesizer. Briefly, TGR resin was mixed with amino acid (5 equiv/equiv resin), HCTU (5 equiv/equiv resin) and DIPEA (12 equiv/equiv resin) in DMF and reacted for 10 min at room temperature. Fmoc was deprotected by 20% piperidine in DMF for 20 min at room

temperature. Ba moiety was coupled to the free N-terminus at the end of the reaction. The subsequent processes were done manually. The allyloxycarbonyl (Aloc) group on the Dap residue was removed by mixing $\text{Pd}(\text{PPh}_3)_4$ (3 equiv) and $\text{CHCl}_3/\text{AcOH}/\text{NMM}$ (37:2:1, 15mL/g of resin) with the peptide for 3 h. Hna moiety was then coupled via exposure of Dap side-chain free amine to 50 equiv Hna, 50 equiv PyBop and 250 equiv NMM in DMF for 3 h. The peptide was cleaved from the resin using TFA/TIS/ H_2O (95:2.5:2.5) along with side chain deprotections.

Peptide **26** was prepared by reacting purified peptide **25** with CFDA-SE. HPLC purified and lyophilized peptide **25** was weighed and dissolved in 1X PBS (pH 7.4) buffer (10 mg peptide/3mL PBS). CFDA-SE (1.5 equiv/equiv peptide) was dissolved in anhydrous DMSO and then slowly added into peptide solution to react for 1.5-3 h. Peptide **27** was prepared by reacting peptide **25** with (5)-FAM-SE. 1 equiv of purified peptide **25** was dissolved in 0.1 M NaHCO_3 , pH 8.4 buffer (~1 mg peptide/1 mL buffer). 1.5 equiv (5)-FAM-SE powder was dissolved in anhydrous DMSO, and slowly added to peptide **25** solution to react for 2-3 h.

Peptides **25**, **26** and **27** were purified by a preparative C18 column on HPLC (Waters) using a binary solvent system, and confirmed by ESI-MS. $\text{C}_{123}\text{H}_{159}\text{Cl}_6\text{N}_{24}\text{O}_{46}\text{PS}$ (peptide **25**) calculated Mass: 2985.47, found 2985.0; $\text{C}_{148}\text{H}_{173}\text{Cl}_6\text{N}_{24}\text{O}_{54}\text{PS}$ (peptide **26**) calculated Mass: 3427.84, found 3426.6; $\text{C}_{144}\text{H}_{169}\text{Cl}_6\text{N}_{24}\text{O}_{52}\text{PS}$ (peptide **27**) calculated Mass: 3343.77, found 3343.5.

IC₅₀ Measurement. Active Src family kinases were purchased from Invitrogen (Src: P3044, Fyn: P3042, Lck: P3043, Blk: PV3683). Other commonly used reagents were purchased from Fisher Scientific or Sigma Aldrich. IC₅₀ values of all bivalent

inhibitors were determined as previously reported (Hah et al., 2006). Specifically, reaction was initiated by addition of 5 μ L of 10 mM ATP to the following solution: 5 μ L of various concentrations of inhibitor, 0.25 μ L 2 mM fluorescent peptide substrate, 1.26 μ L 200 mM MgCl₂, 0.25 μ L 200 mM MnCl₂, 2 μ L 50 mM DTT, 1 μ L 0.5 mg/mL BSA, 2 μ L 0.26 μ M Src family kinase, 8 μ L H₂O and 25.2 μ L 100 mM Tris buffer solution (pH 7.5). The final concentration was: 10 μ M peptide substrate, 10 nM Src family kinase, 1 mM ATP, 50 mM Tris at pH 7.5, 5 mM MgCl₂ 1 mM MnCl₂, 0.01 mg/mL BSA, 2 mM DTT. The fluorescent peptide substrate used in this assay gives a phosphorylation dependent change (~4-fold) in pyrene fluorescence intensity (Wang et al., 2006b). The fluorescence was monitored by bottom reading from a clear bottom multi-well plate on Molecular Devices SpectraMAX Gemini EM fluorescence plate reader at 37 °C (excitation wavelength is 343 nm and emission wavelength is 380 nm). Reaction rates were measured within 10% product formation. Fractional velocities (v/v_0) were plotted against inhibitor concentrations and data was fitted to a full-4 parameter equation to calculate IC₅₀ (Grafit5 software).

$$y = \frac{\text{Range}}{1 + \left(\frac{x}{IC_{50}}\right)^s} + \text{background}$$

Range: the maximum y range.

s: slope factor.

x: the analyte concentration .

Fluorescence microscopy. Uncoated glass bottom dishes (35 mm, glass No. 1.5) were obtained from MatTek Corporation. To facilitate adherence of Jurkat E6-1 cells, the plates were coated with gelatin by adding 200 μ L of 2% gelatin to the glass surface and

incubated at 37 °C for 30 min, followed by washing with DPBS three times. Poly-d-lysine coated glass bottom dishes (MatTek) have also been used to adhere cells. For time-dependent uptake experiments, Jurkat cells were first pelleted at 400 x g for 5 min and washed with DPBS, then resuspended in 500 μ L of DPBS and added to gelatin coated dishes. After letting cells adhere for 10 min at room temperature (RT), 10 μ M final concentration of peptide **26** was added to the dish. Live cell time-course fluorescence images (**Fig. 3.2A**) were taken using a Zeiss 510 Meta laser scanning confocal microscope with a 488 nm argon laser and a 63x oil objective at UNC Michael Hooker microscopy facility.

For the fixed time-point experiment, the cells were first pelleted and washed with DPBS (X3), then incubated with 10 μ M peptide **26** for 30 min. After washing the treated cells once again in DPBS buffer, the cells were plated on poly-d-lysine coated plates and let adhere for about 5 min. The fluorescence image (**Fig. 3.2B**) was taken using an Olympus IX81 inverted wide-field microscope equipped with a Hamamatsu C8484 camera, a xenon arc lamp, a 60x oil objective and a FITC filter cube.

The trypan blue staining was performed by incubating 10 μ M peptide **26** pre-treated Jurkat cells with 0.2% trypan blue (Sigma Aldrich) for 2 min and then diluted in PBS buffer before imaging. The images (**Fig. 3.2C**) were taken using an Olympus IX81-ZDC inverted fluorescence microscope equipped with a QImaging RETIGA 4000R color camera, an Hg Arc lamp, a 40x objective and a FITC filter cube at UNC-CH Lineberger Microscopy Services Laboratory.

Affinity pull-down assay. Peptide **25** affinity pull-down column was prepared according to manufacturer's instruction using Affigel-15 resin purchased from Bio-Rad.

Specifically, 600 μ L of uniformly suspended Affigel-15 resin was added to the column, washed with 3-5 mL of ice-cold isopropyl alcohol (IPA), and centrifuge at 1000 x g for 1 min to remove all solvent. Purified and lyophilized peptide **25** was dissolved in 200 μ L anhydrous DMF and added to the resin. The reaction was carried out by adding 300 μ L additional anhydrous DMF and 5 μ L DIPEA to the resin and rotated at RT for 4 h. The resin was then washed with 5-10 mL ice-cold IPA. The unreacted N-hydroxysuccinimide (NHS) ester was blocked by reacting with 200 μ L of ethanolamine for 1 h at RT. The affinity column was stored in IPA or PBS buffer at 4 °C.

Before use, the column was washed with 500 μ L PBS buffer 10 times. Native cell lysates were added to the resin and rotated for 5-7 h at 4 °C. The flow through was collected by spinning the column at 1000 x g for 1 min and washed with flow through buffer (5 mM $MgCl_2$, 1 mM $MnCl_2$, 2 mM DTT, 10 μ g/mL BSA, 1 mM ATP in 100 mM Tris HCl pH 7.5 buffer) 6 times. The flow through was condensed using a Vivaspinn 6 (10 kD) concentrator. The Affigel-peptide bound proteins were eluted by boiling in 1X SDS loading buffer (50 mM Tris HCl pH 6.8, 100 mM DTT, 20% SDS and 12.5% glycerol) for 10 min.

Native cell lysate preparation and total protein concentration measurement.

Jurkat E6-1 cells were pelleted at 1000 x g for 2 min, and washed with 5 ml of ice-cold DPBS twice. M-PER mammalian protein extraction reagent with 1X Halt protease and phosphatase inhibitor cocktail (Thermo Scientific) was added to the cells and mixed at 4 °C for 10 min. Cell debris was removed by centrifuging samples at 16,000 x g for 10 min at 4 °C. The total protein concentrations were determined by comparing to known concentrations of BSA using Dc Protein assay (Bio-Rad).

T cell growth and stimulation. Jurkat E6-1 cells were obtained from ATCC, cultured and stimulated essentially as described before (Collins et al., 2010b). In brief, the cells were cultured in RPMI1640 medium (Cellgro) supplemented with 10% FBS (Omega Scientific) and 1% penicillin/streptomycin (Cellgro) at a 37°C, 5% CO₂ humidified incubator. For Fyn inhibitor treatment, cells were grown to a concentration of $2-5 \times 10^5$ cells/mL (counted by Scepter™ 2.0 Cell Counter, Millipore), collected and washed in DPBS (GIBCO) for 3 times. Then resuspended to $5-6 \times 10^7$ cells/mL in DPBS and incubated for 10 min at 37°C. The cells were treated with different concentrations of peptide **26** (stock solutions in DMSO were diluted 100X in cell containing PBS) for 10 min at 37°C. For Lck inhibitor damnacanthal (EMD chemicals) treatment, cells were washed and resuspended in RPMI1640 medium without supplement and incubated for 10 min at 37°C. The cells were then treated with different concentrations of Lck inhibitors (stock solutions in DMSO were diluted 100X in cell containing PBS) for 4 h in a 37°C, 5% CO₂ humidified incubator.

Without washing, the cells were stimulated with 10 µg/mL anti-CD3 antibody [OKT3] (Abcam, ab86883) for 1 min at 37°C. Stimulation was stopped by lysing cells with a 4 fold excess (v/v) of 95°C denaturing lysis buffer (20 mM Tris pH 8.0, 2 mM EDTA, 2 mM Na₃VO₄, 20 mM DTT, 2% SDS and 20% glycerol). The lysates were kept at 95°C for 4 min and then sonicated briefly using Fisher Scientific model 50 sonic dismembrator (10 amplitude, 5-10 s) to reduce viscosity.

Western blot experiments. Primary antibodies phospho-Pyk2 (Tyr402) and phospho-Pyk2 (Tyr580) were purchased from Invitrogen; phospho-LAT (Tyr191) was purchased from Cell Signaling Technology; β-actin antibody was purchased from Sigma

Aldrich (A5441); Fyn antibody and Lck antibody were obtained from BD Biosciences. Secondary antibodies (Amersham ECL anti-rabbit/mouse IgG HRP linked species-specific whole antibody from donkey) were purchased from GE healthcare. 20X TBS buffer was obtained from AMRESCO. Ultrapure Tris, glycine and SDS were obtained from Invitrogen. Methanol was obtained from Fisher Scientific.

In affinity pull-down experiment, proteins were separated using NuPage 4-12% Bis-Tris gel (Invitrogen), running at 200 V for 60 min. Gels were then transferred to PVDF membranes using iBlot dry blotting system (Invitrogen). Blocking, antibody incubation, and washes were performed on SNAPid (Millipore). Specifically, the membranes were first blocked using 0.5% non-fat milk in PBST (1X PBS with 0.1% Tween-20) buffer for 1 min. After removing the blocking buffer, the membranes were incubated with primary antibodies (Fyn antibody was diluted 1:250; Lck antibody was diluted 1:1000 in blocking buffer) for 15 min (X2). The membranes were then washed with PBST for 3 times. Then secondary antibodies (1:400 dilution in blocking buffer for Fyn; 1:1000 dilution for Lck) were applied for 15 min. The membranes were subsequently washed with PBST (X3), 0.5% NaCl (X3) and PBS (X3). The blots were detected by Amersham ECL Plus (GE Healthcare) and the chemiluminescence images were obtained by the FluoChemFC2 system (Alpha Innotech).

In experiments detecting Pyk2 and LAT proteins, cell lysates were separated using Novex 4–20% Tris-Glycine pre-cast gel in Novex Tris-Glycine SDS buffer (Invitrogen) at 125 V for 2 h. The proteins were then transferred to PVDF membrane (Invitrogen) using transfer buffer (25 mM Tris, 190 mM glycine, 0.1% SDS and 20% methanol), 120 mA constant current at 4°C overnight. To analyze site-specific

phosphorylation, the membranes were blocked for 1 h at RT in a blocking buffer consisting of TBST (1X TBS with 0.1% Tween-20) with 5% nonfat dry milk (Santa Cruz Biotechnology). The membranes were then washed in TBST for 5 min (X3). Primary antibodies were diluted 1:1000 (1:3000 for β -actin antibody) in TBST containing 5% BSA (Sigma) and then incubated with the membrane at 4°C overnight. After washing with TBST for 5 min (X3), the membranes were incubated with the secondary antibody (1:1000 diluted in blocking buffer) at RT for 1 h, followed by washing in TBST for 10 min (X3). Antibody binding was identified with Amersham ECL Plus (GE Healthcare) and the chemiluminescence images were obtained by the FluoChemFC2 system (Alpha Innotech). The densitometry analysis of the bands was performed using the AlphaView software. Three independent replicates were performed for each experiment. To perform the loading control, all membranes were stripped for 20 min at RT using Restore plus Western blot stripping buffer (Pierce), washed in TBS for 5 min (X3), and reprobed for β -actin.

Results and Discussion

Determination of IC₅₀ and selectivity of light-deactivatable peptide inhibitors for Fyn and Lck. Src kinase family members share highly homologous domain structures. However, specific differences exist in the linker region between the SH1 and SH2 domain. These differences correlate with the subgrouping of Src family kinases (SFKs) (Group A: Src, Yes, Fgr, Yrk and Fyn; Group B: Blk, Lck, Hck and Lyn) (Williams et al., 1998). Moreover, studies by Miller *et al.* suggest that the relative positioning of SH1 domain to SH2 domain is important for proper substrate recognition (Yadav and Miller, 2008). A highly potent “group A” selective Src kinase inhibitor has been developed based on the spatial orientation of the SH1-SH2 domain. This inhibitor contains SH1- and SH2-directed components linked by a three β -Ala tether. The tether length between the two components is believed to be critical for inhibitor potency and selectivity (Hah et al., 2006). Based on this “group A” selective inhibitor, Li *et al.* have prepared a small library of photo-cleavable peptide inhibitors by changing the three β -Ala tether into a photo-labile moiety containing linker. Several potent inhibitors for Src kinase have been identified from this library (Li et al., 2008a). However, the selectivity of these photo-cleavable inhibitors between “group A” and “group B” of Src family members has not been examined. Although these inhibitors were designed based on the “group A” selective peptide sequence, the linker region has been changed to contain a photo-cleavable moiety, which might affect the inhibitor potency and selectivity. Therefore, we tested the IC₅₀ and selectivity of this small library of photo-cleavable peptides towards four Src family members: Src, Fyn, Lck and Blk.

As shown in **Table 3.1**, IC_{50} values of these peptides are similar for Src and Fyn, which is expected since Fyn and Src are both members of the “group A” SFKs. In contrast, these peptides are poorer inhibitors for Lck and Blk (“group B” SFKs), and exhibit different selectivity between Fyn and Lck. The control peptide **16** [Fyn ($IC_{50} = 1.34 \mu M$), Lck ($IC_{50} = 26.7 \pm 0.5 \mu M$)] is a 1:1 mixture of the two components of the bivalent inhibitor, which is used to mimic the resulting compounds after light induced cleavage. Among these inhibitors, we have identified a lead compound peptide **24** [Src ($IC_{50} = 0.056 \pm 4 \mu M$); Fyn ($IC_{50} = 0.025 \pm 0.003 \mu M$); Lck ($IC_{50} = 13.6 \pm 1.4 \mu M$); Blk ($IC_{50} = 2.29 \pm 0.42 \mu M$)]. Although peptide **24** is not able to discriminate within “group A” (Src and Fyn) or “group B” (Lck and Blk), the 543-fold selectivity for Fyn versus Lck should prove sufficient to study signaling mechanisms of these two kinases in T cells.

#	*Peptide	Src IC ₅₀ (nM)	Fyn IC ₅₀ (nM)	Lck IC ₅₀ (nM)	Blk IC ₅₀ (nM)	Lck/Fyn
15	Ba-EEEIFGEF-Dap(Hna)-βA ₃ -pYEEIEIX	21±1.5	16±1.6	2250±140	5100±160	141
16	Ba-EEEIFGEF-Dap(Hna)X + AcpYEEIE-NH ₂	627±48	1340	26700±510	4860±2120	20
17	Ba-EEEIFGEF-Dap(Hna)-βA-I-βA-pYEEIEIX	48±4	88±15	4960±600	2920±260	56
18	Ba-EEEIFGEF-Dap(Hna)-βA-II-βA-pYEEIEIX	12±1	51±12	8450±4000	2950±370	166
19	Ba-EEEIFGEF-Dap(Hna)-βA-III-βA-pYEEIEIX	6.6±0.4	15±0.8	1560±100	2930±550	104
20	Ba-EEEIFGE-II-Dap(Hna)-βA ₃ -pYEEIEIX	632±113	350±34	>59000	8550±2530	171
21	Ba-EEEI-III-GEF-Dap(Hna)-βA ₃ -pY-III-EIEX	>56000	>37000	>56000	>43000	NA
22	Ba-EEEIFGE-III-Dap(Hna)-βA ₃ -pY-III-EIEX	12800	16000	>19000	4400±2760	NA
23	Ba-EEEIFGEF-Dap(Hna)-βA-III-βA-pY-III-EIEX	211±86	360±48	>12000	3770±3400	NA
24	Ba-EEEIFGEF-Dap(Hna)C-III-βA-pYEEIE-NH ₂	74±7	25±3	13600±1400	2290±420	543

*

X

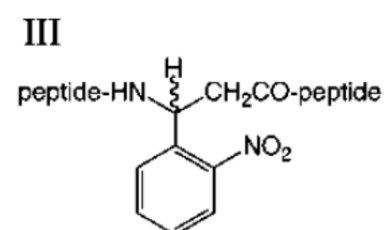
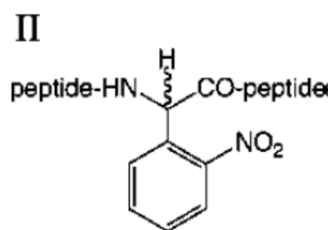
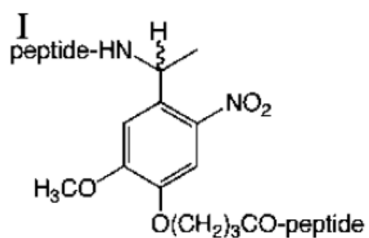
peptide-NH(CH₂)₂SH

Table 3.1 IC₅₀ and selectivity of peptide inhibitors for Src, Fyn, Lck and Blk.

The * labeled peptide sequences and the compound structures were adapted from the previously published paper:

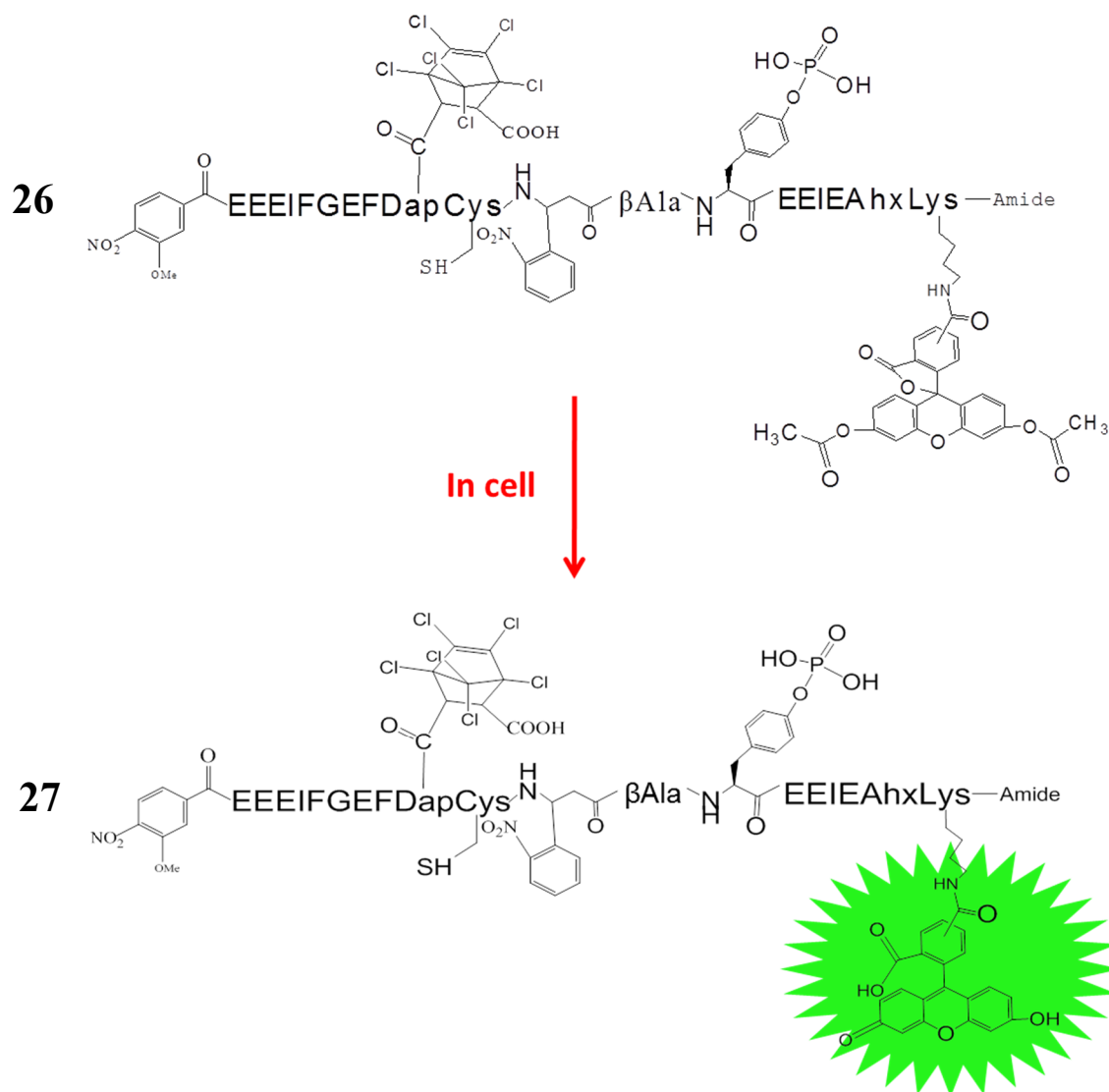
Li, H., Hah, J.-M., and Lawrence, D.S. (2008). Light-mediated liberation of enzymatic activity: “small molecule” caged protein equivalents. *Journal of the American Chemical Society* 130, 10474–10475. © 2008 American Chemical Society, used with permission.

The IC₅₀ measurements of peptide **15-24** for Src kinase were repeated in this study, and showed comparable results with previously published data. IC₅₀ values for Fyn, Lck and Blk kinases were measured, and the selectivity between Fyn and Lck was compared.

Cellular delivery of the Fyn selective inhibitor. One of the challenges to applying bioactive peptide reagents is cellular delivery. Many techniques have been used to introduce cell impermeable proteins and peptides into intact cells, including microinjection, electroporation, osmotic lysis of pinosomes, liposome mediated delivery and red blood cell ghost fusion. These techniques have their advantages and disadvantages. For example, microinjection allows precise control over delivering concentration and timing, but is only appropriate for single cell analysis (Zhang and Yu, 2008a, 2008b). The osmotic lysis of pinosomes utilizes a hypertonic reagent to allow molecules carried into cells via pinosomes, which was later released into cytosol by changing to hypotonic solution. However, osmotic treatment can cause unwanted changes in cell signaling and behavior (Okada and Rechsteiner, 1982; Chakrabarti et al., 1989). Permeabilizing peptides can also be achieved by attaching cell penetrating peptides (CPP) (Stewart et al., 2008) or fatty alkyl chains (Toth, 1994) via disulfide bond. However, the Fyn selective inhibitor **24** is a heavily modified peptide, thus we would anticipate encountering synthesis, purification and solubility difficulties if using these methods. Moreover, the efficiency of CPP- or fatty alkyl chain-mediated delivery is largely dependent on the cell type and cargo properties (Maiolo et al., 2005). Nelson *et al.* have shown that cell penetrating peptide TAT failed to deliver an Abl peptide inhibitor into Jurkat T cells, whereas HeLa cells can be readily loaded under similar conditions (Nelson et al., 2007).

Unsatisfied with the current cell delivering methods, we wanted to screen a compound library aiming to identify a novel cellular delivery agent for the Fyn inhibitor peptide. In order to monitor the uptake of peptide **24** by cells, we prepared a

profluorescent **peptide 26** (synthesis is shown in **Scheme 3.1**). A short Ahx-Lys spacer was added to the C-terminus of the parent peptide **24** to reduce interference of the fluorophore to peptide binding affinity for Fyn, and also provide a lysine side-chain amine for fluorophore conjugation (peptide **25**). A profluorescent carboxyfluorescein diacetate (CFDA) moiety was used so that only those taken up by cells will be fluorescent upon intracellular hydrolysis of the diacetate groups. This uptake-and-report design eliminates the washing steps and therefore is more feasible for high-throughput screening (especially when non-adherent T cells are used). Moreover, after intracellular hydrolysis of CFDA, the resulting carboxyfluorescein (FAM) is not cell permeable, which should help to retain the peptide inside cells (**Scheme 3.2**).



Scheme 3.2 The “uptake and report” design of peptide 26.

Surprisingly, live cell images revealed that the CFDA labeled peptide **26**, without any additives, efficiently penetrated Jurkat E6-1 cells within 10 min. As shown in **Fig. 3.2A**, Jurkat T cells clearly show an increase in green fluorescence signal as a function of incubation time, indicating uptake and accumulation of the peptide inside cells. We suspect that since the parent peptide **24** is heavily negatively charged, it is not likely to be able to penetrate cells. Therefore, the cell permeable profluorescent moiety CFDA may be the key for delivering the entire molecule into cells. However, we do note that punctate-endosome like structures were observed in Jurkat cells incubated with 10 μ M of peptide **26** for 30 min (**Fig. 3.2B**). More studies are needed to identify the punctate pattern and the cellular uptake mechanisms of CFDA labeled peptides. We suspect that peptide **26** was taken up by Jurkat cells via a combination of direct permeabilization and endocytosis.

We have also examined cytotoxicity of peptide **26** to Jurkat T cells. The cells were first incubated with 10 μ M peptide **26** for 30 min, and then stained with cell vital dye trypan blue. Trypan blue is commonly used not only to assess cell viability, but also to quench extracellular fluorescence in flow cytometry analysis (Van Amersfoort and Van Strijp, 1994; Rejman et al., 2005). In our experiment, the dead cells would be stained with trypan blue and also lose fluorescence. As shown in **Fig. 3.2C**, the arrow is pointing to a dead cell, which has lost cell membrane integrity, thus stained by trypan blue and fluorescence quenched. However, most of the cells treated with peptide **26** for 30 min are viable and fluorescent. This result shows that when used at 10 μ M, Fyn inhibitor peptide **26** can readily penetrate Jurkat T cells, and doesn't seem to be cytotoxic. However, in the later experiments, higher concentrations of peptide **26** were used to treat Jurkat cells.

Therefore, further studies are needed to determine cytotoxicity of peptide **26** when used at higher concentrations.

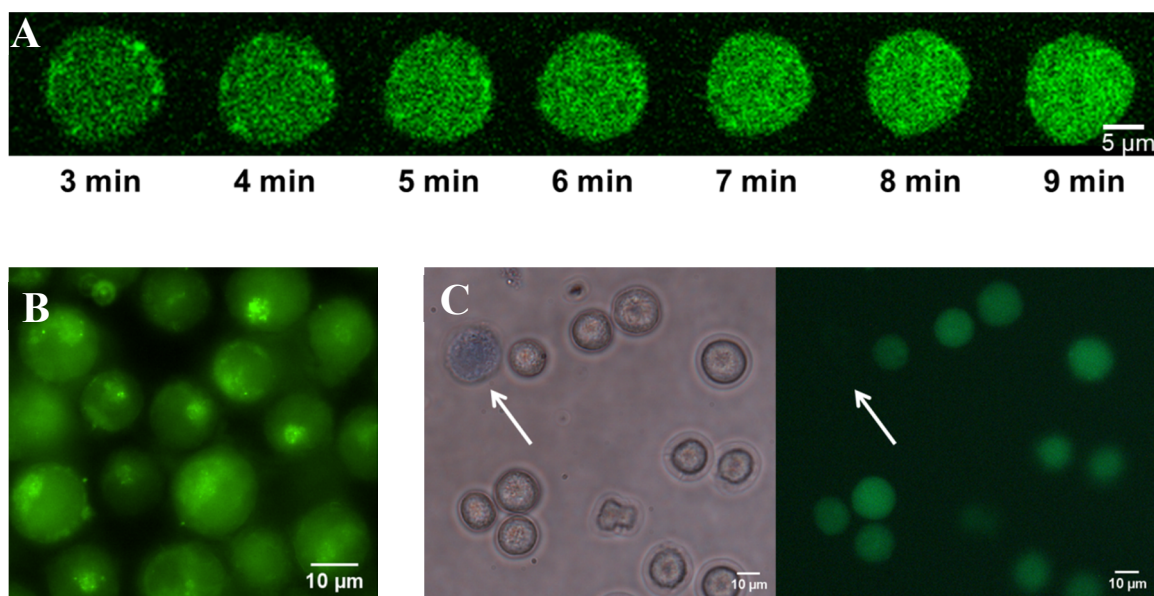


Figure 3.2 Fluorescence microscopy imaging of peptide 26 uptake by Jurkat T cell.

(A) Cellular uptake and accumulation of peptide **26** was observed as green fluorescence signal in live Jurkat T cells. Confocal images of a gradual increase of cellular fluorescence were captured every 1 min after adding peptide **26** to cells for 3 min. (B) Wide-field fluorescence image of Jurkat T cells incubated with 10 µM peptide **26** for 30 min, then adhered on a poly-d-lysine coated plate. Fluorescein fluorescence is largely cytosolic, but a punctate pattern is observed. (C) 10 µM of peptide **26** was incubated with Jurkat cells for 30 min, then 0.2% trypan blue solution was added to stain for dead cells. The fluorescein fluorescence from the dead cells is quenched by trypan blue (arrow).

Determination of IC₅₀ and selectivity of cell permeable Fyn inhibitor. After taken up by cells, peptide **26** is hydrolyzed to a fluorescein labeled peptide **27** (**Scheme 3.2**). Compared to the lead compound **24** from the library, **27** not only contains two extra amino acids, but also a bulky negatively charged moiety close to the SH2 domain targeting component. Although we placed a spacer between the SH2 domain targeting sequence and the fluorophore, we suspect that these modifications are likely to alter the potency and selectivity of peptide **27** as a Fyn inhibitor. Therefore, we evaluated the IC₅₀ and the selectivity of peptide **27** (**Table 3.2**). As expected, the addition of extra amino acids and fluorescein had a negative influence on the potency and selectivity of the inhibitor. We have also tested the IC₅₀ of peptide **25**, which contains the Ahx and Lys amino acid spacer, but not labeled with fluorescein. With the extra amino acids only, the IC₅₀ of peptide **25** for Fyn (IC₅₀ = 0.046 μ M) and Lck (IC₅₀ = 10 μ M) did not change much from the parent peptide **24** [Fyn (IC₅₀ = 0.025 μ M) and Lck (IC₅₀ = 13.6 μ M)]. In contrast, the fluorescein conjugated peptide **27** has a 0.41 μ M IC₅₀ for Fyn, and 65.3 μ M IC₅₀ for Lck, and the selectivity for Fyn over Lck is 159-fold. From these results, we decided that the cell permeable peptide exhibits good inhibitory behavior and high selectivity for Fyn, and therefore should serve as a good Fyn-selective inhibitor in subsequent cell based studies.

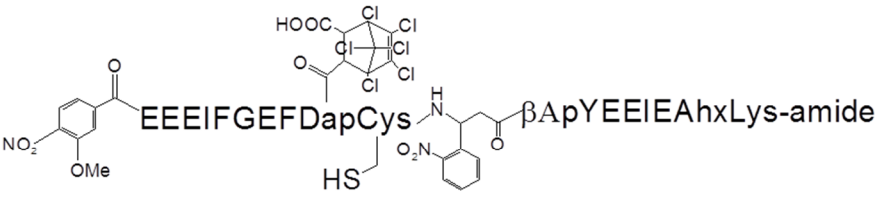
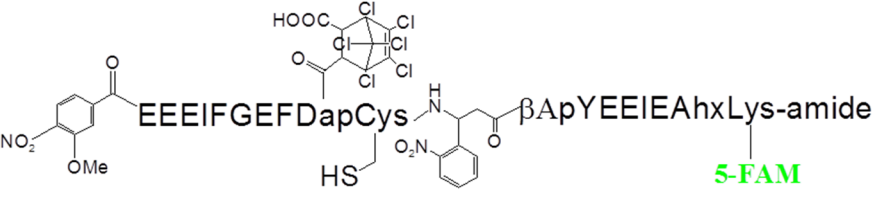
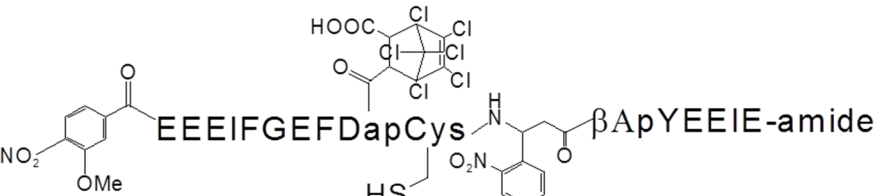
#	Peptide	IC ₅₀ Fyn (μM)	IC ₅₀ Lck (μM)	Lck/ Fyn
25		0.046 ± 0.012	10.01±1.62	218
27		0.41 ± 0.06	65.3±4	159
24		0.025 ± 0.003	13.58±1.4	543

Table 3.2 IC₅₀ and selectivity of peptide 24, 25 and 27 for Fyn and Lck.

Peptide 25 selectively pulls down Fyn over Lck from Jurkat cell lysate. To see if the Fyn inhibitor peptide **25** is able to selectively bind to Fyn versus Lck in Jurkat T cell lysates, we performed an affinity pull-down assay. The affinity column was prepared by immobilizing peptide **25** on an Affigel resin through conjugation to the lysine side chain. Jurkat E6-1 cell lysate was added to the Affigel-peptide **25** affinity column. After incubation, the unbound proteins were collected from the flow through fraction, and the bound proteins were subsequently eluted by boiling the resins in SDS containing buffer. The relative amount of Fyn and Lck in cell lysate, flow through and elution was compared by Western blot using Fyn and Lck specific antibodies (**Fig. 3.3**). Denny *et al.* have previously determined that the relative levels of Fyn and Lck in Jurkat cells is 1:30 (Denny et al., 2000). We found that, when used at the same dilution, the Lck antibody produces a much stronger signal than the Fyn antibody. Thus different dilutions for these two antibodies were used in the pull-down analysis to generate comparable chemiluminescence signals. Therefore, the Fyn and Lck signal strength shown in **Fig. 3.3 (INPUT)** is not representative of the relative amount of Fyn and Lck expressed in Jurkat E6-1 cells.

The pull-down assay demonstrated that the immobilized Fyn inhibitor **25** was able to selectively bind to Fyn over Lck in Jurkat cell lysate. However, we do note that not all Fyn protein has been pulled-down, and a small fraction of Lck also bound to the affinity column. We suspect this is because the Jurkat cells were lysed and used without TCR stimulation, thus Fyn and Lck kinases present in the cell lysate were not in the fully activated form. The bivalent inhibitor is designed to bind to the fully active Fyn kinase which exhibits an “open” conformation. When Fyn is in a “closed” inactive conformation,

the SH1 and SH2 domains are not positioned for the optimal binding by the bivalent inhibitor. Therefore, the selectivity of this peptide for inactive Fyn and Lck is likely to be moderate.

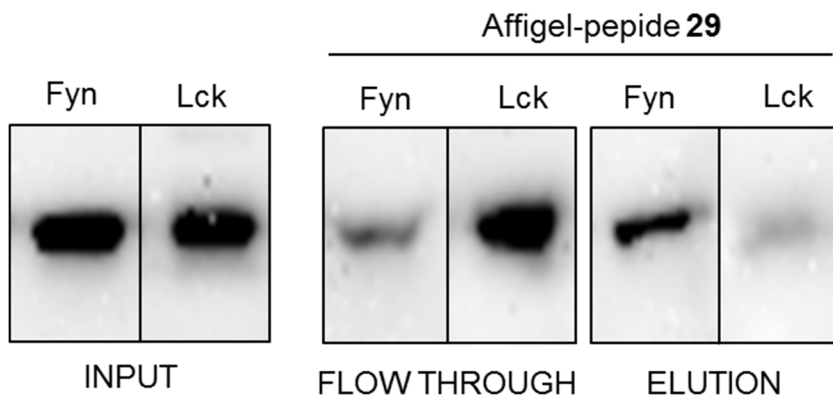


Figure 3.3 Immobilized peptide 25 selectively pulls-down Fyn over Lck from Jurkat lysate.

Jurkat E6-1 cell lysate was used for pull-down analysis by Affigel-peptide **25**. The amount of Fyn and Lck from cell lysate (input), unbound fraction (flow through) and peptide bound fraction (elution) was analyzed by Western blot.

Effect of Fyn and Lck inhibitors on Pyk2 and LAT phosphorylation in stimulated Jurkat T cells. Many studies have indicated that Fyn is able to selectively phosphorylate several protein substrates upon T cell stimulation, including Pyk2 (Qian et al., 1997), c-Cbl (Tsygankov et al., 1996; Feshchenko et al., 1998), Sam68 (Feuillet et al., 2002), SKAP55 (Wu et al., 2002) and WASP (Badour et al., 2004). However, controversial data exists indicating that although not required, Lck may also play a role in phosphorylating some of these proteins. For example, knocking out Fyn doesn't completely abolish Pyk2 phosphorylation (Collins et al., 2010b), and knocking down Lck causes a reduction in c-Cbl phosphorylation (Methi et al., 2008).

Lck is generally believed to be the major contributor in proximal TCR signaling (Salmond et al., 2009), and has attracted more attention than Fyn. Proteins including ZAP-70 (Wang et al., 2010a), LAT (Jiang and Cheng, 2007), PLC γ 1 (Lovatt et al., 2006), ezrin (Autero et al., 2003) and magicin (Lee et al., 2006) were shown to be selectively phosphorylated by Lck, although Fyn may also mediate LAT phosphorylation in the absence of Lck (Lovatt et al., 2006). In our study, considering the availability of phospho-specific antibodies, we choose to examine the phosphorylation of Pyk2 and LAT upon Jurkat TCR stimulation, and how the phosphorylation is affected by selective inhibition of Fyn or Lck.

TCR stimulation induces rapid phosphorylation of Pyk2 on tyrosine residues 402 and 580, and phosphorylation of LAT on tyrosine residue 191. As shown in **Fig. 3.4A**, stimulating Jurkat E6-1 cells with soluble anti-CD3 (OKT3) antibody induces fast phosphorylation of Pyk2 Tyr-580 and LAT Tyr-191. The maximum phosphorylation occurs between 1 - 2 min after stimulation for both sites. Previous studies have shown

that the Src family kinase inhibitor PP2 [Fyn ($IC_{50} = 6$ nM); Lck ($IC_{50} = 5$ nM)] is able to completely suppress Fyn and Lck activity in T cells (Collins et al., 2010b). To confirm this finding, we used another potent cell permeable Src kinase inhibitor AZD0530 [Fyn ($IC_{50} < 10$ nM); Lck ($IC_{50} < 4$ nM)] (Green et al., 2009). After pre-treating Jurkat cells with 10 μ M AZD0530 for 10 min, no detectable Pyk2 and LAT tyrosine phosphorylation was observed in stimulated T cells (**Fig. 3.4B**). Therefore, our results confirm that TCR induced phosphorylation of Pyk2 and LAT requires Src family kinase activity.

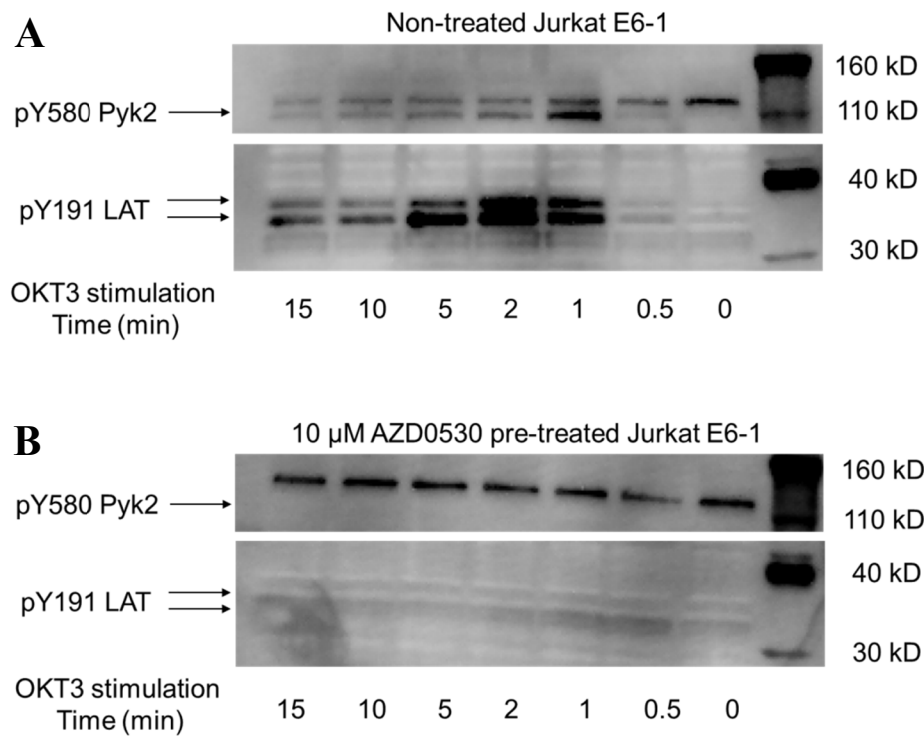


Figure 3.4 TCR induced Pyk2 and LAT phosphorylation requires Src family kinase activity.

(A) Jurkat E6-1 cells were stimulated with 10 μ g/mL anti-CD3 antibody (OKT3) for 0–15 min. Phosphorylation of Pyk2 Tyr-580 and LAT Tyr-191 was examined by Western blot. (B) Phosphorylation of both proteins was abolished by pre-treating the cells with 10 μ M SFK inhibitor AZD0530 for 10 min.

The previous experiment demonstrated that phosphorylation of Pyk2 and LAT upon TCR stimulation requires Src family kinase activity. Therefore, we wanted to examine if Lck and Fyn play different roles in phosphorylating Pyk2 and LAT. Jurkat E6-1 cells were pre-treated with various doses of cell permeable kinase selective inhibitors, and then stimulated with anti-CD3 (OKT3) antibody for 1 min. The phosphorylation of Pyk2 Tyr-402 and LAT Tyr-191 was examined by Western blot. As shown in **Fig. 3.5A** and **Fig. 3.6A**, minimum phosphorylation of Pyk2 and LAT is observed prior to TCR stimulation, whereas 1 min incubation with OKT3 induces significant phosphorylation for both proteins. Treatment with Lck inhibitor damnacanthal [Lck (IC_{50} = 17 nM), ~20-fold selective for Lck versus Fyn) (Faltynek et al., 1995)] induces a concentration dependent LAT phosphorylation reduction, with a 50% suppression in 30 μ M damnacanthal treated Jurkat cells. In contrast, for all the doses tested, damnacanthal does not significantly affect Pyk2 phosphorylation compared to a DMSO treated control (**Fig. 3.5B**). These data are consistent with previously reported results by Collins *et al.*, indicating Pyk2 phosphorylation does not require Lck activity, whereas LAT Tyr-191 phosphorylation is dependent on Lck activation (Samelson, 2002; Collins et al., 2010b).

To test if Pyk2 phosphorylation is dependent on Fyn activity, we pre-treated Jurkat cells for 10 min with an increasing concentrations of cell permeable Fyn selective inhibitor peptide **26** [the in cell hydrolyzed form **27** has a 0.41 μ M IC_{50} for Fyn and 159-fold selective for Fyn versus Lck] (**Fig. 3.6**). However, no significant change of Pyk2 phosphorylation was observed for doses up to 30 μ M. This result might indicate that Fyn kinase activity is not required for Pyk2 phosphorylation. However, we were surprised to

find that LAT phosphorylation is suppressed over 20% in 1 μ M or 30 μ M peptide **26** pre-treated cells, but not in 5-20 μ M dose range. With the current data in hand, we are not able to give an explanation for this observation. However, we suspect that during cell delivery, some peptides were trapped in the endosome-like structures. Therefore not enough peptide is present in the cytosol after 10 min incubation. In addition, it is also possible that peptide **26** (or the hydrolyzed **27**) might have been degraded or dephosphorylated in cells. Indeed, rapid peptide degradation and dephosphorylation have been observed in living cells by CE analysis, as demonstrated in **Chapter 2**.

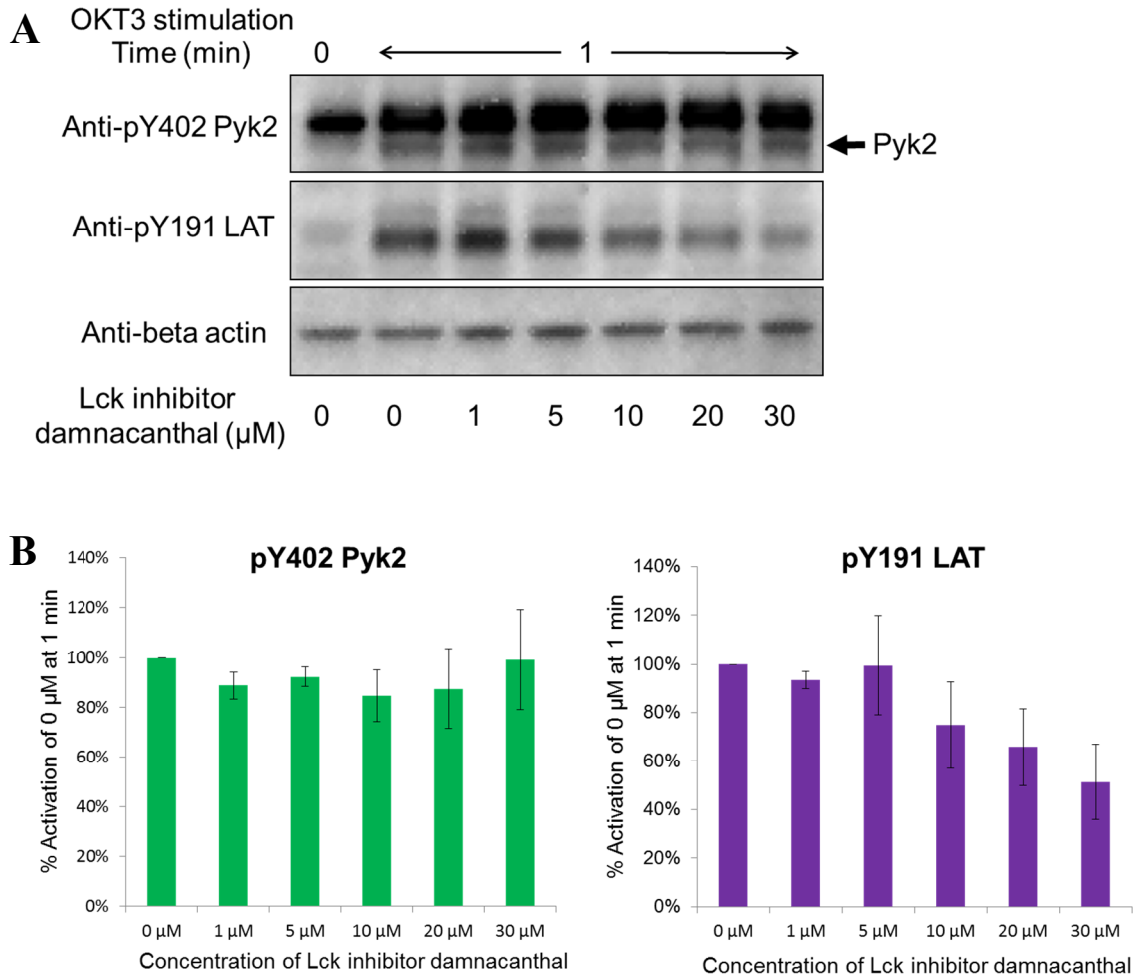


Figure 3.5 Effect of Lck inhibitor damnacanthal treatment on Pyk2 and LAT phosphorylation.

(A) Western blot analysis of Pyk2 Tyr-402 and LAT Tyr-191 phosphorylation upon OKT3 stimulation in the absence or presence of increasing concentrations of cell permeable Lck selective inhibitor damnacanthal. (B) Densitometry analysis of Western blot results. The signal from pY402 Pyk2 and pY191 LAT was normalized to β -actin loading control. The normalized phosphorylation levels from inhibitor treated samples were compared to DMSO treated sample (0 μ M). Data was averaged from at least 3 independent experiments. Error bars are showing SEM.

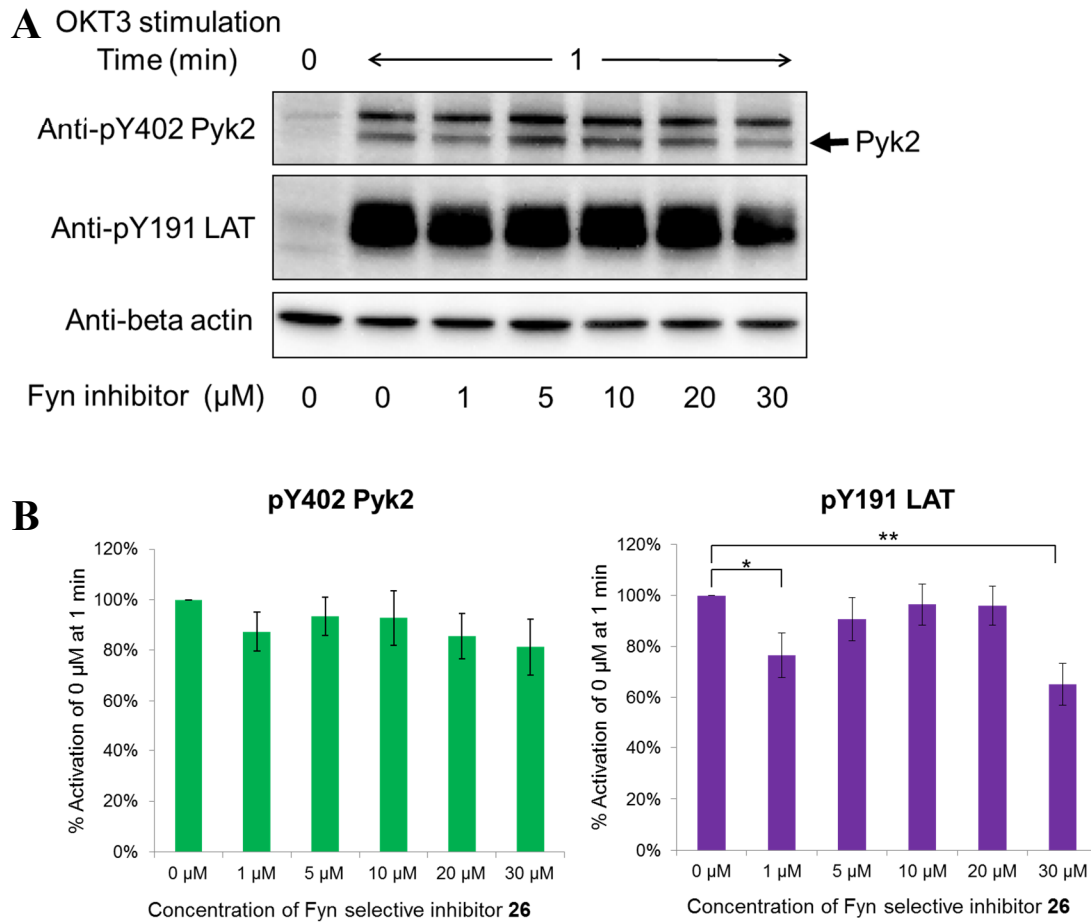


Figure 3.6 Effect of cell permeable Fyn selective inhibitor **26 treatment on Pyk2 and LAT phosphorylation.**

(A) Western blot analysis of Pyk2 Tyr-402 and LAT Tyr-191 phosphorylation upon OKT3 stimulation in the absence or presence of increasing concentrations of cell permeable Fyn selective peptide inhibitor **26**. (B) Densitometry analysis of Western blot results. The signal from pY402 Pyk2 and pY191 LAT was normalized to β -actin loading control. The normalized phosphorylation levels from inhibitor treated samples were compared to DMSO treated sample (0 μ M). Data was averaged from at least 3 independent experiments (except for 30 μ M inhibitor treated pY191 LAT level, which is the average of two experiments). Error bars are showing SEM. * $p=0.0105$, ** $p=0.0253$

Conclusions

We have discovered a potent and selective Fyn kinase inhibitor from screening a small library of photo-cleavable bivalent peptides. This inhibitor (peptide **24**) exhibits a 25 nM IC₅₀ for Fyn and a ~550-fold selectivity against Lck. To utilize this inhibitor for cellular studies, we designed an uptake-and-report strategy by attaching a profluorescent CFDA moiety to the C-terminus of the inhibitor peptide, aiming to screen for novel cell delivery agents. We were surprised to find that the CFDA conjugated peptide **26** is permeable to Jurkat E6-1 cells. However, punctate endosome-like patterns were observed. Therefore, it would be useful to further study the uptake mechanism of CFDA labeled peptide, and also explore the application of this new cell delivery strategy to other peptide sequences and other cell types.

Some studies showed that Pyk2 can be specifically phosphorylated by activated Fyn kinase (Qian et al., 1997), whereas other indicates that Lck may also play a role in Pyk2 phosphorylation (Collins et al., 2010b). We found that pretreating Jurkat E6-1 cells with various doses of Fyn inhibitor **26** or Lck inhibitor damnacanthal does not significantly affect Pyk2 phosphorylation. However, a potent Src family kinase inhibitor AZD0530 abolishes phosphorylation of both proteins. This might support the findings by Collins *et al.* that Lck is not required, but is sufficient to phosphorylate Pyk2 (Collins et al., 2010b). However, the phosphorylation of a T cell adaptor protein LAT is suppressed not only in a dose dependent manner by Lck inhibitor damnacanthal, but also by pretreatment of 1 μ M or 30 μ M of Fyn inhibitor. From these results, we can't conclude that LAT phosphorylation requires both Fyn and Lck activity. However, we suspect that the observed effect of Fyn inhibitor on Pyk2 and LAT phosphorylation might be due to

different cytosol concentrations after 10 min pre-incubation, due to intracellular peptide degradation and/or dephosphorylation of the peptide. Therefore, further characterization of the cellular concentration as a function of incubation time and concentration, as well as the stability of the Fyn inhibitor inside living Jurkat cells, is essential in understanding the observed phenomenon, and to proceed with further investigations.

CHAPTER IV

CONSTRUCTION OF A PHOTOACTIVATABLE PROFLUORESCENT ENZYME VIA PROPINQUITY LABELING

Elucidation of protein structure/function relationships has a long and storied history. However, for a wide variety of reasons, these relationships can be difficult to discern. For example, there is often a pronounced spatiotemporal component associated with protein action and the attendant biological consequences. In this regard, one particularly noteworthy protein is the cAMP-dependent protein kinase (PKA), which is associated with an array of organelles and supramolecular complexes, yet the ramifications of its action at these sites are distinct (Taskén and Aandahl, 2004).

In recent years, one of the emerging areas of chemical biology is the use of photo-sensitive molecules to study the signaling networks in cells (Priestman and Lawrence, 2010), and cell behavior upon activation (or deactivation) of these light-responsive compounds (Ellis-Davies, 2007; Gorostiza and Isacoff, 2008). Among the photo-sensitive biological effectors, light-activatable (“caged”) proteins are a very interesting category and have attracted much attention. Caged proteins represent a potentially powerful means to address the relationship between protein activity and cellular behavior as a function of time and location (Lawrence, 2005; Mayer and Heckel, 2006; Lee et al., 2009; Priestman and Lawrence, 2010; Gautier et al., 2011). Caged proteins allow researchers to control protein activity by light irradiation at the cellular and tissue level. This provides a tool to allow the study of their biological functions in a spatial and temporal manner. Caged

biological effectors (including caged proteins) can be introduced into a biological system and subsequently turned-on by a UV lamp (global uncaging, appropriate for a large cell population) (Lee et al., 2011), or by a focused laser beam under the microscope (local uncaging, appropriate for single cells or subcellular studies) (Ghosh et al., 2004).

Protein caging has been achieved in several ways: (a) chemical modification of existing critical nucleophilic residues with photo-cleavable moieties (Marriott, 1994; Golan et al., 1996; Marriott and Heidecker, 1996; Priestman et al., 2011), (b) site-directed mutagenesis-mediated insertion or deletion of reactive residues (Chang et al., 1995, 1998; Ghosh et al., 2004), (c) enzyme-directed insertion of reactive functionality (Zou et al., 2002), (d) unnatural amino acid mutagenesis-mediated introduction of caged amino acids (Wang et al., 2006a; Lee et al., 2009; Riggsbee and Deiters, 2010), (e) semisynthetic proteins generated by expressed protein ligation (Hahn and Muir, 2004; Pellois et al., 2004; Hahn et al., 2007), (f) using caged small molecule effectors or light-deactivatable inhibitors (Kawakami et al., 2008; Li et al., 2008a; Georgianna et al., 2010; Karginov et al., 2010; Riggsbee and Deiters, 2010; Priestman et al., 2011), and (g) genetically encoded incorporation of light-responsive proteins (Lee et al., 2008a; Strickland et al., 2008; Levskaya et al., 2009; Wu et al., 2009; Kennedy et al., 2010).

The cAMP-dependent protein kinase (PKA) plays important roles in several signaling pathways, and is one of the most studied protein kinases. The PKA holoenzyme consists of two catalytic domains and two regulatory domains. The catalytic subunit has been used to develop the caged derivatives. There are three reactive residues on PKA catalytic subunit, Cys-199, Cys-343 and Thr-197. Cys-199 and Thr-197 are in the activation loop, and are critical for the enzymatic activity. Bayley *et al.* covalently

modified Cys-199 with nitrobenzyl caging groups and reported 5% residual activity and up to 30-fold activity recovery after photolysis (Chang et al., 1998). Thr-197 has also been modified by first inserting a reactive thiophosphate via an enzyme-directed reaction, then caging the phosphate group with a photo-cleavable moiety. This strategy resulted in 6% residual activity and up to 90% activity recovery after photolysis (Zou et al., 2002). PKA Cys-199 has also been selectively modified via an active-site directed peptide, which was designed to promote a weak active-site binding and thus induce an affinity labeling of Cys-199. This design successfully reduced PKA activity to less than 2%, and photolysis induced a 25-fold activity enhancement (Curley and Lawrence, 1998).

In addition to controlling protein activity by light, it would also be useful if the uncaging and location of the modified species could be observed. When researchers use caged molecules to decipher the complex intracellular pathways, the only feedback from the experiment is the biological response that is directly or indirectly generated from the photo-activated effectors. However, if no desired biological response is observed, it can be extremely difficult to decide if this is due to unsuccessful uncaging or some other unexpected mechanism. Therefore, a strategy that allows visual evaluation of the extent of photo-uncaging, and, the location and movement of the photo-activated effectors in real time is desirable. There are two different approaches to generate the uncage-and-report system. One is to use a profluorescent caging group. This type of caging group, after photolysis, is transformed into an active fluorophore, hence the extent of photolysis can be visually evaluated fluorescently. Kutateladze and co-workers have developed a thioxanthone-based system that furnishes an up to 17-fold enhancement in response to photo-cleavage (Majjigapu et al., 2005). Another uncage-and-report strategy is to use a

fluorophore tethered to a quencher via a photolabile linker. Compared to the small profluorescent caging groups, this design has the advantage of being used for real-time tracking if the fluorophore, after photolysis, remains on the activated protein. Muir and co-workers prepared a caged protein construct (Smad2) via expressed protein ligation using a fluorescein-photolabile linker-dabcyl cassette and reported a 26-fold fluorescence enhancement upon photo-activation in the test tube (Pellois et al., 2004).

In this project, we have successfully developed a new uncage-and-report system that utilizes peptide-based active site recognition and affinity labeling strategy (Yan et al., 1996; Curley and Lawrence, 1998; Harvey and Trauner, 2008) to modify a non-active site residue in PKA catalytic subunit, and prepared a caged profluorescent PKA (**Fig. 4.1**).

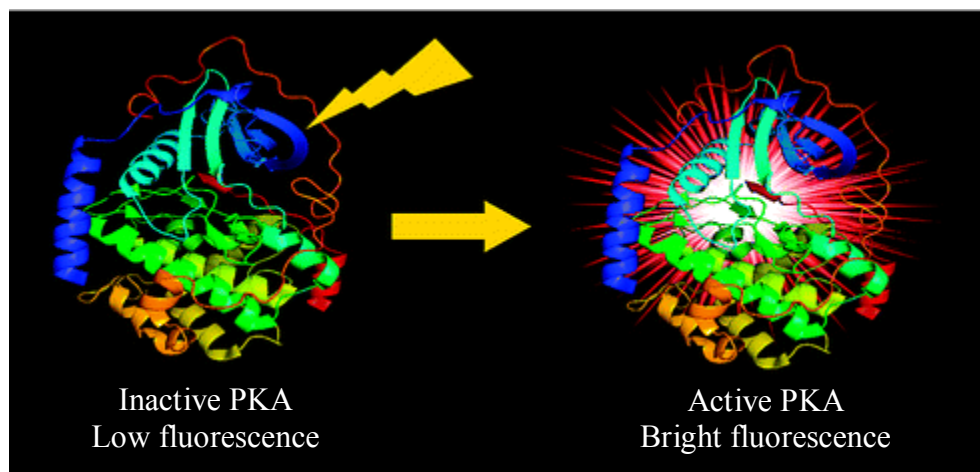


Figure 4.1 The uncage-and-report design of a caged profluorescent PKA.

Materials and Methods

Peptide synthesis. All amino acids, Fmoc-PEG-linker, NovaSyn TGR resin, HCTU were obtained from NovaBiochem. 4-{4-[1-(9-fluorenylmethyloxycarbonylamino)ethyl]-2-methoxy-5-nitrophenoxy}butanoic acid (Fmoc-photolabile linker) was purchased from Advanced ChemTech. DMF, DCM, and other general solvents were purchased from Fisher Scientific. DIPEA was purchased from Sigma. 5-carboxytetramethylrhodamine (5-TAMRA) was purchased from ChemPep. QSY7-maleimide was purchased from Invitrogen. N-succinimidyl 6-maleimidohexanoate was purchased from TCI America.

Ac-G-R(pbf)-T(tBu)-G-R(pbf)-R(pbf)-N(OtBu)-A-I-H(trt)-D(OtBu)-PEG-C(trt)-photolinker-K(ivDde)-K(Boc)-CONH₂ was synthesized on the TGR resin (0.2 mmol/g, 500 mg resin, 0.1 mmol scale). A standard peptide coupling protocol was used for all amino acid couplings including the Fmoc-photolabile linker. Amino acid (5 equiv/equiv resin), HCTU (5 equiv/equiv resin) and DIPEA (12 equiv/equiv resin) were mixed with resin in DMF and reacted for 10 min at room temperature using a Protein Technology International Prelude peptide synthesizer. Fmoc deprotection was achieved using 20% piperidine in DMF for 20 min at RT. The N-terminus was capped using acetic anhydride with 20% DIPEA for 20 min.

The dye labeling procedure was performed by Dr. Hsien-ming Lee. Briefly, after Lys side chain (ivDde) was deprotected and labeled with TAMRA, the peptide was cleaved from the resin and purified by HPLC. The purified TAMRA labeled peptide was then reacted with QSY7-maleimide quencher to generate the fluorescence quenched peptide.

Preparation of caging agent 28-PKA catalytic subunit conjugate. The caging agent **28** was prepared by Dr. Hsien-ming Lee. Briefly, the fluorescently quenched peptide was HPLC purified and then reacted with N-succinimidyl 6-maleimidohexanoate to install the maleimide functional group at the lysine side chain. The reaction mixture was then HPLC purified to obtain the caging agent **28**.

20 μ M mouse c-AMP dependent protein kinase (PKA) catalytic subunit α (purchased from Promega: V5161, or expressed and purified by Dr. Hsien-ming Lee) was dialyzed against the “reaction buffer” (100 mM Tris buffer with 10% glycerol, 100 mM KCl at pH 7.5) at 4 °C overnight. Two reaction solutions were prepared: (1) PKA solution: 5 μ L of 200 mM ATP and 200 mM $MgCl_2$ mixture stock solution was added to reaction buffer containing PKA (100 μ L, 20 μ M, 2.0 nmol) to furnish a solution that contained 9.5 mM ATP and 9.5 mM $MgCl_2$. (2) Caging agent solution: 2.2 eq of caging agent **28** (5 mM, 4.4 nmol, 0.8 μ L) stock in DMSO was diluted using the reaction buffer containing 10 mM ATP and 10 mM $MgCl_2$ to make a 15 μ L caging agent (266 μ M) solution. The caging agent solution was slowly added into the PKA solution and the resulting mixture was incubated at 4 °C for 12 h. The resultant caged PKA was dialyzed against PBS containing 100 μ M DTT overnight for buffer exchange, and then stored at 4 °C. Prionex was added (to 1% final concentration) to caged PKA destined for intracellular microinjection to prevent aggregation that might clog the microinjection needle. Purchased (from Sigma Aldrich) Prionex solution 10% (w/v) was dialyzed against 100 mM Tris buffer with 100 mM KCl prior to use.

SDS-PAGE analysis of caged PKA. As a consequence of the significant molecular weight associated with the caging agent **28** (3680 g/mol), the SDS-PAGE

technique provides a mean to assess the extent of PKA labeling. NuPAGE 4 - 12% Bis-Tris precast gel from Invitrogen was chosen for this purpose due to its high resolution performance. Molecular weight marker and samples (5 μ L of each protein solution was mixed with 5 μ L of 4X loading buffer, water was added up to a volume of 20 μ L) were gel loaded. Samples were loaded without heating. The gel was run at 200 V for 40 min. The gel was stained using Bio-Safe Coomassie and pictures obtained using the FluoChem system.

Labeling yield (i.e. yield of caged PKA) was estimated using SDS-PAGE analysis. In brief, the band corresponding to caged PKA was compared to that of unmodified PKA. Quantification of the bands furnishes an estimation of labeling yield for the desired caged PKA conjugate.

PKA catalytic activity measurement. PKA activity was measured as previously described (Cook et al., 1982). In brief, the assay couples the formation of ADP to the generation of pyruvate (catalyzed by pyruvate kinase), which is in turn reduced to lactate via the NADH-dependent lactate dehydrogenase. 198 μ L of the assay solution containing 50 mM Tris pH 7.5, 100 mM NaCl, 10% glycerol, 10 mM $MgCl_2$, 1 mM ATP, 1 mM DTT, 1 mM Leu-Arg-Arg-Ala-Ser-Leu-Gly (kemptide), 1 mM phosphoenolpyruvate, 0.2 mM NADH (Sigma) and 1X coupling enzymes (lactic dehydrogenase and pyruvate kinase) was added into a 200 μ L quartz cell and the NADH absorbance over time at 340 nm was measured for 1 min as the background. 2 μ L of PKA solution with unknown activity was then added into the assay mixture and the NADH absorbance decrease over time was measured. The slope of the absorbance decrease, after subtracting the background slope, directly reflects the activity of the kinase being measured.

Kinase activity as a function of irradiation time. 20 μL of 15 μM caged PKA was diluted to 60 μL (5 μM PKA) using the uncaging solution (100 mM Tris pH 7.5, 100 mM KCl, 10 mM DTT with 1% Prionex as a protein stabilizer, with freshly added DTT). The caged PKA in the uncaging solution was placed in an ice water bath and irradiated using a Hg Arc lamp in the presence of a color glass filter UG-1 (250 mW/cm^2) for different time periods (from 5 to 180 s). For every time point, 5 μL of irradiated PKA solution was aliquoted. Activity measurements were obtained using a coupled assay (Cook et al., 1982) for each time point. The activity of non-irradiated PKA was also measured. Specific activity was calculated as the slope of the change in absorbance/time divided by the PKA concentration. The specific activity of uncaged PKA is reported as a percentage of the specific activity of wild type PKA.

Mass spectrometry characterization. Both the wild type catalytic subunit of PKA and its caged counterpart were subjected to in-gel trypsin digestion prior to mass spectral analysis (MALDI-TOF and MS/MS was performed by the Proteomic core facility in University of North Carolina at Chapel Hill). In brief, the gel pieces were destained via treatment with a 1:1 mixture of CH_3CN :50 mM NH_4HCO_3 by shaking in a thermomixer for 10 min at 25 $^\circ\text{C}$ and removing the solution (3x). The gel was then “dehydrated” via three washings with pure CH_3CN (10 min at 25 $^\circ\text{C}$ in thermomixer) and then dried. The gel was then exposed to trypsin on ice for 20 min and the solution drained. The gel was subsequently incubated with 25 mM NH_4HCO_3 in a thermomixer at 36 $^\circ\text{C}$ overnight. CH_3CN was added to the solution, shaken for 10 min at RT and the combined solution transferred to an Axygen tube.

Inhibition of active site-directed caging of PKA. An assessment of whether the labeling of PKA is driven by active site recognition of the caging agent was performed by conducting the labeling reaction with caging agent **28** in the absence and presence of “PKI 5-24”, an active site-targeted reversible inhibitor (purchased from Sigma-Aldrich). The reaction was performed as described above in the **Preparation of caging agent 28-PKA catalytic subunit conjugate** section except that the reaction time was 4 h (instead of 12 h). The reactions in the presence or absence of PKI 5-24 fragment were carried out simultaneously. Absence of PKI 5-24: sequentially mix 22.2 μ L PKA solution, 22 μ L H₂O and 1.66 μ L caging agent **28**. Presence of PKI 5-24: sequentially mix 22.2 μ L PKA solution, 22 μ L PKI 5-24 (1 mM, 22 nmol, 100 eq) and 1.66 μ L caging agent **28**. The resulting mixtures were incubated at 4 °C for 4 h. After 4 h, 22 μ L of the reaction mixtures were taken out from each tube, and 0.25 μ L of 100 mM DTT was added to stop the reaction. Then 8 μ L 4X NuPAGE loading buffer was added to the mixtures, and the solutions (30.25 μ L) were gel loaded.

Cell culture. REF52 cells (provided by Professor Rudy Juliano at UNC-CH) were grown in Dulbecco’s Modified Eagle Medium supplemented with 10% fetal calf serum (FCS) and 1% P/S at 37 °C in a 5% CO₂ incubator. 24 h prior to the microscopy experiments, 2-3 X 10⁴ cells were seeded onto fibronectin-coated glass bottom plates in 10% FCS containing Leibovitz’s L-15 medium. MatTek 50 mm gridded glass bottom dishes were used for experiments requiring microinjection or photolysis. MatTek 6-well glass bottom plates were used for experiment with cell permeable reagents.

Fibronectin glass bottom plate coating was achieved by incubating 5 μ g/mL fibronectin (BD Biosciences) with the glass bottom plates for 1 h at 37 °C in a 5% CO₂

incubator. After removing the fibronectin containing buffer, the plates were let dry in a cell culture hood overnight.

Fluorescence microscopy. All fluorescence imaging experiments were performed using an inverted Olympus IX81 microscope with a Hamamatsu C8484 camera and FITC, Cy3 and Cy5.5 filter cubes (Semrock). Microinjection was performed using an Eppendorf FemtoJet and Injectman NI 2 system. Photolysis experiments were performed by centering the cell culture dish under an Oriel Hg arc lamp system (NewPort, power supply model 69907, 200 W Hg Arc lamp). A 360 nm color glass filter (300-400 nm band pass, NewPort, model UG-1) was placed on top of the cell plate cover. All imaging analyses were performed using Metamorph software.

CPT-cAMP induced stress fiber disappearance. REF52 cells were seeded on fibronectin-coated wells for 24 h prior to experiments using 6-well plates. Cells were incubated with CPT-cAMP (500 μ M) in 10% FCS L-15 medium for 30 min, washed with PBS, permeabilized with 0.1% Triton X-100/PBS for 10 min at RT, and stained with Alexa Fluor 488 phalloidin (Invitrogen) in 1% BSA containing PBS buffer for 20 min at room temperature. Fluorescent images of phalloidin-labeled actin were taken at 100 ms exposures using a FITC filter cube.

Photolysis-induced change in fluorescence of REF52 cells microinjected with caged PKA. 20 μ M caged PKA catalytic subunit with 10 μ M dextran Alexa 680 in the microinjection needle (Femtotips II, Eppendorf) was microinjected (injection pressure 100 hPa, injection time 2 s, compensation pressure 20 hPa) into REF52 cells. Cells were subsequently washed with 2 mL of 10% FCS containing L-15 medium. Images were acquired using 500 ms exposure with the Cy3 filter cube (TAMRA), furnishing initial

fluorescence prior to photolysis. The sample was illuminated (360 nm filter) under an Hg Arc lamp for 5 min. Following photolysis, the cells were allowed to recover at 37 °C for 1 h (5% CO₂ incubator) and subsequently fixed (4% paraformaldehyde/PBS for 10 min). Images of TAMRA fluorescence were then reacquired as described above. The fluorescence change upon photolysis was obtained by subtracting both the initial cell fluorescence and the photobleaching from the acquired fluorescence for each microinjected cell.

Photolysis-induced loss of stress fibers in REF52 cells microinjected with caged PKA. Following the acquisition of TAMRA fluorescence as described in the previous paragraph, the fixed cells were permeabilized in 0.1% Triton X-100/PBS (10 min), and stained with Alexa Fluor 488 phalloidin (Invitrogen) in 1% BSA/PBS (20 min). Fluorescent images of phalloidin-labeled actin were taken using a 100 ms exposure time with a FITC filter cube.

TAMRA photobleaching. Free TAMRA (50 µM in microinjection needle; injection conditions as described above with caged PKA) were microinjected into REF52 cells to measure the fluorescence decrease during photolysis and imaging. Following microinjection, the cells were washed, imaged and photolyzed in a fashion identical to that described with caged PKA. However, since free TAMRA is not fixed by paraformaldehyde, the fluorescence images of TAMRA after photolysis were performed without fixation.

Results and Discussion

Design and synthesis of the caging agent 28. The catalytic subunit (C) of PKA contains two readily modifiable Cys residues, one at the base of the active site (Cys-199) and the other approximately 20 Å removed (Cys-343) (**Fig. 4.2A**). Covalent modification of Cys-199 destroys catalytic activity and thus represents a poor choice for tagging the enzyme with a fluorophore label (Mobashery et al., 1990; Salerno and Lawrence, 1993; Yan et al., 1996; Chang et al., 1998; Curley and Lawrence, 1998). Consequently, we focused our attention on the non-active site Cys-343 moiety for this purpose. The C subunit catalyzes the phosphorylation of Ser and Thr residues ensconced within targeted sequences (-Arg-Arg-Xaa-Ser-) of protein and peptide substrates (Pinna and Ruzzene, 1996). In addition, peptide-based inhibitors have been constructed by replacing the phosphorylatable Ser moiety with a nonphosphorylatable Ala residue (Dalton and Dewey, 2006). The caging agent **28** contains a (i) validated active site-directed inhibitory peptide sequence, GRTGRRNAIHD (“PKI”) (Dalton and Dewey, 2006), (ii) a polyethylene glycol (PEG) spacer to optimally position an appended electrophilic maleimide near Cys-343, and (iii) a tripeptide cassette composed of a photolabile (PL) moiety inserted between a fluorophore and a fluorescent quencher. The cassette employed in this study [Cys(QSY7)-PL-Lys(TAMRA)], shown explicitly in the caging agent **28** (**Fig. 4.3**) and schematically in **Figs 4.2B** and **4.2C**, was derived from a library of fluorescently quenched cassettes (Lee et al., 2010a). The latter were screened to identify an arrangement of fluorophore, quencher, and photolabile moiety that optimizes the fluorescent response upon photo-cleavage. Consequently, photolysis of the covalently modified, and therefore inactive, protein kinase (**Fig. 4.2C**), is designed to both restore

enzymatic activity and simultaneously generate a fluorescent protein via release of the active site-directed PKI fragment and the appended quencher moiety (**Fig. 4.2D**).

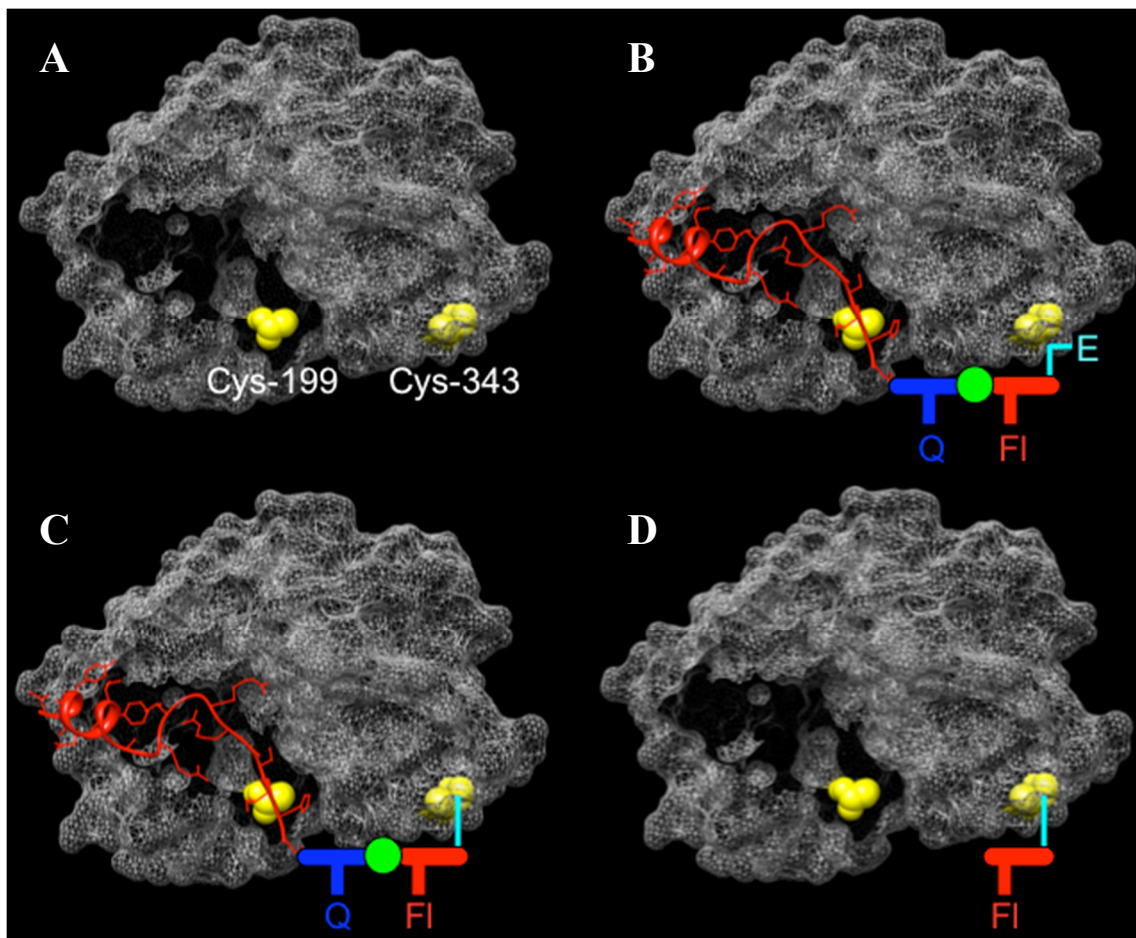


Figure 4.2 Design of the caged profluorescent PKA.

(A) Native PKA C subunit highlighting the active site Cys-199 and its non-active site Cys-343 counterpart. (B) Active site-directed alignment of the maleimide (E) of the caging agent near Cys-343. (C) Caged profluorescent PKA C subunit. (D) Photolyzed C subunit, with fluorophore remains on the protein. Q = Quencher; F = Fluorophore; ● = PL (photolabile linker).

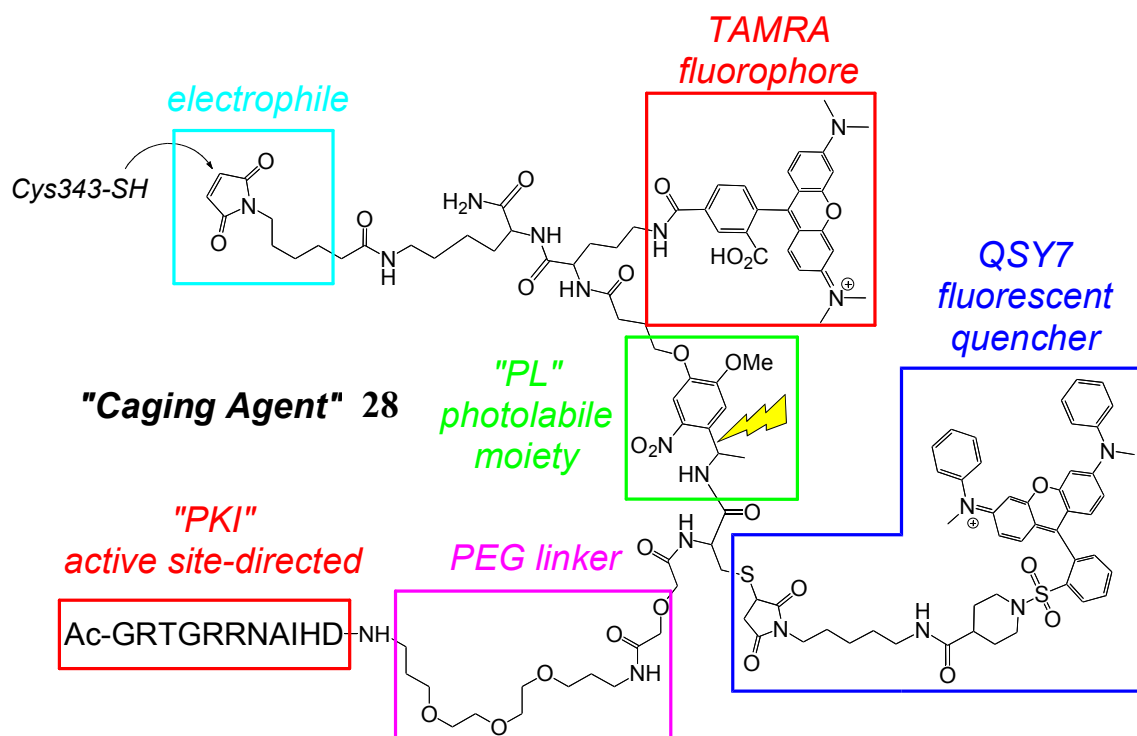


Figure 4.3 Structure of the caging agent 28.

Preparation of caged PKA catalytic subunit. The caged enzyme (<3% residual activity) was acquired by exposing the native PKA C subunit to caging agent **28** (details are described in **Preparation of caging agent 28-PKA catalytic subunit conjugate** section). To demonstrate that the labeling reaction is indeed driven by protein-ligand recognition, we compared the modification efficiency of the caging agent **28** to PKA in the presence or absence of the active site-directed reversible inhibitor PKI 5-24. As shown in **Fig. 4.4**, 25% of caged PKA was formed in the absence of reversible inhibitor, whereas the presence of reversible inhibitor competitively prohibited modification of PKA with the caging agent.

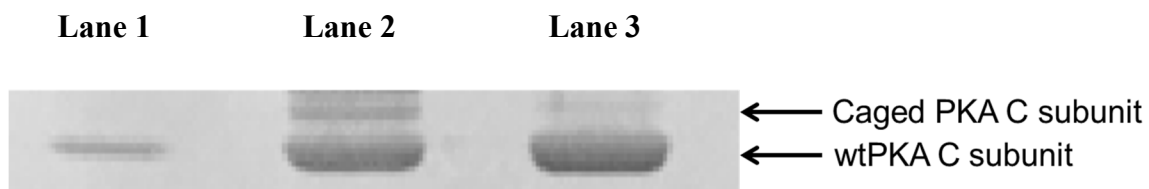
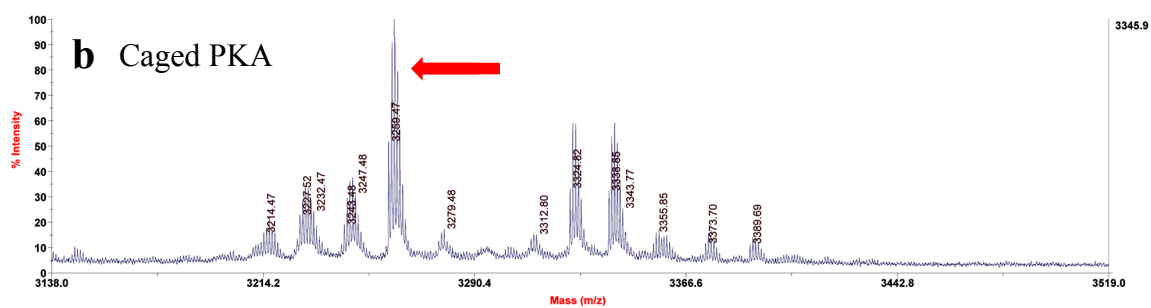
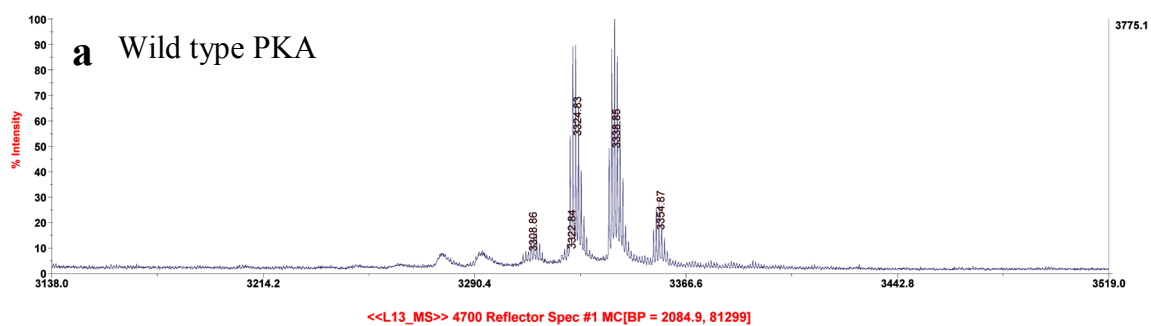
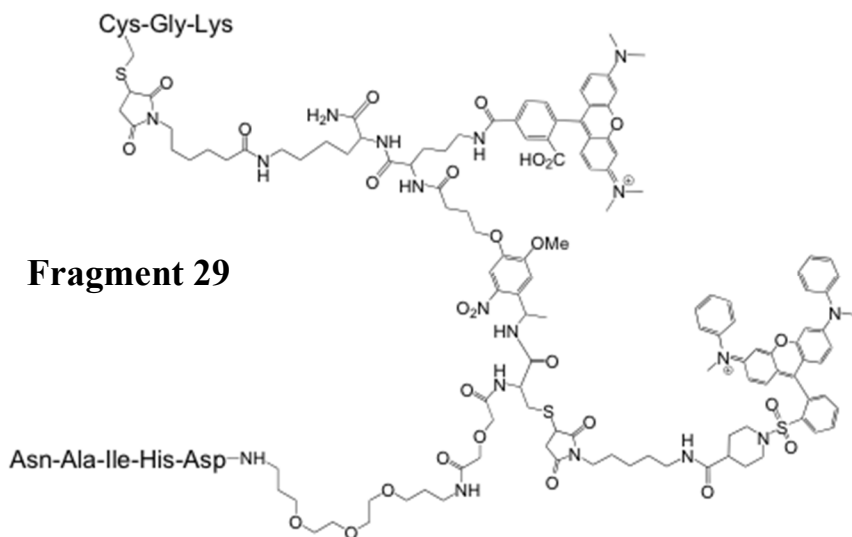


Figure 4.4 Caging agent 28 labeling PKA reaction is driven by protein-ligand recognition.

SDS-PAGE of wild type C subunit of PKA (lane 1), C subunit treated with the caging agent **28** (lane 2), and C subunit treated with the caging agent **28** in the presence of the active site-directed reversible inhibitor PKI 5-24 (lane 3) for 4 h. The densities of the bands were analyzed using ImageJ. In the absence of reversible inhibitor: caged PKA is 25% and unmodified PKA is 75%. In the presence of reversible inhibitor: caged PKA is 9.6% and unmodified PKA is 90.4%.

Mass spectrometry characterization of caged PKA. Mass spectrometric comparison of the wild type PKA and caged PKA revealed a series of unique masses for the latter. Specifically, trypsin-treated caged PKA displays a distinctive mass of 3259.45, which corresponds to a Cys-Gly-Lys containing fragment **29**, a fragment that can only be derived from the Cys343 sequence (-Asn340-Glu-Lys-Cys-Gly-Lys-Glu-Phe-Thr-Glu-Phe350) (**Fig. 4.5A**). In addition, mass spectrometric analysis of trypsinized photolyzed caged PKA revealed a distinctive mass of 1434.1, which corresponds to the fragment **30**, a fragment also can only be derived from the Cys343 sequence (**Fig. 4.5B**). Because photolysis was performed in the presence of dithiothreitol, which can convert photocleavage byproduct arylnitroso derivatives into arylamines (Dölle et al., 1980), therefore, fragment **30** contains an arylamine, and not the initially formed arylnitroso.

A



B

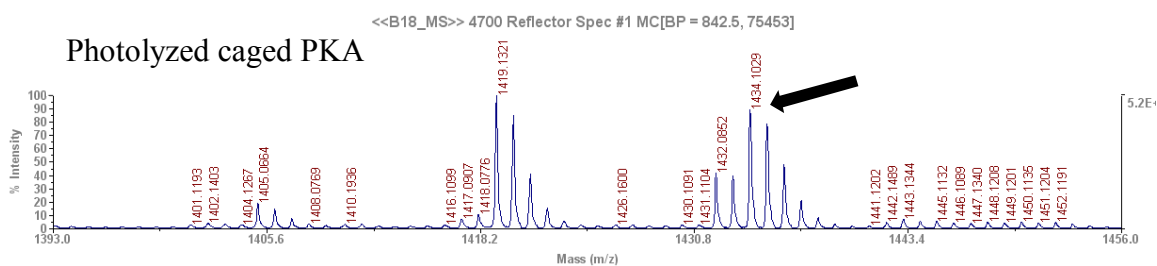
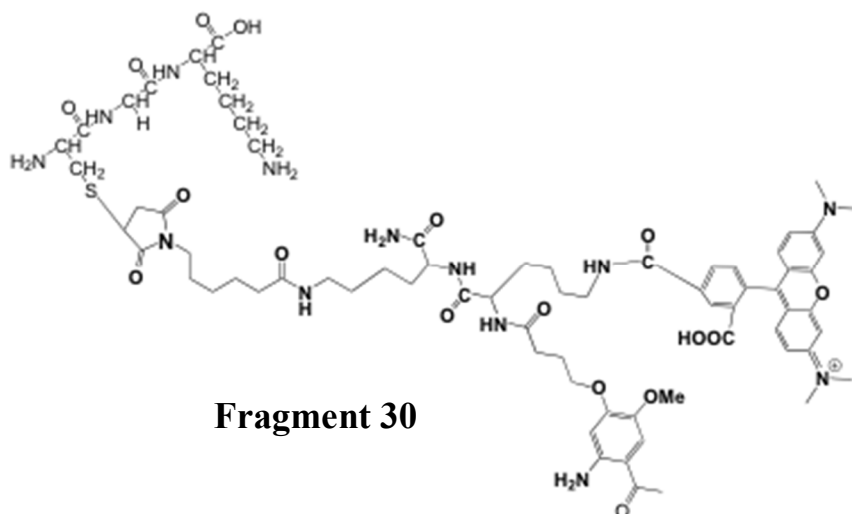


Figure 4.5 Mass spectrometry characterization of caged PKA.

(A) 3138 – 3519 m/z region of trypsin-treated (a) wild type PKA and (b) caged PKA.

Highlighted peak (red arrow) corresponds to Cys343-modified fragment **29**.

(B) 1393 - 1456 m/z region of trypsin-treated photolyzed caged PKA. Highlighted peak

(black arrow) corresponds to Cys343-modified fragment **30**.

Photolyzation of caged PKA in live cells. Stress fibers are bundles of actin that interface with focal adhesions and thereby link the cytoskeleton of the cell with the extracellular matrix. cAMP, as well as active PKA, drives the disassembly of stress fibers along with attendant morphological changes, and therefore serves as a good biological readout for PKA activation (Lamb et al., 1988; Roger et al., 1988; McNamee et al., 1995). The effect of active PKA on stress fiber disassembly is mediated via several pathways, including suppression of collagen-induced actin polymerization (in endothelial cells) (Whelan and Senger, 2003), phosphorylation and inhibition of Rho function, which is important for stress fiber formation (Kreisberg et al., 1997), and stimulation of the SHP2 (SH2-domain containing phosphotyrosine phosphatase) phosphatase activity, which negatively regulates Rho function and stress fiber integrity (Alan K, 2004).

We decided to examine the ability of caged PKA to promote stress fiber disassembly in a light-dependent fashion. We choose rat embryo fibroblasts (REF52) for our study because of its flattened cell shape and well organized actin stress fibers. We first treated REF52 cells with a cell-permeable form of cAMP (CPT-cAMP), and, as expected, we observed complete or partial loss of actin stress fibers in most cells. The cells also rounded up and left long processes, displaying a characteristic cAMP induced stellate morphology (**Fig. 4.6**) (Dong et al., 1998). Similar morphological changes were also observed in cells microinjected with wild-type PKA C subunit (**Fig. 4.7**).

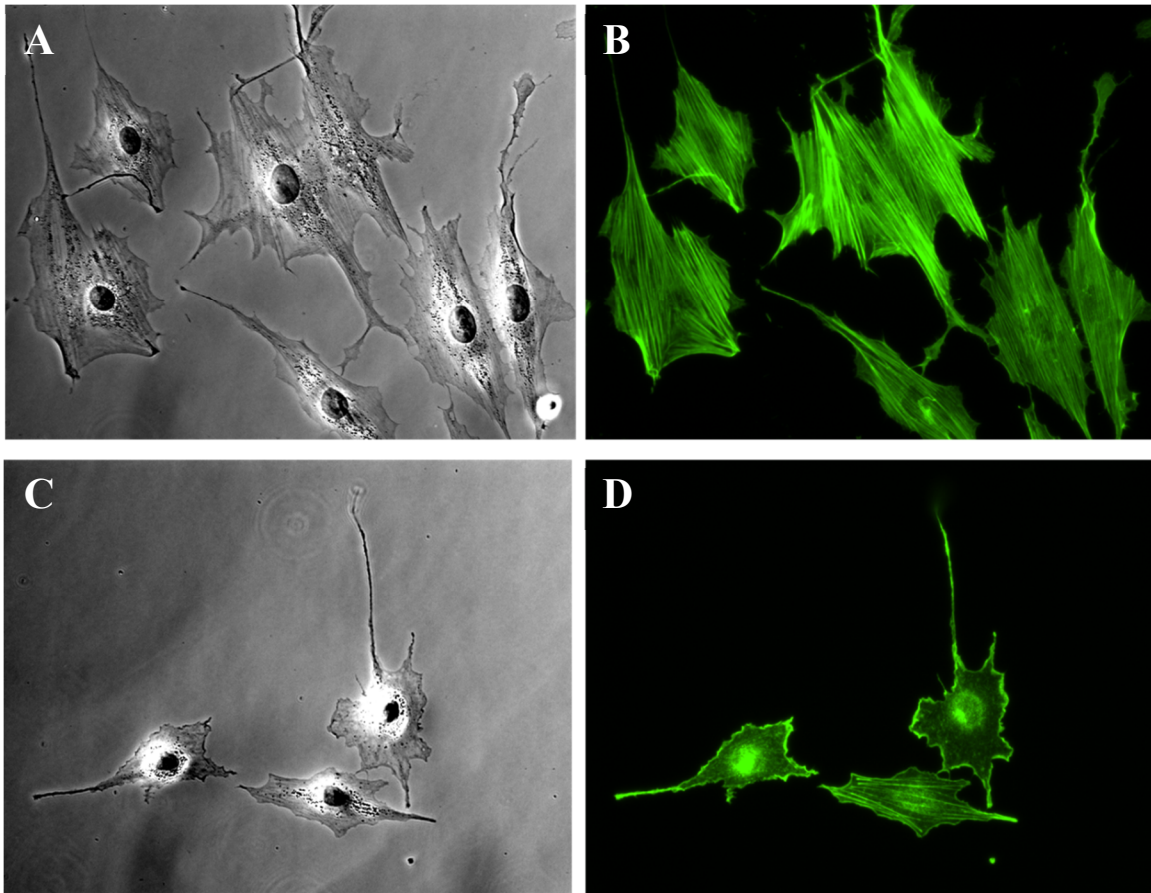


Figure 4.6 Actin staining of untreated and CPT-cAMP-treated REF52 cells.

(A, B) REF52 cells seeded on fibronectin coated plate with 10% FCS in L-15 media are flat and tightly adherent, and contain stress fibers. (C, D) Treating cells with 500 μ M CPT-cAMP in L-15 media containing 10% FCS for 30 min induces either partial or complete loss of stress fibers. The cells also round up and leave long processes, which is the characteristic stellate morphology induced by increased intracellular cAMP level. [(A) and (C) are transmitted light images; (B) and (D) are fluorescence images taken using a FITC filter cube.]

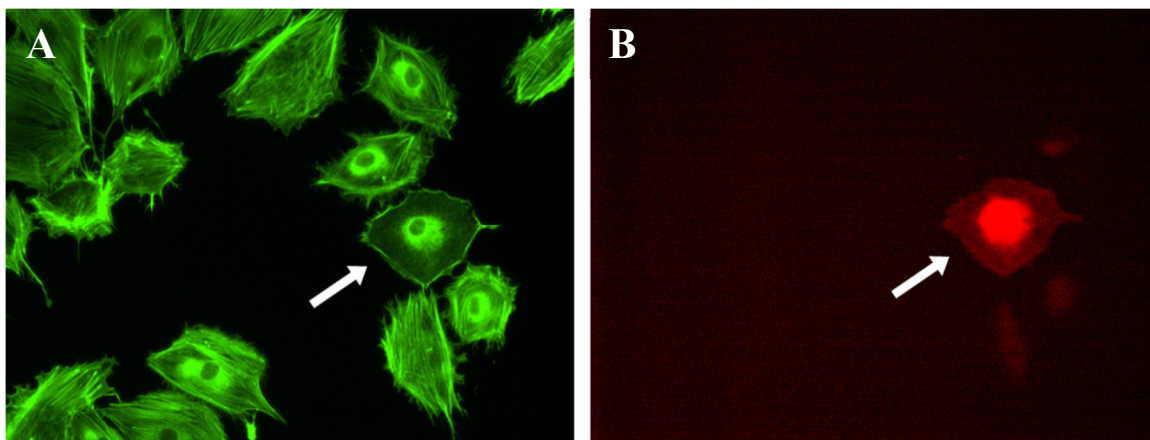


Figure 4.7 Morphology change in wtPKA injected REF52 cell.

(A) Fluorescence image (FITC filter cube) of 10 μ M wtPKA microinjected (arrow) and non-microinjected cells fixed, permeabilized and stained with phalloidin-Alexa 488. (B) Fluorescence image (Cy5.5 filter cube) of microinjected cell (arrow) showing microinjection marker dextran-Alexa 680 fluorescence. Images were taken after 1 h incubation post-microinjection and subsequent fixation. Both images are of the same field.

After demonstrating that active PKA can induce stress fiber loss and cell shape change, we examined whether the same cell behavior is induced by light using caged PKA, and at the same time observe fluorescence enhancement. To exclude the possibility that microinjection and/or light illumination might perturb cell signaling and induce unwanted cell behavior, we first examined if these two treatments have any effect on cell morphology. As shown in **Fig. 4.8**, photolysis alone does not affect REF52 cell morphology and stress fiber integrity. In addition, microinjection of REF52 cells with caged PKA, in the absence of subsequent photolysis, also has no effect on cell shape and stress fibers. Moreover, in microinjected cells, the dim TAMRA fluorescence from the caged PKA is reduced, possibly due to photobleaching during image captures. (**Fig. 4.9**).

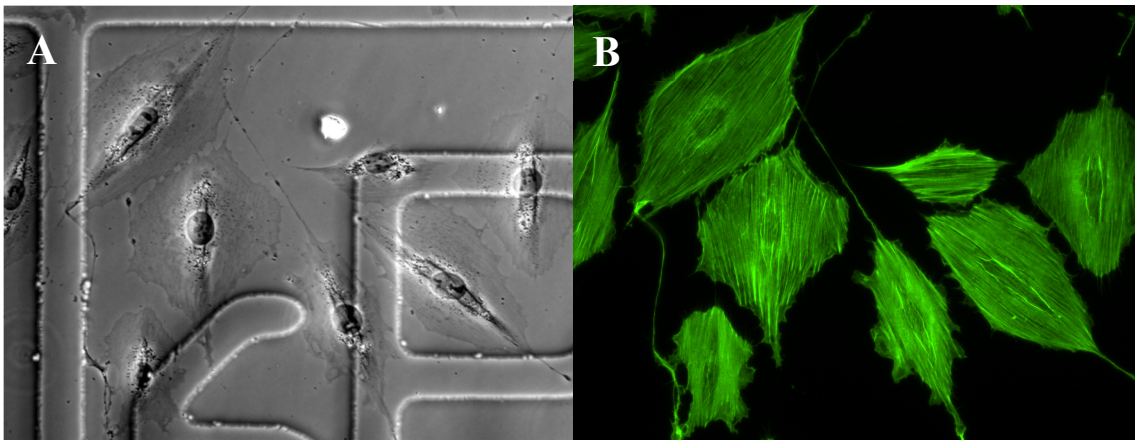


Figure 4.8 Stress fibers in photolyzed non-microinjected cells were retained.

(A) Transmitted light image of photolyzed REF52 cells. (B) REF52 cells were photolyzed for 5 min under a Hg Arc lamp, incubated for 1 h post-photolyzation and then fixed, permeabilized and stained with phalloidin-Alexa 488. Both images are of the same field.

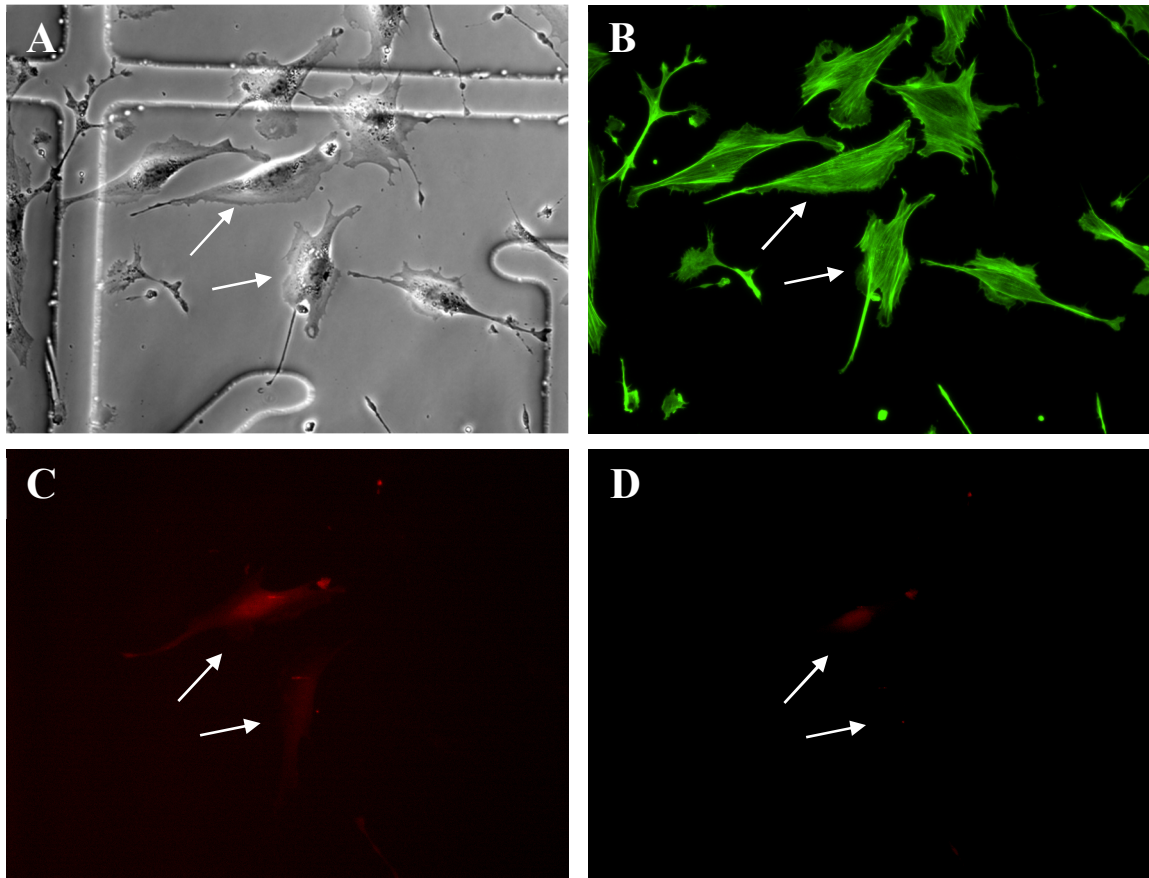


Figure 4.9 Microinjected REF52 cells in the absence of illumination.

(A) Transmitted light image of caged PKA microinjected (arrows) and non-microinjected cells incubated for 1 h after microinjection and then fixed. (B) Stress fibers in microinjected (arrows) and non-microinjected cells are retained. (C) and (D) TAMRA fluorescence intensity from the injected cells decreased 1.42-fold after fixation (without subtracting TAMRA photobleaching). [(C) Image taken immediately after microinjection; (D) image taken after 1 h incubation post-microinjection and subsequent fixation.] All images are of the same field.

In contrast, as shown in **Fig. 4.10**, cells microinjected with caged PKA, which were subsequently photolyzed for 5 min under a Hg Arc lamp, lost stress fibers. The morphological change from flat to round shape and the long processes are also apparent. At the same time, we observe a 6.2 ± 2.1 -fold (after subtracting TAMRA photobleaching control shown in **Fig. 4.11**) enhancement in TAMRA fluorescence after photolysis. The fluorescence intensity appears strongest in the nuclear region of the cells. This is because the PKA construct is freely diffusible, and therefore associated TAMRA fluorescence is strongest in the region (nuclear) where the cell has the thickest path length.

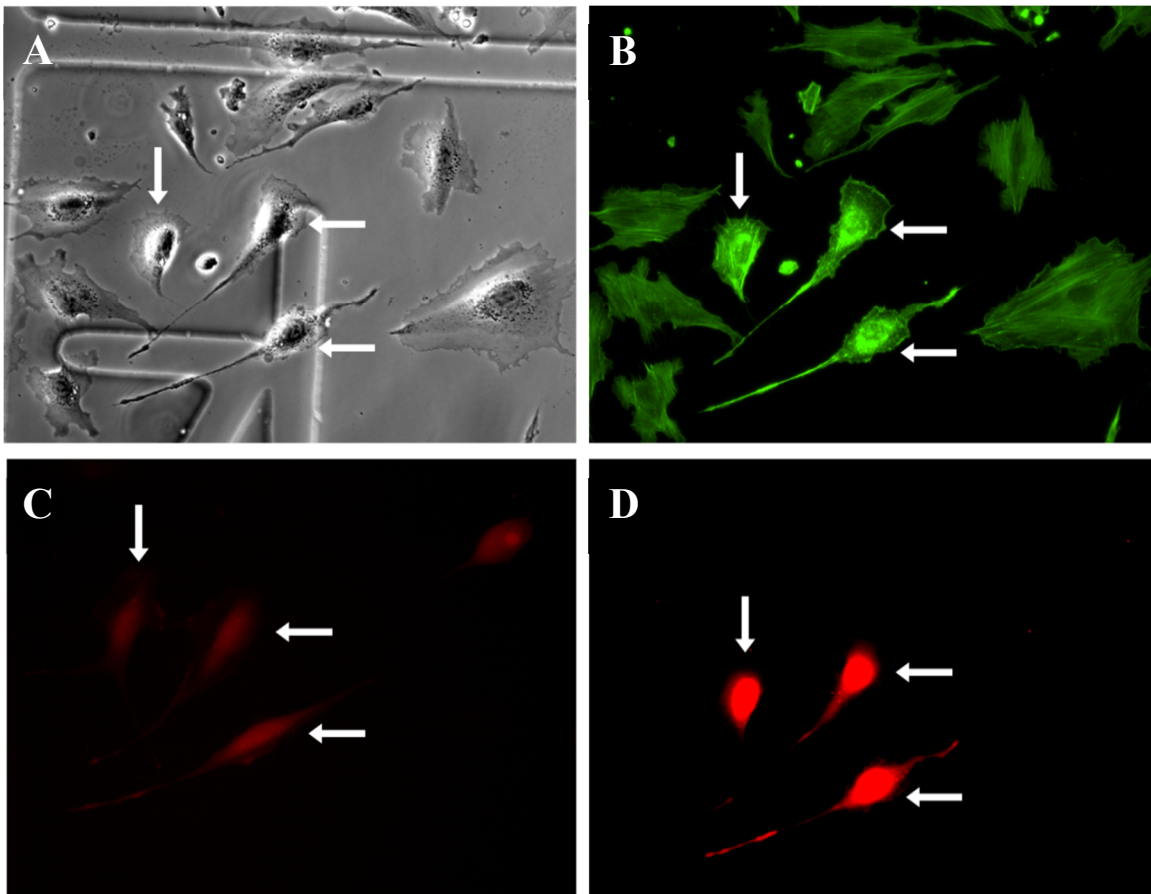


Figure 4.10 Photolysis of caged PKA induced stress fiber disappearance and fluorescence increase.

(A) Transmitted light image of caged PKA microinjected (arrows) and non-microinjected cells incubated for 1 h after photolysis and then fixed. (B) Only microinjected cells (arrows) display stress fiber loss and morphological changes upon global illumination of all cells. (C) and (D) TAMRA fluorescence intensity increases 6.2 ± 2.1 fold (after subtracting TAMRA photobleaching) upon photolysis. [(C) Image taken immediately after microinjection; (D) image taken after 1 h incubation post-microinjection and subsequent fixation.] All images are of the same field.

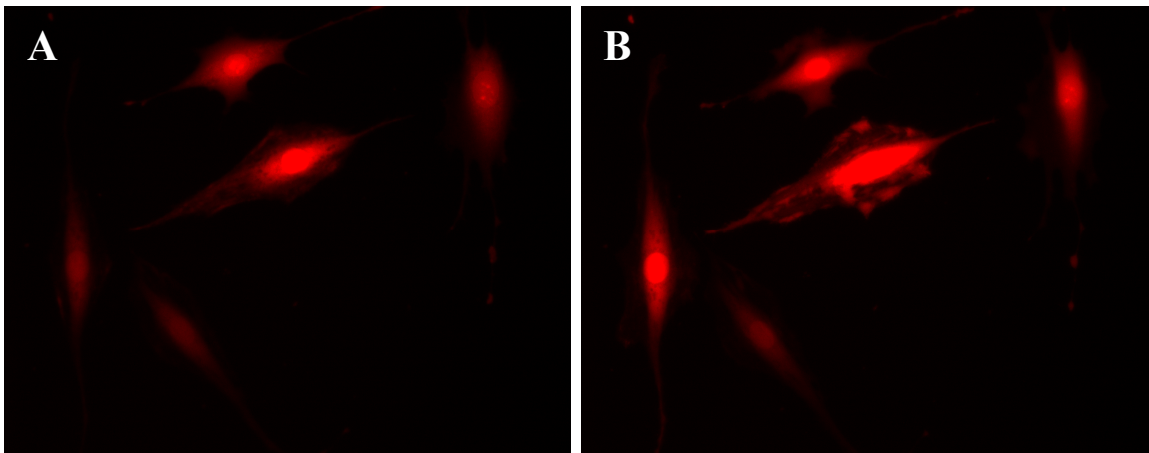


Figure 4.11 TAMRA fluorescence prior to and after photolysis.

The fluorescence intensity of TAMRA prior to (A) and after (B) photolysis was quantified and used as a photobleaching control. A 1.39 ± 0.33 fold fluorescence intensity decrease was observed (averaged from 31 cells). All images are of the same field.

Conclusions

Using the active site-directed peptide-based affinity labeling strategy, we have designed and developed a profluorescent caged PKA catalytic subunit. We have confirmed by activity measurement, protein gel analysis and mass spectrometry that the non-active site Cys-343 residue is modified. The caged PKA displays less than 3% residual activity, and photolysis results in up to 80% activity recovery and 20-fold fluorescence enhancement in the test tube. We have also successfully applied the caged PKA in living REF52 cells and observe a light-dependent loss of stress fiber integrity and the stellate morphology that is characteristic of elevated cAMP and PKA activity. Moreover, photolysis also induces a 6.2-fold TAMRA fluorescence enhancement in REF52 cells microinjected with caged PKA.

We do note that many, but not all protein kinases possess a non-active site Cys residue positioned at the Cys-343 site in PKA. However, any modifiable Cys moiety that lies outside, but within the vicinity of, the active site could potentially serve as a covalent anchoring residue. Alternatively, it is relatively straightforward to incorporate a reactive Cys at an appropriate position via site-directed mutagenesis. In addition, although microinjection is a common biological tool, only a relatively small number of cells (~100) can be treated in this fashion at any given time. By contrast, cell permeable reagents offer a more robust strategy applicable to large cell populations. Therefore, cell permeable analogs of caging agent **28**, could prove useful in this regard, since they can potentially modify the target protein in situ.

References

- Abram, C.L., and Courtneidge, S.A. (2000). Src family tyrosine kinases and growth factor signaling. *Exp. Cell Res.* 254, 1–13.
- Alan K, H. (2004). Regulation of actin-based cell migration by cAMP/PKA. *Biochimica Et Biophysica Acta (BBA) - Molecular Cell Research* 1692, 159–174.
- Alessi, D.R., James, S.R., Downes, C.P., Holmes, A.B., Gaffney, P.R., Reese, C.B., and Cohen, P. (1997). Characterization of a 3-phosphoinositide-dependent protein kinase which phosphorylates and activates protein kinase Balph. *Curr. Biol.* 7, 261–269.
- Allen, M.D., and Zhang, J. (2006). Subcellular dynamics of protein kinase A activity visualized by FRET-based reporters. *Biochem. Biophys. Res. Commun.* 348, 716–721.
- Alonso, G., Koegl, M., Mazurenko, N., and Courtneidge, S.A. (1995). Sequence Requirements for Binding of Src Family Tyrosine Kinases to Activated Growth Factor Receptors. *Journal of Biological Chemistry* 270, 9840 –9848.
- Van Amersfoort, E.S., and Van Strijp, J.A.G. (1994). Evaluation of a flow cytometric fluorescence quenching assay of phagocytosis of sensitized sheep erythrocytes by polymorphonuclear leukocytes. *Cytometry* 17, 294–301.
- Autero, M., Heiska, L., Rönstrand, L., Vaheri, A., Gahmberg, C.G., and Carpen, O. (2003). Ezrin is a substrate for Lck in T cells. *FEBS Lett.* 535, 82–86.
- Ayala, G., Thompson, T., Yang, G., Frolov, A., Li, R., Scardino, P., Otori, M., Wheeler, T., and Harper, W. (2004). High levels of phosphorylated form of Akt-1 in prostate cancer and non-neoplastic prostate tissues are strong predictors of biochemical recurrence. *Clin. Cancer Res.* 10, 6572–6578.
- Badour, K., Zhang, J., Shi, F., Leng, Y., Collins, M., and Siminovitch, K.A. (2004). Fyn and PTP-PEST-mediated Regulation of Wiskott-Aldrich Syndrome Protein (WASp) Tyrosine Phosphorylation Is Required for Coupling T Cell Antigen Receptor Engagement to WASp Effector Function and T Cell Activation. *The Journal of Experimental Medicine* 199, 99–112.
- BD Biosciences (2006). BD Calcein AM Fluorescent Dye.
- BD Biosciences (2008). BD Matrigel Basement Membrane Matrix.
- BD Biosciences (2010). BD FluoroBlok Cell Culture Inserts Fluorescence blocking membranes and optimized assay systems.
- Behrens, J., Vakaet, L., Friis, R., Winterhager, E., Van Roy, F., Mareel, M.M., and Birchmeier, W. (1993). Loss of epithelial differentiation and gain of invasiveness correlates with tyrosine phosphorylation of the E-cadherin/beta-catenin complex in cells transformed with a temperature-sensitive v-SRC gene. *J. Cell Biol.* 120, 757–766.

- Belsches, A.P., Haskell, M.D., and Parsons, S.J. (1997). Role of c-Src tyrosine kinase in EGF-induced mitogenesis. *Front. Biosci.* 2, d501–518.
- Benati, D., and Baldari, C.T. (2008). SRC family kinases as potential therapeutic targets for malignancies and immunological disorders. *Curr. Med. Chem.* 15, 1154–1165.
- Berrier, A.L., and Yamada, K.M. (2007). Cell-matrix adhesion. *J. Cell. Physiol.* 213, 565–573.
- Bhatnagar, N., Li, X., Padi, S.K.R., Zhang, Q., Tang, M., and Guo, B. (2010). Downregulation of miR-205 and miR-31 confers resistance to chemotherapy-induced apoptosis in prostate cancer cells. *Cell Death and Dis* 1, e105.
- Boerner, R.J., Kassel, D.B., Barker, S.C., Ellis, B., DeLacy, P., and Knight, W.B. (1996). Correlation of the Phosphorylation States of pp60c-src with Tyrosine Kinase Activity: The Intramolecular pY530–SH2 Complex Retains Significant Activity If Y419 Is Phosphorylated†. *Biochemistry* 35, 9519–9525.
- Boggon, T.J., and Eck, M.J. (2004). Structure and regulation of Src family kinases. *Oncogene* 23, 7918–7927.
- Bolenz, C., Gupta, A., Hotze, T., Ho, R., Cadeddu, J.A., Roehrborn, C.G., and Lotan, Y. (2010). Cost comparison of robotic, laparoscopic, and open radical prostatectomy for prostate cancer. *Eur. Urol.* 57, 453–458.
- Borland, L.M., Kottegoda, S., Phillips, K.S., and Allbritton, N.L. (2008). Chemical analysis of single cells. *Annu Rev Anal Chem (Palo Alto Calif)* 1, 191–227.
- Bowden, E.T., Onikoyi, E., Slack, R., Myoui, A., Yoneda, T., Yamada, K.M., and Mueller, S.C. (2006). Co-localization of cortactin and phosphotyrosine identifies active invadopodia in human breast cancer cells. *Exp. Cell Res.* 312, 1240–1253.
- Bozinovski, S., Cristiano, B.E., Marmy-Conus, N., and Pearson, R.B. (2002). The synthetic peptide RPRAATF allows specific assay of Akt activity in cell lysates. *Anal. Biochem.* 305, 32–39.
- Braunwaler, A.F., Yarwood, D.R., Hall, T., Missbach, M., Lipson, K.E., and Sills, M.A. (1996). A solid-phase assay for the determination of protein tyrosine kinase activity of c-src using scintillating microtitration plates. *Anal. Biochem.* 234, 23–26.
- Bromann, P.A., Korkaya, H., and Courtneidge, S.A. (2004). The interplay between Src family kinases and receptor tyrosine kinases. *Oncogene* 23, 7957–7968.
- Buccione, R., Caldieri, G., and Ayala, I. (2009). Invadopodia: specialized tumor cell structures for the focal degradation of the extracellular matrix. *Cancer Metastasis Rev.* 28, 137–149.

- Calleja, V., Alcor, D., Laguerre, M., Park, J., Vojnovic, B., Hemmings, B.A., Downward, J., Parker, P.J., and Larijani, B. (2007). Intramolecular and intermolecular interactions of protein kinase B define its activation in vivo. *PLoS Biol.* 5, e95.
- Calleja, V., Ameer-Beg, S.M., Vojnovic, B., Woscholski, R., Downward, J., and Larijani, B. (2003). Monitoring conformational changes of proteins in cells by fluorescence lifetime imaging microscopy. *Biochem. J.* 372, 33–40.
- Carrera, A.C., Paradis, H., Borlado, L.R., Roberts, T.M., and Martinez, C. (1995). Lck unique domain influences Lck specificity and biological function. *J. Biol. Chem.* 270, 3385–3391.
- Carrigan, C.N., and Imperiali, B. (2005). The engineering of membrane-permeable peptides. *Analytical Biochemistry* 341, 290–298.
- Chakrabarti, R., Pfeiffer, N.E., Wylie, D.E., and Schuster, S.M. (1989). Incorporation of monoclonal antibodies into cells by osmotic permeabilization. Effect on cellular metabolism. *J. Biol. Chem.* 264, 8214–8221.
- Chang, C., Fernandez, T., Panchal, R., and Bayley, H. (1998). Caged Catalytic Subunit of cAMP-Dependent Protein Kinase. *J. Am. Chem. Soc.* 120, 7661–7662.
- Chang, C.Y., Niblack, B., Walker, B., and Bayley, H. (1995). A photogenerated pore-forming protein. *Chem. Biol.* 2, 391–400.
- Chang, Y.-M., Bai, L., Liu, S., Yang, J.C., Kung, H.-J., and Evans, C.P. (2008). Src family kinase oncogenic potential and pathways in prostate cancer as revealed by AZD0530. *Oncogene* 27, 6365–6375.
- Chang, Y.-M., Kung, H.-J., and Evans, C.P. (2007). Nonreceptor Tyrosine Kinases in Prostate Cancer. *Neoplasia* 9, 90–100.
- Chen, C.-A., Yeh, R.-H., and Lawrence, D.S. (2002). Design and Synthesis of a Fluorescent Reporter of Protein Kinase Activity. *J. Am. Chem. Soc.* 124, 3840–3841.
- Chen, H., Ahsan, S.S., Santiago-Berrios, M.B., Abruña, H.D., and Webb, W.W. (2010). Mechanisms of Quenching of Alexa Fluorophores by Natural Amino Acids. *J. Am. Chem. Soc.* 132, 7244–7245.
- Chen, R., Kim, O., Yang, J., Sato, K., Eisenmann, K.M., McCarthy, J., Chen, H., and Qiu, Y. (2001a). Regulation of Akt/PKB activation by tyrosine phosphorylation. *J. Biol. Chem.* 276, 31858–31862.
- Chen, X., Thakkar, H., Tyan, F., Gim, S., Robinson, H., Lee, C., Pandey, S.K., Nwokorie, C., Onwudiwe, N., and Srivastava, R.K. (2001b). Constitutively active Akt is an important regulator of TRAIL sensitivity in prostate cancer. *Oncogene* 20, 6073–6083.

Collins, M., Bartelt, R.R., and Houtman, J.C.D. (2010a). T cell receptor activation leads to two distinct phases of Pyk2 activation and actin cytoskeletal rearrangement in human T cells. *Mol. Immunol.* *47*, 1665–1674.

Collins, M., Tremblay, M., Chapman, N., Curtiss, M., Rothman, P.B., and Houtman, J.C.D. (2010b). The T cell receptor-mediated phosphorylation of Pyk2 tyrosines 402 and 580 occurs via a distinct mechanism than other receptor systems. *J. Leukoc. Biol.* *87*, 691–701.

Cook, P.F., Neville, M.E., Jr, Vrana, K.E., Hartl, F.T., and Roskoski, R., Jr (1982). Adenosine cyclic 3',5'-monophosphate dependent protein kinase: kinetic mechanism for the bovine skeletal muscle catalytic subunit. *Biochemistry* *21*, 5794–5799.

Curley, K., and Lawrence, D.S. (1998). Photoactivation of a Signal Transduction Pathway in Living Cells. *J. Am. Chem. Soc.* *120*, 8573–8574.

Dalton, G.D., and Dewey, W.L. (2006). Protein kinase inhibitor peptide (PKI): a family of endogenous neuropeptides that modulate neuronal cAMP-dependent protein kinase function. *Neuropeptides* *40*, 23–34.

Danhauser-Riedl, S., Warmuth, M., Druker, B.J., Emmerich, B., and Hallek, M. (1996). Activation of Src kinases p53/56lyn and p59hck by p210bcr/abl in myeloid cells. *Cancer Res.* *56*, 3589–3596.

Dar, A.C., Lopez, M.S., and Shokat, K.M. (2008). Small Molecule Recognition of c-Src via the Imatinib-Binding Conformation. *Chemistry & Biology* *15*, 1015–1022.

Datta, S., and Milner, J.D. (2011). Altered T-cell receptor signaling in the pathogenesis of allergic disease. *J. Allergy Clin. Immunol.* *127*, 351–354.

Davidson, D., Schraven, B., and Veillette, A. (2007). PAG-Associated FynT Regulates Calcium Signaling and Promotes Anergy in T Lymphocytes. *Molecular and Cellular Biology* *27*, 1960–1973.

Denny, M.F., Patai, B., and Straus, D.B. (2000). Differential T-Cell Antigen Receptor Signaling Mediated by the Src Family Kinases Lck and Fyn. *Molecular and Cellular Biology* *20*, 1426–1435.

Dimri, M., Naramura, M., Duan, L., Chen, J., Ortega-Cava, C., Chen, G., Goswami, R., Fernandes, N., Gao, Q., Dimri, G.P., et al. (2007). Modeling Breast Cancer–Associated c-Src and EGFR Overexpression in Human MECs: c-Src and EGFR Cooperatively Promote Aberrant Three-dimensional Acinar Structure and Invasive Behavior. *Cancer Res* *67*, 4164–4172.

Dölle, B., Töpner, W., and Neumann, H.G. (1980). Reaction of aryl nitroso compounds with mercaptans. *Xenobiotica* *10*, 527–536.

- Dong, J.-M., Leung, T., Manser, E., and Lim, L. (1998). cAMP-induced Morphological Changes Are Counteracted by the Activated RhoA Small GTPase and the Rho Kinase ROK α . *J. Biol. Chem.* 273, 22554–22562.
- Eck, M.J., Shoelson, S.E., and Harrison, S.C. (1993). Recognition of a high-affinity phosphotyrosyl peptide by the Src homology-2 domain of p56lck. 362, 87.
- Edwards, J. (2010). Src kinase inhibitors: an emerging therapeutic treatment option for prostate cancer. *Expert Opin. Investig. Drugs* 19, 605–614.
- Eliceiri, B.P., Puente, X.S., Hood, J.D., Stupack, D.G., Schlaepfer, D.D., Huang, X.Z., Sheppard, D., and Cheresch, D.A. (2002). Src-Mediated Coupling of Focal Adhesion Kinase to Integrin $\text{Av}\beta 5$ in Vascular Endothelial Growth Factor Signaling. *J Cell Biol* 157, 149–160.
- Ellis-Davies, G.C.R. (2007). Caged compounds: photorelease technology for control of cellular chemistry and physiology. *Nat Meth* 4, 619–628.
- Erickson, J.R., Patel, R., Ferguson, A., Bossuyt, J., and Bers, D.M. (2011). Fluorescence resonance energy transfer-based sensor Camui provides new insight into mechanisms of calcium/calmodulin-dependent protein kinase II activation in intact cardiomyocytes. *Circ. Res.* 109, 729–738.
- Faltynek, C.R., Schroeder, J., Mauvais, P., Miller, D., Wang, S., Murphy, D., Lehr, R., Kelley, M., Maycock, A., and Michne, W. (1995). Damnacanthal is a highly potent, selective inhibitor of p56lck tyrosine kinase activity. *Biochemistry* 34, 12404–12410.
- Feng, S., Chen, J.K., Yu, H., Simon, J.A., and Schreiber, S.L. (1994). Two binding orientations for peptides to the Src SH3 domain: development of a general model for SH3-ligand interactions. *Science* 266, 1241–1247.
- Feshchenko, E.A., Langdon, W.Y., and Tsygankov, A.Y. (1998). Fyn, Yes, and Syk Phosphorylation Sites in c-Cbl Map to the Same Tyrosine Residues That Become Phosphorylated in Activated T Cells. *J. Biol. Chem.* 273, 8323–8331.
- Feuillet, V., Semichon, M., Restouin, A., Harriague, J., Janzen, J., Magee, A., Collette, Y., and Bismuth, G. (2002). The distinct capacity of Fyn and Lck to phosphorylate Sam68 in T cells is essentially governed by SH3/SH2-catalytic domain linker interactions. *Oncogene* 21, 7205–7213.
- Filby, A., Seddon, B., Kleczkowska, J., Salmond, R., Tomlinson, P., Smida, M., Lindquist, J.A., Schraven, B., and Zamoyska, R. (2007). Fyn regulates the duration of TCR engagement needed for commitment to effector function. *J. Immunol.* 179, 4635–4644.
- Filipp, D., Moemeni, B., Ferzoco, A., Kathirkamathamby, K., Zhang, J., Ballek, O., Davidson, D., Veillette, A., and Julius, M. (2008). Lck-dependent Fyn activation requires

C terminus-dependent targeting of kinase-active Lck to lipid rafts. *J. Biol. Chem.* **283**, 26409–26422.

Filipp, D., Zhang, J., Leung, B.L., Shaw, A., Levin, S.D., Veillette, A., and Julius, M. (2003). Regulation of Fyn through translocation of activated Lck into lipid rafts. *J. Exp. Med.* **197**, 1221–1227.

Fizazi, K. (2007). The role of Src in prostate cancer. *Annals of Oncology* **18**, 1765–1773.

Frame, M.C. (2002). Src in cancer: deregulation and consequences for cell behaviour. *Biochimica Et Biophysica Acta (BBA) - Reviews on Cancer* **1602**, 114–130.

Fujioka, A., Terai, K., Itoh, R.E., Aoki, K., Nakamura, T., Kuroda, S., Nishida, E., and Matsuda, M. (2006). Dynamics of the Ras/ERK MAPK Cascade as Monitored by Fluorescent Probes. *J. Biol. Chem.* **281**, 8917–8926.

Gao, X., Loggie, B.W., and Nawaz, Z. (2002). The roles of sex steroid receptor coregulators in cancer. *Molecular Cancer* **1**, 7.

Geho, D.H., Bandle, R.W., Clair, T., and Liotta, L.A. (2005). Physiological Mechanisms of Tumor-Cell Invasion and Migration. *Physiology* **20**, 194–200.

Georgianna, W.E., Lusic, H., McIver, A.L., and Deiters, A. (2010). Photocleavable Polyethylene Glycol for the Light-Regulation of Protein Function. *Bioconjugate Chem.* **21**, 1404–1407.

Ghosh, M., Song, X., Mouneimne, G., Sidani, M., Lawrence, D.S., and Condeelis, J.S. (2004). Cofilin promotes actin polymerization and defines the direction of cell motility. *Science* **304**, 743–746.

Ghosh, P.M., Malik, S., Bedolla, R., and Kreisberg, J.I. (2003). Akt in prostate cancer: possible role in androgen-independence. *Curr. Drug Metab.* **4**, 487–496.

Golan, R., Zehavi, U., Naim, M., Patchornik, A., and Smirnoff, P. (1996). Inhibition of *Escherichia coli* β -galactosidase by 2-nitro-1-(4,5-dimethoxy-2-nitrophenyl)ethyl, a photoreversible thiol label. *Biochimica Et Biophysica Acta (BBA) - Protein Structure and Molecular Enzymology* **1293**, 238–242.

González-Vera, J.A. (2012). Probing the kinome in real time with fluorescent peptides. *Chemical Society Reviews* **41**, 1652–1664.

González-Vera, J.A., Luković, E., and Imperiali, B. (2009). Synthesis of red-shifted 8-hydroxyquinoline derivatives using click chemistry and their incorporation into phosphorylation chemosensors. *J. Org. Chem.* **74**, 7309–7314.

Gora-Tybor, J., and Robak, T. (2008). Targeted drugs in chronic myeloid leukemia. *Curr. Med. Chem.* **15**, 3036–3051.

- Gorostiza, P., and Isacoff, E.Y. (2008). Optical Switches for Remote and Noninvasive Control of Cell Signaling. *Science* 322, 395–399.
- Green, T.P., Fennell, M., Whittaker, R., Curwen, J., Jacobs, V., Allen, J., Logie, A., Hargreaves, J., Hickinson, D.M., Wilkinson, R.W., et al. (2009). Preclinical anticancer activity of the potent, oral Src inhibitor AZD0530. *Molecular Oncology* 3, 248–261.
- Guarino, M. (2009). Src signaling in cancer invasion. *J. Cell. Physiol.* n/a-n/a.
- Gulyani, A., Vitriol, E., Allen, R., Wu, J., Gremyachinskiy, D., Lewis, S., Dewar, B., Graves, L.M., Kay, B.K., Kuhlman, B., et al. (2011). A biosensor generated via high-throughput screening quantifies cell edge Src dynamics. *Nat. Chem. Biol.* 7, 437–444.
- Hah, J.-M., Sharma, V., Li, H., and Lawrence, D.S. (2006). Acquisition of a “Group A”-Selective Src Kinase Inhibitor via a Global Targeting Strategy. *Journal of the American Chemical Society* 128, 5996–5997.
- Hahn, M.E., and Muir, T.W. (2004). Photocontrol of Smad2, a Multiphosphorylated Cell-Signaling Protein, through Caging of Activating Phosphoserines. *Angewandte Chemie International Edition* 43, 5800–5803.
- Hahn, M.E., Pellois, J.-P., Vila-Perelló, M., and Muir, T.W. (2007). Tunable photoactivation of a post-translationally modified signaling protein and its unmodified counterpart in live cells. *Chembiochem* 8, 2100–2105.
- Hakak, Y., and Martin, G.S. (1999). Ubiquitin-dependent degradation of active Src. *Curr. Biol* 9, 1039–1042.
- Harris, K.F., Shoji, I., Cooper, E.M., Kumar, S., Oda, H., and Howley, P.M. (1999). Ubiquitin-mediated degradation of active Src tyrosine kinase. *Proc Natl Acad Sci U S A* 96, 13738–13743.
- Harvey, J.H., and Trauner, D. (2008). Regulating Enzymatic Activity with a Photoswitchable Affinity Label. *ChemBioChem* 9, 191–193.
- zur Hausen, J.D., Burn, P., and Amrein, K.E. (1997). Co-localization of Fyn with CD3 complex, CD45 or CD28 depends on different mechanisms. *European Journal of Immunology* 27, 2643–2649.
- Hiscox, S., Morgan, L., Green, T., and Nicholson, R.I. (2006). Src as a therapeutic target in anti-hormone/anti-growth factor-resistant breast cancer. *Endocr. Relat. Cancer* 13 Suppl 1, S53–59.
- HSIEH, T.-C., and WU, J.M. (2009). Targeting CWR22Rv1 Prostate Cancer Cell Proliferation and Gene Expression by Combinations of the Phytochemicals EGCG, Genistein and Quercetin. *Anticancer Research* 29, 4025–4032.

- Huveneers, S., and Danen, E.H.J. (2009). Adhesion Signaling – Crosstalk Between Integrins, Src and Rho. *J Cell Sci* 122, 1059–1069.
- Irby, R.B., Mao, W., Coppola, D., Kang, J., Loubeau, J.M., Trudeau, W., Karl, R., Fujita, D.J., Jove, R., and Yeatman, T.J. (1999). Activating SRC mutation in a subset of advanced human colon cancers. *Nat. Genet.* 21, 187–190.
- Jabeen, R., Payne, D., Wiktorowicz, J., Mohammad, A., and Petersen, J. (2006). Capillary electrophoresis and the clinical laboratory. *Electrophoresis* 27, 2413–2438.
- Jia, C.Y.H., Nie, J., Wu, C., Li, C., and Li, S.S.-C. (2005). Novel Src homology 3 domain-binding motifs identified from proteomic screen of a Pro-rich region. *Mol. Cell Proteomics* 4, 1155–1166.
- Jiang, Y., and Cheng, H. (2007). Evidence of LAT as a dual substrate for Lck and Syk in T lymphocytes. *Leuk. Res.* 31, 541–545.
- Kaneko, T., Li, L., and Li, S.S.-C. (2008). The SH3 domain--a family of versatile peptide- and protein-recognition module. *Front. Biosci.* 13, 4938–4952.
- Karginov, A.V., Zou, Y., Shirvanyants, D., Kota, P., Dokholyan, N.V., Young, D.D., Hahn, K.M., and Deiters, A. (2010). Light Regulation of Protein Dimerization and Kinase Activity in Living Cells Using Photocaged Rapamycin and Engineered FKBP. *J. Am. Chem. Soc.* 133, 420–423.
- Kawakami, T., Cheng, H., Hashiro, S., Nomura, Y., Tsukiji, S., Furuta, T., and Nagamune, T. (2008). A caged phosphopeptide-based approach for photochemical activation of kinases in living cells. *Chembiochem* 9, 1583–1586.
- Kelley, L.C., Ammer, A.G., Hayes, K.E., Martin, K.H., Machida, K., Jia, L., Mayer, B.J., and Weed, S.A. (2010). Oncogenic Src requires a wild-type counterpart to regulate invadopodia maturation. *J. Cell. Sci.* 123, 3923–3932.
- Kennedy, M.J., Hughes, R.M., Peteya, L.A., Schwartz, J.W., Ehlers, M.D., and Tucker, C.L. (2010). Rapid blue-light-mediated induction of protein interactions in living cells. *Nature Methods* 7, 973–975.
- Kim, L.C., Song, L., and Haura, E.B. (2009). Src kinases as therapeutic targets for cancer. *Nat Rev Clin Oncol* 6, 587–595.
- Kim, P.W., Sun, Z.-Y.J., Blacklow, S.C., Wagner, G., and Eck, M.J. (2003). A zinc clasp structure tethers Lck to T cell coreceptors CD4 and CD8. *Science* 301, 1725–1728.
- Kong, M., Mounier, C., Dumas, V., and Posner, B.I. (2003). Epidermal growth factor-induced DNA synthesis. Key role for Src phosphorylation of the docking protein Gab2. *J. Biol. Chem.* 278, 5837–5844.

- Kottegoda, S., Aoto, P.C., Sims, C.E., and Allbritton, N.L. (2008). Biarsenical–Tetracysteine Motif as a Fluorescent Tag for Detection in Capillary Electrophoresis. *Anal. Chem.* *80*, 5358–5366.
- Kovarik, M.L., and Allbritton, N.L. (2011). Measuring enzyme activity in single cells. *Trends Biotechnol.* *29*, 222–230.
- Kreisberg, J.I., Ghosh-Choudhury, N., Radnik, R.A., and Schwartz, M.A. (1997). Role of Rho and Myosin Phosphorylation in Actin Stress Fiber Assembly in Mesangial Cells. *Am J Physiol Renal Physiol* *273*, F283–F288.
- Kremers, G.-J., Piston, D.W., and Davidson, M.W. Nikon MicroscopyU | Fluorescence Microscopy | FRET Basics.
- Kunkel, M.T., Ni, Q., Tsien, R.Y., Zhang, J., and Newton, A.C. (2005). Spatio-Temporal Dynamics of Protein Kinase B/Akt Signaling Revealed by a Genetically Encoded Fluorescent Reporter. *J. Biol. Chem.* *280*, 5581–5587.
- Kuo, L., Chang, H.-C., Leu, T.-H., Maa, M.-C., and Hung, W.-C. (2006). Src oncogene activates MMP-2 expression via the ERK/Sp1 pathway. *J. Cell. Physiol.* *207*, 729–734.
- Lamb, N.J., Fernandez, A., Conti, M.A., Adelstein, R., Glass, D.B., Welch, W.J., and Feramisco, J.R. (1988). Regulation of actin microfilament integrity in living nonmuscle cells by the cAMP-dependent protein kinase and the myosin light chain kinase. *J. Cell Biol.* *106*, 1955–1971.
- Lawrence, D.S., and Wang, Q. (2007). Seeing is believing: peptide-based fluorescent sensors of protein tyrosine kinase activity. *Chembiochem* *8*, 373–378.
- Lee, H.-M., Larson, D.R., and Lawrence, D.S. (2009). Illuminating the chemistry of life: design, synthesis, and applications of “caged” and related photoresponsive compounds. *ACS Chem. Biol.* *4*, 409–427.
- Lee, H.-M., Priestman, M.A., and Lawrence, D.S. (2010a). Light-Mediated Spatial Control via Photolabile Fluorescently Quenched Peptide Cassettes. *J. Am. Chem. Soc.* *132*, 1446–1447.
- Lee, J., Natarajan, M., Nashine, V.C., Socolich, M., Vo, T., Russ, W.P., Benkovic, S.J., and Ranganathan, R. (2008a). Surface Sites for Engineering Allosteric Control in Proteins. *Science* *322*, 438–442.
- Lee, J.H., Kumar, S., and Lawrence, D.S. (2008b). Stepwise combinatorial evolution of Akt bisubstrate inhibitors. *Chembiochem* *9*, 507–509.
- Lee, J.H., Nandy, S.K., and Lawrence, D.S. (2004). A Highly Potent and Selective PKC α Inhibitor Generated via Combinatorial Modification of a Peptide Scaffold. *Journal of the American Chemical Society* *126*, 3394–3395.

- Lee, K.C., Ouwehand, I., Giannini, A.L., Thomas, N.S., Dibb, N.J., and Bijlmakers, M.J. (2010b). Lck is a key target of imatinib and dasatinib in T-cell activation. *Leukemia* *24*, 896–900.
- Lee, M.-F., Beauchamp, R.L., Beyer, K.S., Gusella, J.F., and Ramesh, V. (2006). Magicin associates with the Src-family kinases and is phosphorylated upon CD3 stimulation. *Biochem. Biophys. Res. Commun.* *348*, 826–831.
- Lee, T.R., and Lawrence, D.S. (1999). Acquisition of high-affinity, SH2-targeted ligands via a spatially focused library. *J. Med. Chem.* *42*, 784–787.
- Lee, T.R., and Lawrence, D.S. (2000). SH2-Directed Ligands of the Lck Tyrosine Kinase. *J. Med. Chem.* *43*, 1173–1179.
- Leung, D.W., Otomo, C., Chory, J., and Rosen, M.K. (2008). Genetically encoded photoswitching of actin assembly through the Cdc42-WASP-Arp2/3 complex pathway. *Proc. Natl. Acad. Sci. U.S.A.* *105*, 12797–12802.
- Levskaya, A., Weiner, O.D., Lim, W.A., and Voigt, C.A. (2009). Spatiotemporal control of cell signalling using a light-switchable protein interaction. *Nature* *461*, 997.
- Ley, S.C., Marsh, M., Bebbington, C.R., Proudfoot, K., and Jordan, P. (1994). Distinct intracellular localization of Lck and Fyn protein tyrosine kinases in human T lymphocytes. *J Cell Biol* *125*, 639–649.
- Li, H., Hah, J.-M., and Lawrence, D.S. (2008a). Light-Mediated Liberation of Enzymatic Activity: “Small Molecule” Caged Protein Equivalents. *Journal of the American Chemical Society* *130*, 10474–10475.
- Li, H., and Lawrence, D.S. (2005). Acquisition of Fyn-Selective SH3 Domain Ligands via a Combinatorial Library Strategy. *Chemistry & Biology* *12*, 905–912.
- Li, H., Sims, C.E., Kaluzova, M., Stanbridge, E.J., and Allbritton, N.L. (2004). A quantitative single-cell assay for protein kinase B reveals important insights into the biochemical behavior of an intracellular substrate peptide. *Biochemistry* *43*, 1599–1608.
- Li, H., Wu, H.Y., Wang, Y., Sims, C.E., and Allbritton, N.L. (2001). Improved capillary electrophoresis conditions for the separation of kinase substrates by the laser micropipet system. *Journal of Chromatography B: Biomedical Sciences and Applications* *757*, 79–88.
- Li, L., Ittmann, M.M., Ayala, G., Tsai, M.-J., Amato, R.J., Wheeler, T.M., Miles, B.J., Kadmon, D., and Thompson, T.C. (2005). The emerging role of the PI3-K-Akt pathway in prostate cancer progression. *Prostate Cancer and Prostatic Diseases* *8*, 108.
- Li, S.S.-C. (2005). Specificity and versatility of SH3 and other proline-recognition domains: structural basis and implications for cellular signal transduction. *Biochem. J.* *390*, 641–653.

- Li, Y., Liu, D., and Bao, J.J. (2011). Characterization of tyrosine kinase and screening enzyme inhibitor by capillary electrophoresis with laser-induced fluorescence detector. *J. Chromatogr. B Analyt. Technol. Biomed. Life Sci* *879*, 107–112.
- Li, Y., Xie, W., and Fang, G. (2008b). Fluorescence detection techniques for protein kinase assay. *Anal Bioanal Chem* *390*, 2049–2057.
- Liu, X., Brodeur, S.R., Gish, G., Songyang, Z., Cantley, L.C., Laudano, A.P., and Pawson, T. (1993). Regulation of c-Src tyrosine kinase activity by the Src SH2 domain. *Oncogene* *8*, 1119–1126.
- Lovatt, M., Filby, A., Parravicini, V., Werlen, G., Palmer, E., and Zamoyska, R. (2006). Lck Regulates the Threshold of Activation in Primary T Cells, While both Lck and Fyn Contribute to the Magnitude of the Extracellular Signal-Related Kinase Response. *Mol. Cell. Biol.* *26*, 8655–8665.
- Luković, E., González-Vera, J.A., and Imperiali, B. (2008). Recognition-domain focused chemosensors: versatile and efficient reporters of protein kinase activity. *J. Am. Chem. Soc.* *130*, 12821–12827.
- Luo, Y., Shoemaker, A.R., Liu, X., Woods, K.W., Thomas, S.A., de Jong, R., Han, E.K., Li, T., Stoll, V.S., Powlas, J.A., et al. (2005). Potent and selective inhibitors of Akt kinases slow the progress of tumors in vivo. *Mol Cancer Ther* *4*, 977–986.
- Mader, C.C., Oser, M., Magalhaes, M.A.O., Bravo-Cordero, J.J., Condeelis, J., Koleske, A.J., and Gil-Henn, H. (2011). An EGFR-Src-Arg-cortactin pathway mediates functional maturation of invadopodia and breast cancer cell invasion. *Cancer Res.* *71*, 1730–1741.
- Maiolo, J.R., Ferrer, M., and Ottinger, E.A. (2005). Effects of cargo molecules on the cellular uptake of arginine-rich cell-penetrating peptides. *Biochimica Et Biophysica Acta (BBA) - Biomembranes* *1712*, 161–172.
- Majid, S., Saini, S., Dar, A.A., Hirata, H., Shahryari, V., Tanaka, Y., Yamamura, S., Ueno, K., Zaman, M.S., Singh, K., et al. (2011). MicroRNA-205 inhibits Src-mediated oncogenic pathways in renal cancer. *Cancer Res.* *71*, 2611–2621.
- Majjigapu, J.R.R., Kurchan, A.N., Kottani, R., Gustafson, T.P., and Kutateladze, A.G. (2005). Release and Report: A New Photolabile Caging System with a Two-Photon Fluorescence Reporting Function. *J. Am. Chem. Soc.* *127*, 12458–12459.
- Marriott, G. (1994). Caged Protein Conjugates and Light-Directed Generation of Protein Activity: Preparation, Photoactivation, and Spectroscopic Characterization of Caged G-Actin Conjugates. *Biochemistry* *33*, 9092–9097.
- Marriott, and Heidecker, M. (1996). Light-directed generation of the actin-activated ATPase activity of caged heavy meromyosin. *Biochemistry* *35*, 3170–3174.

- Martín-Cófreces, N.B., Sancho, D., Fernández, E., Vicente-Manzanares, M., Gordón-Alonso, M., Montoya, M.C., Michel, F., Acuto, O., Alarcón, B., and Sánchez-Madrid, F. (2006). Role of Fyn in the rearrangement of tubulin cytoskeleton induced through TCR. *J. Immunol.* *176*, 4201–4207.
- McNamee, C.J., Pennington, S.R., and Sheterline, P. (1995). Cell cycle-dependent morphological changes in the actin cytoskeleton induced by agents which elevate cyclic AMP. *Cell Biol. Int.* *19*, 769–775.
- Mellado, B., Codony, J., Ribal, M.J., Visa, L., and Gascón, P. (2009). Molecular biology of androgen-independent prostate cancer: the role of the androgen receptor pathway. *Clin Transl Oncol* *11*, 5–10.
- Meredith, G.D., Sims, C.E., Sougayer, J.S., and Allbritton, N.L. (2000). Measurement of kinase activation in single mammalian cells. *Nat Biotech* *18*, 309–312.
- Methi, T., Berge, T., Torgersen, K.M., and Taskén, K. (2008). Reduced Cbl phosphorylation and degradation of the zeta-chain of the T-cell receptor/CD3 complex in T cells with low Lck levels. *Eur. J. Immunol.* *38*, 2557–2563.
- Meyn, M.A., 3rd, and Smithgall, T.E. (2008). Small molecule inhibitors of Lck: the search for specificity within a kinase family. *Mini Rev Med Chem* *8*, 628–637.
- Mitra, S.K., and Schlaepfer, D.D. (2006). Integrin-regulated FAK–Src signaling in normal and cancer cells. *Current Opinion in Cell Biology* *18*, 516–523.
- Moarefi, I., LaFevre-Bernt, M., Sicheri, F., Huse, M., Lee, C.-H., Kuriyan, J., and Miller, W.T. (1997). Activation of the Src-family tyrosine kinase Hck by SH3 domain displacement. *Nature* *385*, 650–653.
- Mobashery, S., Doughty, M., and Kaiser, E.T. (1990). Inactivation of the catalytic subunit of bovine cAMP-dependent protein kinase by a peptide-based affinity inactivator. *Biopolymers* *29*, 131–138.
- Mukhopadhyay, D., Tsiokas, L., and Sukhatme, V.P. (1995). Wild-type p53 and v-Src exert opposing influences on human vascular endothelial growth factor gene expression. *Cancer Res.* *55*, 6161–6165.
- Neininger, A., Thielemann, H., and Gaestel, M. (2001). FRET-based detection of different conformations of MK2. *EMBO Rep.* *2*, 703–708.
- Nel, A.E. (2002). T-cell activation through the antigen receptor. Part 1: signaling components, signaling pathways, and signal integration at the T-cell antigen receptor synapse. *J. Allergy Clin. Immunol.* *109*, 758–770.
- Nelson, A.R., Borland, L., Allbritton, N.L., and Sims, C.E. (2007). Myristoyl-Based Transport of Peptides into Living Cells†. *Biochemistry* *46*, 14771–14781.

- Newman, R.H., Fosbrink, M.D., and Zhang, J. (2011). Genetically encodable fluorescent biosensors for tracking signaling dynamics in living cells. *Chem. Rev.* *111*, 3614–3666.
- Okada, C.Y., and Rechsteiner, M. (1982). Introduction of macromolecules into cultured mammalian cells by osmotic lysis of pinocytotic vesicles. *Cell* *29*, 33–41.
- Oser, M., and Condeelis, J. (2009). The cofilin activity cycle in lamellipodia and invadopodia. *J. Cell. Biochem.* *108*, 1252–1262.
- Palacios, E.H., and Weiss, A. (2004). Function of the Src-family kinases, Lck and Fyn, in T-cell development and activation. *Oncogene* *23*, 7990–8000.
- Pang, H., Kenseth, J., and Coldiron, S. (2004). High-throughput multiplexed capillary electrophoresis in drug discovery. *Drug Discovery Today* *9*, 1072–1080.
- Parsons, S.J., and Parsons, J.T. (2004). Src family kinases, key regulators of signal transduction. *Oncogene* *23*, 7906–7909.
- Patwardhan, P., and Resh, M.D. (2010). Myristoylation and Membrane Binding Regulate c-Src Stability and Kinase Activity. *Mol. Cell. Biol.* *30*, 4094–4107.
- Pellois, J.-P., Hahn, M.E., and Muir, T.W. (2004). Simultaneous triggering of protein activity and fluorescence. *J. Am. Chem. Soc.* *126*, 7170–7171.
- Pereira, A.M., Tudor, C., Kanger, J.S., Subramaniam, V., and Martin-Blanco, E. (2011). Integrin-dependent activation of the JNK signaling pathway by mechanical stress. *PLoS ONE* *6*, e26182.
- Pinna, L.A., and Ruzzene, M. (1996). How do protein kinases recognize their substrates? *Biochim. Biophys. Acta* *1314*, 191–225.
- Priestman, M.A., and Lawrence, D.S. (2010). Light-mediated remote control of signaling pathways. *Biochim. Biophys. Acta* *1804*, 547–558.
- Priestman, M.A., Sun, L., and Lawrence, D.S. (2011). Dual Wavelength Photoactivation of cAMP- and cGMP-Dependent Protein Kinase Signaling Pathways. *ACS Chem. Biol.* *6*, 377–384.
- Proctor, A., Wang, Q., Lawrence, D.S., and Allbritton, N.L. (2012). Metabolism of peptide reporters in cell lysates and single cells. *Analyst*.
- Qian, D., Lev, S., Oers, N.S.C. van, Dikic, I., Schlessinger, J., and Weiss, A. (1997). Tyrosine Phosphorylation of Pyk2 Is Selectively Regulated by Fyn During TCR Signaling. *J Exp Med* *185*, 1253–1260.
- Rauf, F., Huang, Y., Muhandiramlage, T.P., and Aspinwall, C.A. (2010). Analysis of protein kinase A activity in insulin-secreting cells using a cell-penetrating protein substrate and capillary electrophoresis. *Anal Bioanal Chem* *397*, 3359–3367.

- Rejman, J., Bragonzi, A., and Conese, M. (2005). Role of Clathrin- and Caveolae-Mediated Endocytosis in Gene Transfer Mediated by Lipo- and Polyplexes. *Molecular Therapy* 12, 468.
- Resh, M.D. (1999). Fatty acylation of proteins: new insights into membrane targeting of myristoylated and palmitoylated proteins. *Biochim. Biophys. Acta* 1451, 1–16.
- Riggsbee, C.W., and Deiters, A. (2010). Recent advances in the photochemical control of protein function. *Trends Biotechnol.* 28, 468–475.
- Rijksen, G., Adriaansen-Slot, S.S., and Staal, G.E. (1996). An enzyme-linked immunosorbent assay for the determination of src-family tyrosine kinase activity in breast cancer. *Breast Cancer Res. Treat.* 39, 139–145.
- Robinson, D.R., Wu, Y.M., and Lin, S.F. (2000). The protein tyrosine kinase family of the human genome. *Oncogene* 19, 5548–5557.
- Roger, P.P., Rickaert, F., Huez, G., Authelet, M., Hofmann, F., and Dumont, J.E. (1988). Microinjection of catalytic subunit of cyclic AMP-dependent protein kinase triggers acute morphological changes in thyroid epithelial cells. *FEBS Lett.* 232, 409–413.
- Roskoski, R., Jr (2005). Src kinase regulation by phosphorylation and dephosphorylation. *Biochem. Biophys. Res. Commun.* 331, 1–14.
- Rothman, D.M., Shults, M.D., and Imperiali, B. (2005). Chemical approaches for investigating phosphorylation in signal transduction networks. *Trends Cell Biol.* 15, 502–510.
- Saad, F., and Lipton, A. (2010). SRC kinase inhibition: Targeting bone metastases and tumor growth in prostate and breast cancer. *Cancer Treatment Reviews* 36, 177–184.
- Salerno, A., and Lawrence, D.S. (1993). Covalent modification with concomitant inactivation of the cAMP-dependent protein kinase by affinity labels containing only L-amino acids. *J. Biol. Chem.* 268, 13043–13049.
- Salmond, R.J., Filby, A., Qureshi, I., Caserta, S., and Zamoyska, R. (2009). T-cell receptor proximal signaling via the Src-family kinases, Lck and Fyn, influences T-cell activation, differentiation, and tolerance. *Immunol. Rev.* 228, 9–22.
- Samelson, L.E. (2002). Signal transduction mediated by the T cell antigen receptor: the role of adapter proteins. *Annu. Rev. Immunol.* 20, 371–394.
- Sarbassov, D.D., Guertin, D.A., Ali, S.M., and Sabatini, D.M. (2005). Phosphorylation and Regulation of Akt/PKB by the Rictor-mTOR Complex. *Science* 307, 1098–1101.
- Sasaki, K., Sato, M., and Umezawa, Y. (2003). Fluorescent Indicators for Akt/Protein Kinase B and Dynamics of Akt Activity Visualized in Living Cells. *J. Biol. Chem.* 278, 30945–30951.

Sato, M., Kawai, Y., and Umezawa, Y. (2007). Genetically encoded fluorescent indicators to visualize protein phosphorylation by extracellular signal-regulated kinase in single living cells. *Anal. Chem.* *79*, 2570–2575.

Sharma, V., Agnes, R.S., and Lawrence, D.S. (2007). Deep Quench: An Expanded Dynamic Range for Protein Kinase Sensors. *Journal of the American Chemical Society* *129*, 2742–2743.

Sharma, V., Wang, Q., and Lawrence, D.S. (2008). Peptide-based fluorescent sensors of protein kinase activity: design and applications. *Biochim. Biophys. Acta* *1784*, 94–99.

Shaw, A.S., Chalupny, J., Whitney, J.A., Hammond, C., Amrein, K.E., Kavathas, P., Sefton, B.M., and Rose, J.K. (1990). Short related sequences in the cytoplasmic domains of CD4 and CD8 mediate binding to the amino-terminal domain of the p56lck tyrosine protein kinase. *Mol. Cell. Biol.* *10*, 1853–1862.

Shaw, L.M. (2005). Tumor Cell Invasion Assays. In *Cell Migration*, (New Jersey: Humana Press), pp. 097–106.

Shen, K., Keng, Y.-F., Wu, L., Guo, X.-L., Lawrence, D.S., and Zhang, Z.-Y. (2001). Acquisition of a Specific and Potent PTP1B Inhibitor from a Novel Combinatorial Library and Screening Procedure. *Journal of Biological Chemistry* *276*, 47311–47319.

Sheng, Q., and Liu, J. (2011). The therapeutic potential of targeting the EGFR family in epithelial ovarian cancer. *British Journal of Cancer* *104*, 1241.

Shults, M.D., and Imperiali, B. (2003). Versatile Fluorescence Probes of Protein Kinase Activity. *J. Am. Chem. Soc.* *125*, 14248–14249.

Sims, C.E., and Allbritton, N.L. (2003). Single-cell kinase assays: opening a window onto cell behavior. *Current Opinion in Biotechnology* *14*, 23–28.

Sims, C.E., Meredith, G.D., Krasieva, T.B., Berns, M.W., Tromberg, B.J., and Allbritton, N.L. (1998). Laser-micropipet combination for single-cell analysis. *Anal. Chem.* *70*, 4570–4577.

Songyang, Z., Carraway, K.L., Eck, M.J., Harrison, S.C., Feldman, R.A., Mohammadi, M., Schlessinger, J., Hubbard, S.R., Smith, D.P., Eng, C., et al. (1995). Catalytic specificity of protein-tyrosine kinases is critical for selective signalling. *Nature* *373*, 536–539.

Soon, L.L. (2007). A discourse on cancer cell chemotaxis: where to from here? *IUBMB Life* *59*, 60–67.

Stains, C.I., Luković, E., and Imperiali, B. (2011). A p38 α -selective chemosensor for use in unfractionated cell lysates. *ACS Chem. Biol.* *6*, 101–105.

- Stefanová, I., Hemmer, B., Vergelli, M., Martin, R., Biddison, W.E., and Germain, R.N. (2003). TCR ligand discrimination is enforced by competing ERK positive and SHP-1 negative feedback pathways. *Nat. Immunol.* *4*, 248–254.
- Stewart, K.M., Horton, K.L., and Kelley, S.O. (2008). Cell-penetrating peptides as delivery vehicles for biology and medicine. *Org. Biomol. Chem.* *6*, 2242–2255.
- Strickland, D., Moffat, K., and Sosnick, T.R. (2008). Light-activated DNA binding in a designed allosteric protein. *Pnas* *105*, 10709–10714.
- Sun, H., Low, K.E., Woo, S., Noble, R.L., Graham, R.J., Connaughton, S.S., Gee, M.A., and Lee, L.G. (2005). Real-time protein kinase assay. *Anal. Chem.* *77*, 2043–2049.
- Sundberg, E.J., Deng, L., and Mariuzza, R.A. (2007). TCR recognition of peptide/MHC class II complexes and superantigens. *Seminars in Immunology* *19*, 262–271.
- Takao, K., Okamoto, K.-I., Nakagawa, T., Neve, R.L., Nagai, T., Miyawaki, A., Hashikawa, T., Kobayashi, S., and Hayashi, Y. (2005). Visualization of synaptic Ca²⁺/calmodulin-dependent protein kinase II activity in living neurons. *J. Neurosci.* *25*, 3107–3112.
- Taskén, K., and Aandahl, E.M. (2004). Localized effects of cAMP mediated by distinct routes of protein kinase A. *Physiol. Rev.* *84*, 137–167.
- Tatarov, O., Mitchell, T.J., Seywright, M., Leung, H.Y., Brunton, V.G., and Edwards, J. (2009). Src Family Kinase Activity Is Up-Regulated in Hormone-Refractory Prostate Cancer. *Clinical Cancer Research* *15*, 3540–3549.
- Thomas, J.W., Ellis, B., Boerner, R.J., Knight, W.B., White, G.C., 2nd, and Schaller, M.D. (1998). SH2- and SH3-mediated interactions between focal adhesion kinase and Src. *J. Biol. Chem.* *273*, 577–583.
- Timm, T., von Kries, J.P., Li, X., Zempel, H., Mandelkow, E., and Mandelkow, E.-M. (2011). Microtubule affinity regulating kinase activity in living neurons was examined by a genetically encoded fluorescence resonance energy transfer/fluorescence lifetime imaging-based biosensor: inhibitors with therapeutic potential. *J. Biol. Chem.* *286*, 41711–41722.
- Ting, A.Y., Kain, K.H., Klemke, R.L., and Tsien, R.Y. (2001). Genetically encoded fluorescent reporters of protein tyrosine kinase activities in living cells. *Proceedings of the National Academy of Sciences of the United States of America* *98*, 15003 –15008.
- Toth, I. (1994). A Novel Chemical Approach to Drug Delivery: Lipidic Amino Acid Conjugates. *Journal of Drug Targeting* *2*, 217–239.
- Trevino, J.G., Summy, J.M., Gray, M.J., Nilsson, M.B., Lesslie, D.P., Baker, C.H., and Gallick, G.E. (2005). Expression and activity of SRC regulate interleukin-8 expression in

pancreatic adenocarcinoma cells: implications for angiogenesis. *Cancer Res.* *65*, 7214–7222.

Tsygankov, A.Y., Mahajan, S., Fincke, J.E., and Bolen, J.B. (1996). Specific Association of Tyrosine-phosphorylated c-Cbl with Fyn Tyrosine Kinase in T Cells. *J. Biol. Chem.* *271*, 27130–27137.

Turner, J.M., Brodsky, M.H., Irving, B.A., Levin, S.D., Perlmutter, R.M., and Littman, D.R. (1990). Interaction of the unique N-terminal region of tyrosine kinase p56lck with cytoplasmic domains of CD4 and CD8 is mediated by cysteine motifs. *Cell* *60*, 755–765.

Unni, E., Sun, S., Nan, B., McPhaul, M.J., Cheskis, B., Mancini, M.A., and Marcelli, M. (2004). Changes in Androgen Receptor Nongenotropic Signaling Correlate with Transition of LNCaP Cells to Androgen Independence. *Cancer Res* *64*, 7156–7168.

Uri, A., Lust, M., Vaasa, A., Lavogina, D., Viht, K., and Enkvist, E. (2010). Bisubstrate fluorescent probes and biosensors in binding assays for HTS of protein kinase inhibitors. *Biochim. Biophys. Acta* *1804*, 541–546.

VanEngelenburg, S.B., and Palmer, A.E. (2008). Fluorescent biosensors of protein function. *Current Opinion in Chemical Biology* *12*, 60–65.

Vincent, E.E., Elder, D.J.E., Thomas, E.C., Phillips, L., Morgan, C., Pawade, J., Sohail, M., May, M.T., Hetzel, M.R., and Tavaré, J.M. (2011). Akt phosphorylation on Thr308 but not on Ser473 correlates with Akt protein kinase activity in human non-small cell lung cancer. *Br. J. Cancer* *104*, 1755–1761.

Violin, J.D., Zhang, J., Tsien, R.Y., and Newton, A.C. (2003). A genetically encoded fluorescent reporter reveals oscillatory phosphorylation by protein kinase C. *J. Cell Biol.* *161*, 899–909.

Wakata, A., Cahill, S.M., Blumenstein, M., Gunby, R.H., Jockusch, S., Marti, A.A., Cimbri, B., Gambacorti-Passerini, C., Donella-Deana, A., Pinna, L.A., et al. (2008). A mechanistic design principle for protein tyrosine kinase sensors: application to a validated cancer target. *Org. Lett.* *10*, 301–304.

Wang, H., Kadlecsek, T.A., Au-Yeung, B.B., Goodfellow, H.E.S., Hsu, L.-Y., Freedman, T.S., and Weiss, A. (2010a). ZAP-70: An Essential Kinase in T-cell Signaling. *Cold Spring Harb Perspect Biol* *2*,.

Wang, L., Xie, J., and Schultz, P.G. (2006a). Expanding the genetic code. *Annu Rev Biophys Biomol Struct* *35*, 225–249.

Wang, Q., Cahill, S.M., Blumenstein, M., and Lawrence, D.S. (2006b). Self-Reporting Fluorescent Substrates of Protein Tyrosine Kinases. *Journal of the American Chemical Society* *128*, 1808–1809.

Wang, Q., Dai, Z., Cahill, S.M., Blumenstein, M., and Lawrence, D.S. (2006c). Light-Regulated Sampling of Protein Tyrosine Kinase Activity. *Journal of the American Chemical Society* 128, 14016–14017.

Wang, Q., and Lawrence, D.S. (2005). Phosphorylation-Driven Protein–Protein Interactions: A Protein Kinase Sensing System. *J. Am. Chem. Soc.* 127, 7684–7685.

Wang, Q., Zimmerman, E.I., Touthkine, A., Martin, T.D., Graves, L.M., and Lawrence, D.S. (2010b). Multicolor Monitoring of Dysregulated Protein Kinases in Chronic Myelogenous Leukemia. *ACS Chemical Biology* 5, 887–895.

Wang, W., and Audet, J. (2009). Single-Cell Approaches to Dissect Cellular Signaling Networks. In *Regulatory Networks in Stem Cells*, V.K. Rajasekhar, and M.C. Vemuri, eds. (Totowa, NJ: Humana Press), pp. 337–345.

Wang, Y., Botvinick, E.L., Zhao, Y., Berns, M.W., Usami, S., Tsien, R.Y., and Chien, S. (2005). Visualizing the mechanical activation of Src. *Nature* 434, 1040–1045.

Wang, Y., and McNiven, M.A. (2012). Invasive Matrix Degradation at Focal Adhesions Occurs Via Protease Recruitment by a FAK–p130Cas Complex. *J Cell Biol* 196, 375–385.

Webber, M.M., Quader, S.T.A., Kleinman, H.K., Bello-DeOcampo, D., Storto, P.D., Bice, G., DeMendonca-Calaca, W., and Williams, D.E. (2001). Human cell lines as an in vitro/in vivo model for prostate carcinogenesis and progression. *The Prostate* 47, 1–13.

Weihua, Z., Tsan, R., Huang, W.-C., Wu, Q., Chiu, C.-H., Fidler, I.J., and Hung, M.-C. (2008). Survival of Cancer Cells Is Maintained by EGFR Independent of Its Kinase Activity. *Cancer Cell* 13, 385–393.

Whelan, M.C., and Senger, D.R. (2003). Collagen I initiates endothelial cell morphogenesis by inducing actin polymerization through suppression of cyclic AMP and protein kinase A. *J. Biol. Chem.* 278, 327–334.

Wiegers, G.J., Kaufmann, M., Tischner, D., and Villunger, A. (2011). Shaping the T-cell repertoire: a matter of life and death. *Immunol. Cell Biol.* 89, 33–39.

Wilkinson, B., Downey, J.S., and Rudd, C.E. (2005). T-cell signalling and immune system disorders. *Expert Rev Mol Med* 7, 1–29.

Williams, J.C., Wierenga, R.K., and Saraste, M. (1998). Insights into Src kinase functions: structural comparisons. *Trends in Biochemical Sciences* 23, 179–184.

Wolf, A.M.D., Wender, R.C., Etzioni, R.B., Thompson, I.M., D’Amico, A.V., Volk, R.J., Brooks, D.D., Dash, C., Guessous, I., Andrews, K., et al. (2010). American Cancer Society guideline for the early detection of prostate cancer: update 2010. *CA Cancer J Clin* 60, 70–98.

- Won, J., and Lee, G.H. (2008). T-cell-targeted signaling inhibitors. *Int. Rev. Immunol.* 27, 19–41.
- Wu, L., Yu, Z., and Shen, S.-H. (2002). SKAP55 Recruits to Lipid Rafts and Positively Mediates the MAPK Pathway upon T Cell Receptor Activation. *J. Biol. Chem.* 277, 40420–40427.
- Wu, Y.I., Frey, D., Lungu, O.I., Jaehrig, A., Schlichting, I., Kuhlman, B., and Hahn, K.M. (2009). A genetically encoded photoactivatable Rac controls the motility of living cells. *Nature* 461, 104.
- Xie, L., Lee, S.-Y., Andersen, J.N., Waters, S., Shen, K., Guo, X.-L., Moller, N.P.H., Olefsky, J.M., Lawrence, D.S., and Zhang, Z.-Y. (2003). Cellular effects of small molecule PTP1B inhibitors on insulin signaling. *Biochemistry* 42, 12792–12804.
- Xu, W., Harrison, S.C., and Eck, M.J. (1997). Three-dimensional structure of the tyrosine kinase c-Src. *Nature* 385, 595–602.
- Yadav, S.S., and Miller, W.T. (2008). The Evolutionarily Conserved Arrangement of Domains in Src Family Kinases Is Important for Substrate Recognition†. *Biochemistry* 47, 10871–10880.
- Yan, X., Corbin, J.D., Francis, S.H., and Lawrence, D.S. (1996). Precision targeting of protein kinases. An affinity label that inactivates the cGMP- but not the cAMP-dependent protein kinase. *J. Biol. Chem.* 271, 1845–1848.
- Yasuda, K., Nagafuku, M., Shima, T., Okada, M., Yagi, T., Yamada, T., Minaki, Y., Kato, A., Tani-Ichi, S., Hamaoka, T., et al. (2002). Cutting edge: Fyn is essential for tyrosine phosphorylation of Csk-binding protein/phosphoprotein associated with glycolipid-enriched microdomains in lipid rafts in resting T cells. *J. Immunol.* 169, 2813–2817.
- Yeh, R.-H., Lee, T.R., and Lawrence, D.S. (2002a). From consensus sequence to high-affinity ligands: acquisition of signaling protein modulators. *Pharmacol. Ther.* 93, 179–191.
- Yeh, R.-H., Yan, X., Cammer, M., Bresnick, A.R., and Lawrence, D.S. (2002b). Real time visualization of protein kinase activity in living cells. *J. Biol. Chem.* 277, 11527–11532.
- Zamoyska, R., Basson, A., Filby, A., Legname, G., Lovatt, M., and Seddon, B. (2003). The influence of the src-family kinases, Lck and Fyn, on T cell differentiation, survival and activation. *Immunol. Rev.* 191, 107–118.
- Zhang, J., Hupfeld, C.J., Taylor, S.S., Olefsky, J.M., and Tsien, R.Y. (2005). Insulin disrupts beta-adrenergic signalling to protein kinase A in adipocytes. *Nature* 437, 569–573.

- Zhang, Y., and Yu, L.-C. (2008a). Microinjection as a tool of mechanical delivery. *Current Opinion in Biotechnology* *19*, 506–510.
- Zhang, Y., and Yu, L.-C. (2008b). Single-cell microinjection technology in cell biology. *Bioessays* *30*, 606–610.
- Zheng, X.-M., Resnick, R.J., and Shalloway, D. (2000). A phosphotyrosine displacement mechanism for activation of Src by PTP α . *Embo J* *19*, 964–978.
- Zou, K., Cheley, S., Givens, R.S., and Bayley, H. (2002). Catalytic Subunit of Protein Kinase A Caged at the Activating Phosphothreonine. *J. Am. Chem. Soc.* *124*, 8220–8229.